A PEPTIDE-BASED SMALL INTERFERING RNA DELIVERY SYSTEM AS AN RNA INTERFERENCE APPROACH FOR NEURODEGENERATIVE DISORDERS

by

Pilju Youn

A dissertation submitted to the faculty of
The University of Utah
in partial fulfillment of the requirements for the degree of

Doctor of Philosophy

Department of Pharmaceutics and Pharmaceutical Chemistry

The University of Utah

May 2015

The University of Utah Graduate School

STATEMENT OF DISSERTATION APPROVAL

The dissertation of **Pilju Youn**

has been approved by the following supervisory committee members:

David Grainger	, Chair	**12/31/2014** Date Approved
Darin Furgeson	, Member	**12/04/2014** Date Approved
James Herron	, Member	**01/06/2015** Date Approved
Randy Jensen	, Member	**01/12/2015** Date Approved
Hanseup Kim	, Member	**01/09/2015** Date Approved

and by **David Grainger** , Chair/Dean of

the Department/College/School of **Pharmaceutics and Pharmaceutical Chemistry**

and by David B. Kieda, Dean of The Graduate School.

ABSTRACT

Neurodegenerative disorders (NDDs) have become a major global health burden. Despite persistent advances in understanding the neurodegeneration process, pathogenesis has not been fully clarified and no cures are yet available. As a therapeutic approach for NDDs, RNA interference (RNAi) can be a potent mode of treatment because it can specifically downregulate target genes that are directly or indirectly associated with the onset and progression of neurodegeneration. For example, Keap1, a negative regulator of the antioxidant responsive element (ARE) can be targeted for gene downregulation in order to enhance the endogenous antioxidant capacity and protect brain cells against extensive oxidative stress, a pathological hallmark observed in many NDDs. However, small interfering RNAs (siRNAs) bear limiting factors, including instability in the bloodstream and limited capacity to cross the blood-brain barrier (BBB) mainly due to their bulky size and negatively charged backbone. Thus, there is need for an adequate carrier that can protectively load and deliver bioactive siRNAs to brain cells. In this dissertation we detail the evaluation of a peptide-based siRNA carrier for neurotargeted siRNA delivery and the assessment of Keap1 RNAi therapeutic potential in brain cells. First, we have designed a myristoylated cell-penetrating peptide equipped with a transferrin receptor targeting sequence (myr-TP-Tf) and examined its physicochemical properties and biological functions. The myr-TP-Tf was shown to stably encapsulate siRNAs and deliver them to brain cells, leading to functional silencing

of the target gene. Myr-TP-Tf also transported the siRNAs across a brain endothelial cell monolayer in a transwell system. Second, we have assessed the therapeutic potential of Keap1 RNAi against beta amyloid (Aβ) peptide-induced oxidative stress in a human glioma cell culture. It was found that the Keap1 siRNA-peptide complex-pretreated group had better tolerance to the cytotoxicity from the Aβ and displayed lower levels of oxidative stress and autophagic activity compared to the control groups, demonstrating the neuroprotective effect of Keap1 RNAi. Third, we examined the brain-targeting and functional target gene silencing abilities of the siRNA-peptide carrier complex *in vivo*. Although the direct local injection exerted a greater performance, the systemic administration also delivered a measurable amount of siRNA to the brain, which led to a significant knockdown of the target gene. In summary, results demonstrate that this peptide-based siRNA carrier system can be a promising strategy for neurotargeted siRNA delivery both *in vitro* and *in vivo*.

TABLE OF CONTENTS

LIST OF TABLES

LIST OF FIGURES

LIST OF ABBREVIATIONS

AChEI	Acetylcholinesterase inhibitors
AD	Alzheimer’s disease
AET	Active efflux transporters
ALS	Amyotrophic lateral sclerosis
ANOVA	Analysis of variance
ApoE4	Apolipoprotein E4
APP	Amyloid precursor protein
ARE	Antioxidant response element
BACE1	Beta-secretase 1
BBB	Blood-brain barrier
BCA	Bicinchoninic acid
BCEC	Brain capillary endothelial cell
BMEC	Brain microvascular endothelial cell
CDK5	Cyclin-dependent kinase 5
cDNA	Complementary deoxyribonucleic acid
CED	Convection-enhanced delivery
CNS	Central nervous system
CPP	Cell-penetrating peptide
CSF	Cerebrospinal fluid
CSPD	Chemiluminescent alkaline phosphatase substrate
DLS	Dynamic light scattering
DMEM	Dulbecco's modified eagle medium
DPBS	Dulbecco's phosphate-buffered saline
EMEM	Eagle's minimal essential medium
EOFAD	Early onset familial AD
FBS	Fetal bovine serum
FITC	Fluorescein isothiocyanate
GAPDH	Glyceraldehyde 3-phosphate dehydrogenase
GCLM	Glutamate-cysteine ligase, modifier subunit
GSK-3β	Glycogen synthase kinase-3β
HBSS	Hanks balanced salt solution
HD	Huntington’s disease
HDL	High-density lipoprotein
HIFU	High intensity focused ultrasound
hPAP	Human placental alkaline phosphatase
HPLC	High-performance liquid chromatography
HRP	Horseradish peroxidase
JAMs	Junctional adhesion molecules

Keap1	Kelch-like ECH-associated protein
LC3	Microtubule-associated protein light chain 3 protein
LRP	LDL receptor–related protein
MAP	Microtubule-associated protein
MCI	Mild cognitive impairment
MDA	Malondialdehyde
MPTP	1-methyl-4-phenyl-1,2,3,6-tetrahydropyridine
MRI	Magnetic resonance imaging
MRP	Multidrug resistance protein
NBM	Neurobasal medium
NDD	Neurodegenerative disorder
NFT	Neurofibrillary tangles
NMDA	N-methyl-D-aspartate
NQO1	NAD(P)H dehydrogenase, quinone 1
NRF2	NF-E2-related factor 2
PD	Parkinson's disease
PEG	Polyethylene glycol
PHF	Paired helical filaments
PK/PD	Pharmacokinetics/pharmacodynamics
PSEN1	Presenilin 1
PVDF	Polyvinylidene fluoride
qRT-PCR	Quantitative real time-polymerase chain reaction
RBC	Red blood cell
RES	Reticuloendothelial system
RISC	RNA-induced silencing complex
RMT	Receptor-mediated transcytosis
RNAi	RNA interference
ROS	Reactive oxygen species
RVG	Rabies virus glycoprotein
SCA1	Spinocerebellar ataxia type 1
SDS-PAGE	Sodium dodecyl sulfate-polyacrylamide gel electrophoresis
SET	Single electron transfer mechanism
shRNA	Short hairpin RNAs
siRNA	Small interfering ribonucleic acid
SOD1	Superoxide dismutase 1
SSRI	Selective serotonin reuptake inhibitors
TAC	Total antioxidant capacity
TBA	Tribarbituric acid
TBE	Tris/Borate/EDTA
TCA	Trichloroacetic acid
TEER	Transendothelial electrical resistance
TEM	Transmission electron microscopy
TfR	Transferrin receptor
TMNC	Tris/$MgCl_2$/NaCl/CHAPS
γ-GTP	Gamma-glutamyl transpeptidase

ACKNOWLEDGMENTS

I would like to thank all of my committee members who have willingly invested their time and effort in providing valuable guidance throughout my Ph.D. training. First and foremost, I am very grateful for having Dr. David Grainger as a chair of my supervisory committee. He offered me a lot of scientific advice and helpful suggestions whenever I visited his office to discuss my research. He often invited me to his group meeting, which was another opportunity for me to learn about other interesting areas. On a personal level, I also appreciated his careful concerns and service for students and faculty in our department. I would like to express my sincere gratitude to Dr. James Herron, who willingly provided valuable feedback and considerate points for my research. His vast knowledge across a wide range of disciplines has inspired me throughout individual meetings and classes. I also appreciated his thoughtful listening to my difficulties and providing me unwavering support. Dr. Randy Jensen played a significant role on my *in vivo* studies, particularly on the development of an animal protocol and brain injection techniques. I appreciated the opportunity to experiment in his lab for part of my studies. Dr. Hanseup Kim also provided me with valuable scientific input during the course of my studies. He played a primary role in *in vitro* brain endothelial cell culture experiments and also generously shared his lab folder where I could access a wealth of blood-brain barrier literature. I appreciate his fundamental questions and willingness to support me. I am particularly grateful to my advisor and mentor, Dr. Darin

Furgeson, for allowing me to have research opportunities and guiding me with encouragement in both scientific endeavors and my personal life. Without his constant feedback and support, I could never have come to this point. I truly appreciate it.

I also thank Dr. Jeffrey Johnson and Dr. Eric Shusta at the University of Wisconsin, Madison for generously training me on the primary rodent brain cell culture techniques. I am also obliged to Dr. David Gillespie in Dr. Randy Jensen's lab, who kindly taught me the mouse intracranial injection skills and shared his scientific expertise in *in vitro* and *in vivo* studies. Without these tremendous resources, my research project could not have been so productive.

I appreciate all the professors and colleagues in our department from whom I have always learned a lot in classes, seminars, and casual conversations. It has been a great learning experience for me to interact with these people throughout my Ph.D. years.

I would like to extend my thanks to my lab mate, Dr. Yizhe Chen, who has been an excellent colleague and a good friend to me during our journey here. Our friendship will definitely continue throughout our next steps.

Last but not least, I would like to give my greatest thanks to my parents, my elder brother and sister-in-law, and my friends who consistently send out enormous love and unconditional support. Special thanks to my mom and dad for all that they have done for me since the day I was born. No words can express my deepest thanks to them.

This research project was graciously funded by National Institutes of Health grant 1R21NS064541-01A1 and the University of Utah start-up fund.

CHAPTER 1

INTRODUCTION

1.1 General introduction

Neurodegenerative disorders (NDDs) have become a rapidly growing health issue, with approximately 12 million Americans suffering today from Alzheimer's disease (AD), Parkinson's disease (PD), amyotrophic lateral sclerosis (ALS), and Huntington's disease (HD) (1). The number of patients is increasing with the continuously growing population of age 65 and older. In 2012, approximately $9.1 billion was estimated as the health care cost for dementia caregiving in the US and the economic burden is expected to increase substantially (2).

Despite the global demand for clinically viable therapeutics, as yet, there are no cures or effective treatments for NDDs. It is because the neurodegeneration process has not been fully clarified, and partly because the blood-brain barrier (BBB) poses a major obstacle for drug delivery to the brain (3). The endothelial cells lining the microvessels in the brain form a highly selective barrier prohibiting the passages for the molecules that are hydrophilic or larger than 400 Da. In addition, the tight junction proteins between the endothelial cells block the paracellular transport. Even for the drugs that can exploit the transcellular pathway, the drug efflux pumps may transport those substances out of cells back into the capillaries (4). Therefore, the strategies to overcome the BBB should be investigated in the development of effective central nervous system (CNS)-targeting

drugs.

In the case of AD, the most common type of dementia, there are currently two types of medications approved for patients: cholinesterase inhibitors and memantine (5). However, these drugs can only alleviate the cognitive symptoms and cannot fundamentally prevent the further progression of the neurodegeneration. According to the amyloid hypothesis, the amyloid plaque, the insoluble beta amyloid (Aβ) peptide aggregates, have been considered a major culprit to initiate the AD pathology (6). Therefore, clinical trials have been conducted to evaluate the amyloid plaques-targeting drugs such as solanezumab and bapineuzumab, but both immunotherapy agents failed to prove the efficacy in AD patients. Another antibody-based drug, crenezumab is now focusing on the early-stage of AD because drugs are prone to fail for the advanced stages of AD due to the irreversibly progressed prevailing neuronal damages (7). Another class of drugs is the BACE1 (beta-site APP cleaving enzyme 1) inhibitors, which block the beta secretase enzyme activity, thereby preventing the accumulation of the Aβ peptides. The recent clinical trials have reported promising results showing the decreased level of Aβ peptide in the cerebrospinal fluid (CSF) of mild-to-moderate AD patients (8).

Along with the clinical therapeutics mentioned above, the RNA interference (RNAi) approach can be a promising mode of NDD treatment because this technology allows the highly specific degradation of the target mRNAs that are directly or indirectly associated with the onset and the progression of the neurodegeneration. In AD treatment, for instance, the BACE1 gene can be targeted for the gene silencing in order to reduce the beta amyloid production and amyloid plaque accumulation (9). The amyloid precursor protein (APP) is also a possible candidate as its proteolytic cleavage product generates

the Aβ peptides (10). Aside from the amyloid plaque, phosphorylated tau proteins are a characteristic pathological hallmark of the AD. As the cyclin-dependent kinase 5 (CDK5) has a major role in the tau phosphorylation, the RNAi can be applied against the CDK5 to interfere with the tau phosphorylation (11). In many NDDs, not only the abnormal protein aggregates, but also extensive oxidative stress is considered one of the key pathological factors contributing to the disease progression. In this context, the Nrf2 (NF-E2-related factor 2)-ARE(antioxidant responsive element) pathway can attract attention because the Nrf2 is known to activate the ARE, leading to the upregulation of detoxifying and antioxidant genes which attenuate the oxidative stress (12-16). However, the basal activity of the Nrf2 is normally restricted by the Keap1 protein through cytoplasmic sequestration and the ubiquitin-mediated degradation pathway (17,18). Therefore, the RNAi approach to the Keap1 gene will rescue the Nrf2 activity and thereby boost the endogenous antioxidant capacity providing the cytoprotection to the brain cells against the oxidative stress.

However, the siRNA delivery to the brain has been a challenging task not only because of the defensive vasculature of the BBB, but also because of the susceptibility of naked siRNA to the serum nucleases (19). Therefore, there is a need for the development of siRNA delivery vehicles that can stably encapsulate and protect siRNAs, and deliver them to the brain parenchyma across the BBB. A range of various siRNA delivery modes have been studied including chemically modified siRNA (20,21), polymeric nanoparticles (22,23), liposomes or exosomes (24,25), antibody-fusion molecules (26), and cholesterol-conjugated siRNA (27). However, further investigations are still needed to enhance the essentially required properties such as the physiological stability,

functional target gene knockdown, and sufficient brain-targeting ability.

In this study, we have designed a myristoylated cell-penetrating peptide equipped with a transferrin receptor (TfR)-targeting peptide sequence as a siRNA delivery vehicle for brain-targeted delivery. The peptide-based siRNA carrier can be produced by the solid-phase peptide synthesis in which a series of manipulations can be easily conducted in the automated machine. Among various cell-penetrating peptides, the transportan sequence was chosen based on a recent finding in which the transportan sequence was shown to optimally load siRNAs, deliver them to the cells, and successfully release the bioactive siRNAs in the cytosol resulting in the target gene knockdown (28). As a brain-targeting moiety, we incorporated a TfR-targeting peptide sequence because it has been well identified that TfRs are abundantly expressed on both brain endothelium and neurons/astrocytes (29). Moreover, the relatively short peptide sequence is expected to be less likely to affect the size and the structure of the siRNA-peptide complex. The myristic acid at the N-terminus of the carrier will establish the hydrophobic core of the siRNA-peptide complex contributing to the stable complex formation and possibly enhance the interaction between the complex and the cellular membrane through the hydrophobic interaction (30). We hypothesized that this myr-TP-Tf peptide will serve as a functional siRNA carrier for brain-targeted delivery.

This dissertation is organized into a literature review of the current status of Alzheimer's disease treatments, RNAi therapeutic targets, and siRNA delivery strategies for NDDs. Chapter 3 details the characterization and *in vitro* evaluation of the siRNA-peptide complex. Chapter 4 describes the therapeutic potential of the RNAi approach against the Keap1 gene in the neurodegenerative condition *in vitro*. In Chapter 5, the *in*

vivo validation studies on the brain targeting ability and the functional gene silencing capacity of the siRNA-peptide complex are delineated. Finally, Chapter 6 will briefly summarize the study results and describe future work regarding the optimization of the carrier design and the further evaluation of the siRNA-peptide complex in NDD animal models.

1.2 Specific aims

The RNAi therapy can be a promising approach for NDDs because it can be used specifically to downregulate the genes associated with the pathogenesis. To deliver therapeutic siRNAs to the brain across the BBB, however, there is a need for a siRNA carrier that can achieve the adequate siRNA encapsulation and protection, the effective brain targeting, and the functional cytosolic release of the bioactive siRNAs leading to the successful suppression of the target gene. To this end, we first conceived a peptide-based siRNA carrier which is comprised of an N-terminal myristic acid, a transportan cell-penetrating peptide, and a TfR-targeting short peptide sequence. We hypothesized that a myristoylated cell-penetrating peptide equipped with a TfR-targeting sequence will accomplish the stable condensation and protection of siRNA and targeted delivery of siRNA to the brain cells across the brain endothelial barrier *in vitro*. Next, we proposed the RNAi approach against the Keap1 gene using our peptide-based siRNA carrier as a potential NDD treatment. The fact that many NDDs are associated with elevated oxidative stress is well investigated. Because the Keap1 acts as a negative regulator of Nrf2, which is responsible for the basal expression of antioxidant genes, the downregulation of the Keap1 gene will lead to the augmentation of the endogenous antioxidant capacity, thus providing cytoprotection to the brain cells against the oxidative

assault. We hypothesized that the Keap1 siRNA-peptide complex pretreatment to the brain cells will help maintain the cell viability and protect cells against the Aβ peptide-induced oxidative stress compared to the control group. Finally, an *in vivo* evaluation of the siRNA-peptide complex was planned to assess the brain targeting ability of the siRNA-peptide complex and the functional target gene knockdown in a living system. The following specific aims were designed to evaluate these hypotheses and to perform the validations. The experimental design for each specific aim is shown in Figure 1.1.

- Specific aim 1: Characterization and in vitro evaluation of a myristoylated cell-penetrating peptide equipped with a TfR-targeting sequence (myr-TP-Tf)
    a) Physicochemical characterization of myr-TP-Tf
    b) Evaluation of the functional siRNA delivery and the target gene silencing in a brain cell line and primary brain cells
    c) Examination of the siRNA transport across a brain endothelial cell monolayer
- Specific aim 2: *In vitro* evaluation of the neuroprotective potential from the Keap1 siRNA-peptide complex pretreatment
    a) Examination of the antioxidant activation after the Keap1 siRNA-peptide complex treatment
    b) Assessment of the cell viability after the oxidative assault
    c) Evaluation of the cytoprotective effect against the Aβ peptide-induced oxidative stress
- Specific aim 3: *In vivo* validation of the brain targeting ability and the target gene knockdown capacity of the siRNA-peptide complex

a) Evaluation of the brain-targeted siRNA delivery

b) Examination of the functional downregulation of the target gene

c) Assessment of the toxicity associated with the siRNA-peptide complex treatment

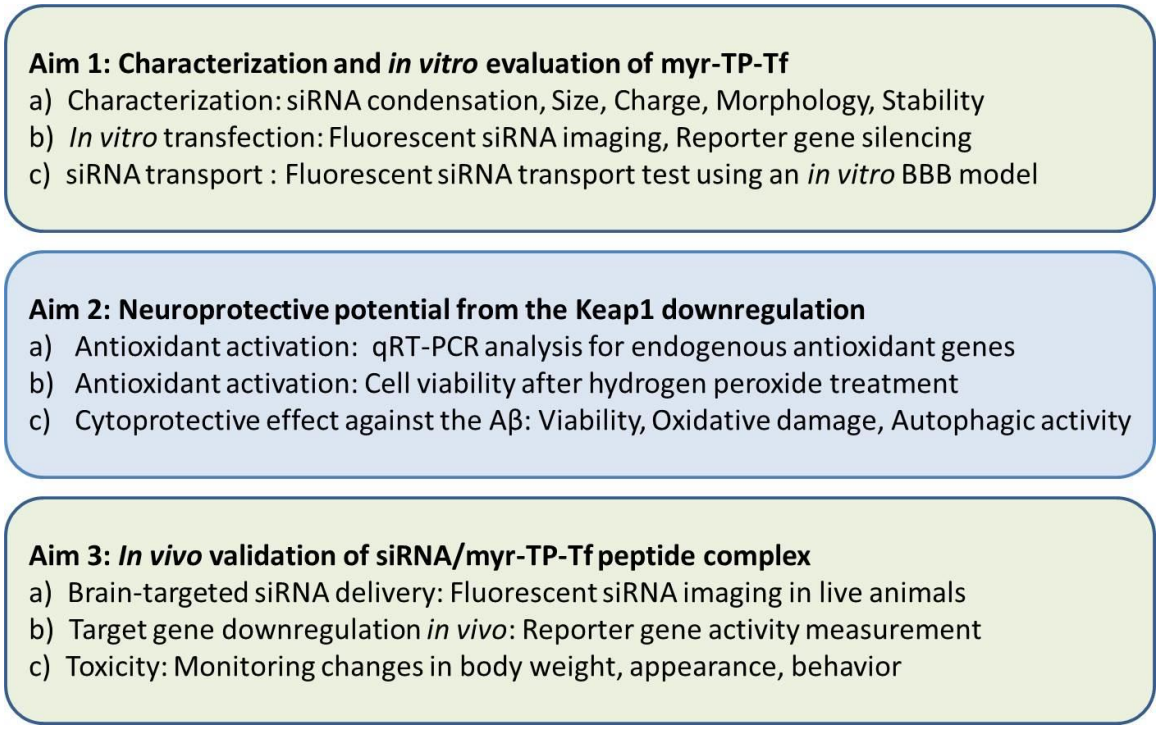

Figure 1.1. Specific aims and corresponding experimental design.

1.3 References

1. Havard Neurodiscovery Centers, http://www.neurodiscovery.harvard.edu/challenge/challenge_2.html, accessed Aug. 19, 2014.

2. Alzheimer's Association. 2013 Alzheimer's disease facts and figures. Alzheimers Dement 2013;9:208-45.

3. Pardridge WM. Blood-brain barrier biology and methodology. J Neurovirol 1999;5:556-69.

4. Toth A, Veszelka S, Nakagawa S, Niwa M, Deli A. Patented *in vitro* blood-brain barrier models in CNS drug discovery. Recent Pat CNS Drug Discov 2011;6:107-18.

5. Alzheimer's Association, http://www.alz.org/alzheimers_disease_standard_prescriptions.asp, accessed Aug. 19, 2014.

6. Hardy J, Selkoe DJ. The amyloid hypothesis of Alzheimer's disease: progress and problems on the road to therapeutics. Science 2002;297:353-56.

7. Corbett A, Pickett J, Burns A, Corcoran J, Dunnett SB, Edison P, et al. Drug repositioning for Alzheimer's disease. Nat Rev Drug Discov 2012;11:833-46.

8. Merck Newsroom, http://www.mercknewsroom.com/press-release/alzheimers-disease/merck-presents-findings-phase-1b-study-investigational-bace-inhibit, accessed Aug. 19, 2014.

9. Singer O, Marr RA, Rockenstein E, Crews L, Coufal NG, Gage FH, et al. Targeting BACE1 with siRNAs ameliorates Alzheimer disease neuropathology in a transgenic model. Nat Neurosci 2005;8:1343-49.

10. Rodríguez-Lebrón E, Gouvion CM, Moore SA, Davidson BL, Paulson HL. Allele-specific RNAi mitigates phenotypic progression in a transgenic model of Alzheimer's disease. Mol Ther 2009;17:1563-73.

11. Piedrahita D, Hernández I, López-Tobón A, Fedorov D, Obara B, Manjunath B, et al. Silencing of CDK5 reduces neurofibrillary tangles in transgenic alzheimer's mice. J Neurosci 2010;30:13966-76.

12. Motohashi H, Yamamoto M. Nrf2-Keap1 defines a physiologically important stress response mechanism. Trends Mol Med 2004;10:549-57.

13. Melo A, Monteiro L, Lima RMF, de Cerqueira MD. Oxidative stress in neurodegenerative diseases: mechanisms and therapeutic perspectives. Oxid Med Cell Longev 2011;2011:Article ID 467180.

14. Barnham KJ, Masters CL, Bush AI. Neurodegenerative diseases and oxidative stress. Nat Rev Drug Discov 2004;3:205-14.

15. Calkins MJ, Johnson DA, Townsend JA, Vargas MR, Dowell JA, Williamson TP, et al. The Nrf2/ARE pathway as a potential therapeutic target in neurodegenerative disease. Antioxid Redox Sign 2009;11:497-508.

16. Element AR. An important role of Nrf2-ARE pathway in the cellular defense mechanism. J Biochem Mol Biol 2004;37:139-43.

17. Itoh K, Wakabayashi N, Katoh Y, Ishii T, Igarashi K, Engel JD, et al. Keap1 represses nuclear activation of antioxidant responsive elements by Nrf2 through binding to the amino-terminal Neh2 domain. Gene Dev 1999;13:76-86.

18. Kobayashi M, Yamamoto M. Molecular mechanisms activating the Nrf2-Keap1 pathway of antioxidant gene regulation. Antioxid Redox Sign 2005;7:385-94.

19. Turner JJ, Jones SW, Moschos SA, Lindsay MA, Gait MJ. MALDI-TOF mass spectral analysis of siRNA degradation in serum confirms an RNAse A-like activity. Mol Biosyst 2006;3:43-50.

20. Layzer JM, McCaffrey AP, Tanner AK, Huang Z, Kay MA, Sullenger BA. *In vivo* activity of nuclease-resistant siRNAs. RNA 2004;10:766-71.

21. Nakajima H, Kubo T, Semi Y, Itakura M, Kuwamura M, Izawa T, et al. A rapid, targeted, neuron-selective, *in vivo* knockdown following a single intracerebroventricular injection of a novel chemically modified siRNA in the adult rat brain. J Biotechnol 2012;157:326-33.

22. Chen C, Mei H, Shi W, Deng J, Zhang B, Guo T, et al. EGFP-EGF1-conjugated PLGA nanoparticles for targeted delivery of siRNA into injured brain microvascular endothelial cells for efficient RNA interference. PloS One 2013;8:e60860.

23. Malmo J, Sandvig A, Vårum KM, Strand SP. Nanoparticle mediated p-glycoprotein silencing for improved drug delivery across the blood-brain barrier: a siRNA-chitosan approach. PloS One 2013;8:e54182.

24. Alvarez-Erviti L, Seow Y, Yin HF, Betts C, Lakhal S, Wood MJA. Delivery of siRNA to the mouse brain by systemic injection of targeted exosomes. Nat Biotechnol 2011;29:341-45.

25. Tao Y, Han J, Dou H. Brain-targeting gene delivery using a rabies virus glycoprotein peptide modulated hollow liposome: bio-behavioral study. J Mater Chem 2012;22:11808-15.

26. Xia CF, Zhang Y, Boado RJ, Pardridge WM. Intravenous siRNA of brain cancer with receptor targeting and avidin–biotin technology. Pharm Res 2007;24:2309-16.

27. Kuwahara H, Nishina K, Yoshida K, Nishina T, Yamamoto M, Saito Y, et al. Efficient *in vivo* delivery of siRNA into brain capillary endothelial cells along with endogenous lipoprotein. Mol Ther 2011;19:2213-21.

28. Ren Y, Hauert S, Lo JH, Bhatia SN. Identification and characterization of receptor-specific peptides for siRNA delivery. ACS Nano 2012;6:8620–31.

29. Lee JH, Engler JA, Collawn JF, Moore BA. Receptor mediated uptake of peptides that bind the human transferrin receptor. Eur J Biochem 2001;268:2004-12.

30. Pham W, Kircher MF, Weissleder R, Tung CH. Enhancing membrane permeability by fatty acylation of oligoarginine peptides. Chembiochem 2004;5:1148-51.

CHAPTER 2

CURRENT STATUS OF ALZHEIMER'S DISEASE TREATMENTS AND RNA INTERFERENCE STRATEGIES AS A PROMISING THERAPEUTIC OPTION: A LITERATURE REVIEW

2.1 Abstract

Alzheimer's disease (AD), the most common form of neurodegenerative disorders (NDDs), has become a significant healthcare concern with the aging population growing worldwide. Despite the expanded understanding of the neurodegenerative process, the AD pathogenesis has not been fully elucidated. Furthermore, the restrictive brain vasculature has been a key hurdle for brain-targeted drug delivery, posing challenges to the development of AD treatments. Here, we briefly overviewed the specialized characteristics of the blood-brain barrier (BBB) in relation to the CNS-targeted drug delivery and examined the current status of AD medicines. In addition, we propose that the RNA interference (RNAi) approach can be a potent mode of NDD treatment via effective suppression of the NDD-associated gene expression. The second part of this article is chiefly devoted to reviewing the potential therapeutic targets of AD and other types of NDDs to which RNAi technology can be applied and the strategies for the brain-targeted siRNA delivery, particularly with a focus on the RNAi delivery systems and the routes of administration. The limitations of the diverse approaches and alternatives are discussed further concerning clinical utility.

2.2 Introduction

As the average lifespan has steadily extended, age-associated diseases have become one of the major public health problems. Particularly, Alzheimer's disease (AD) has ranked 6th among the leading causes of death in the US in 2013 (1). However, current AD medicines provide only temporary symptomatic relief without substantial disease-modifying effects. The AD drugs under laboratory and clinical investigations have also suffered limited pharmacological action largely because of the restrictive blood-brain barrier (BBB) (2). To improve the transport of therapeutics into the brain parenchyma, we need to understand the structural and functional features of the BBB and devise proper drug delivery strategies to overcome this obstacle. The relentless research effort over three decades has identified key pathological processes that are responsible for various neurodegenerative disorders (NDDs), yet much remains unclear. The potential AD drugs which directly address those major disease-causing factors have been evaluated in clinical trials with occasional promising news, but no clinical success in finding AD cures has been reported until now. At present, multiple clinical trials are still in progress with a hope to slow down or stop the AD progression. Along with this effort, the RNA interference (RNAi) therapy as an experimental neurotherapeutics approach for AD and other types of NDDs is worth attempting. The RNAi has emerged as a promising treatment modality for many human diseases owing to the posttranscriptional suppression of the specific target gene expression (3). However, the RNAi approach encounters multifarious hurdles that need to be addressed for successful results in the living system. A wide variety of RNAi delivery vehicles tested in preclinical studies and alternative routes of administration provide the basis to enhance the therapeutic RNAi effect and

possibly to accelerate the RNAi therapy transition to clinical application for NDD treatment.

2.3 Blood-brain barrier (BBB) as a major obstacle for drug delivery to the brain

2.3.1 The restrictive properties of the BBB

The existence of the BBB was first observed by Paul Ehrlich who injected various water-soluble vital dyes to the animals and found that the majority of the organs were stained while the brain and spinal cord remained unstained. He explained this phenomenon as the central nervous system lacks affinity for the vital dyes (4). Later, Lewandowsky named this biological wall bluthirnschranke (BBB) for the first time (5). Today, it has been well known that the endothelial cells that compose brain microvascular capillaries have complex and distinct structures that form the basis of characteristic selective permeability of the BBB. The BBB allows the passage of water, oxygen, and other important nutrients and hormones via various transport systems, as delineated in Figure 2.1. For other types of molecules, however, the following characteristics of the BBB restrict the path to the brain compartment. First of all, the endothelial cells are closely attached together by tight junction proteins that block paracellular passages of substances in the blood circulation. These tight junction proteins include zonula occludins (ZO), claudins, junctional adhesion molecules (JAMs) and others (6). The molecules with small size (< 500 Da) and sufficient lipophilicity may enter the transcellular pathway across the endothelial membrane (7). However, the active efflux transporters (AET) such as P-glycoproteins (Pgp), multidrug resistance proteins (MRPs), and breast cancer resistance proteins (BCRPs) may immediately pump those

substances back into the bloodstream posing a difficulty for the transcellular pathway as well (8,9). In addition, the BBB functions as a biochemical barrier. The enzymatic proteins (e.g., γ-glutamyl transpeptidase (γ-GTP), aromatic acid decarboxylase, and alkaline phosphatase) are widely expressed on plasma membranes of brain endothelial cells, pericytes and astrocyte foot processes, which directs the materials crossing the BBB to the metabolic degradation (10). Therefore, AD treatments as well as other CNS therapeutics require strategies to overcome the major challenges by the BBB for successful brain-targeted drug delivery.

2.3.2 Strategies to circumvent the BBB

Researchers have attempted diverse approaches to transport drugs across the BBB. One is to design small molecule drugs to have more lipid soluble structure. Drugs with high partition coefficient values (LogP) are more likely to migrate across the cellular membrane because of the favorable lipophilicity (11). However, this may also cause unscheduled interaction with hydrophobic proteins, which can lead to toxic effects (12). Therefore, the drug design should pass through an elaborate examination in regard to pharmacokinetic properties as well as physicochemical characteristics. Instead of the systemic administration, CNS drugs can be directly injected to the brain parenchyma via intracerebral injection or intracerebroventricular injection (13). Direct injection ensures BBB circumvention and substantive delivery of therapeutics to the specific brain region. On the contrary, the drugs may not be sufficiently diffused further into the brain tissues, limiting the therapeutic effect. Considering patient convenience, safety, and cost, the craniotomy-based approach may not be a feasible option for certain conditions that need repeated injections. Another approach is to physically disrupt the brain vasculature to

have temporary openings for drug passage. The possible methods for this approach include: injection of hyperosmotic mannitol solution (14), application of high intensity focused ultrasound (HIFU) (15,16) and use of vasoactive compounds such as bradykinin, histamine, and leukotrienes (17,18). However, the disruptive opening approach also allows the entry for all types of blood constituents that may increase the risk of getting toxic substances into the brain. The growing field of pharmaceutical research has suggested various engineered drug delivery vehicles that are constructed for favorable pharmacokinetic behavior, protective drug loading, and improved brain accumulation, often by exploiting targeting moieties that bind to receptors or transporters on brain endothelium (19). Although no unitary method completely satisfies the criteria for a general drug delivery approach for the brain yet, unceasing research efforts have been continually leading a step forward to breaching the BBB.

2.4 Current status of AD treatments

2.4.1 Clinical impact of AD

AD is the most common form of neurodegenerative disorders, affecting over 35 million people worldwide now. The number of AD patients is estimated to reach 115 million by 2050 with an accelerating pace of population aging (20). Along with the growing number of AD patients, the cost for healthcare has become a serious economic burden with approximately $148 billion of total annual health care spending for AD patients (21). The neurodegeneration typically develops and worsens over many years, afflicting patients in their memory, judgment, communication, orientation, and ability to perform daily tasks depending on the severity of the cognitive impairment. Moreover, the AD progression also affects the personality and behavior of patients. That being said,

not only the individual patients but also their immediate caregivers, usually their family, suffer from the high emotional burden. However, the effort to develop a potent cure for AD has not been successful yet. The currently prescribed drugs for AD patients merely provide temporary amelioration of symptoms without having significant disease modifying effects. This unmet clinical need is one of the most urgent health problems on which researchers have steadily worked.

2.4.2 Risk factors for AD incidence

Several known risk factors for AD incidence include aging, family history, genetic predisposition, cardiovascular disease risk factors (e.g., obesity, diabetes, and smoking), education, social and cognitive engagement, and traumatic brain injury (1). Among these, the largest risk factor is aging. Lopez et al. found that the prevalence of mild cognitive impairment (MCI) increased with age, showing that 19% of people 75 years or younger had MCI while it increased to 29% for those 85 years or older (22). Despite the fact that aging plays a significant role in AD incidence, it should be noted that AD is not a normal process of healthy aging. Family history also poses a risk factor. A study reported that individuals having AD patients in their first degree relatives are at a greater risk to develop AD in life (23). Regarding the genetic predisposition, the apolipoprotein E4 (ApoE4) variant may partly account for family history-related AD occurrence. ApoE, a major class of apolipoprotein responsible for cholesterol transport, exists as one of three isoforms (E2, E3, E4) that are encoded by ε2, ε3, and ε4 allele (24). These variants possess different amino acid residues at positions 112 and 158 on their primary structures (25). In particular, the arginine residue at position 112 of ApoE4 is known to direct domain interaction via Arg61 and Glu255 within the ApoE4 structure,

which is known to mediate the production of NFT-like intracellular deposits resulting in neurotoxicity (26). Individuals bearing either one or two ε4 alleles are more likely to develop late-onset familial AD with ~2.8-fold greater risk (27). However, possessing one or two ε4 alleles does not necessarily translate to a definitive diagnosis of AD. It appears that the AD onset is governed not only by the individual genetic profile but also by many other factors. Lifestyle can also influence AD occurrence. Studies have shown that midlife obesity is related to increased risk of AD development later in life (28,29). Ott et al. also showed that smoking contributes to the incidence of AD and other types of dementia with a doubled risk compared to the AD incidence for nonsmokers (30). The known risk factors and other factors that contribute to the pathogenesis of Alzheimer's disease are delineated in Figure 2.2.

2.4.3 Neuropathological features and clinical symptoms of AD

From the neuropathological point of view, AD is typically represented by gradual neuronal demise and loss of synapses in the cerebral cortex, hippocampus, and other brain regions (31). The progressive loss of neurons leads to severe brain shrinkage, (i.e., cerebral atrophy), in late-stage AD. A magnetic resonance imaging (MRI)-based volumetric measurement study confirmed that the medial temporal lobe structures in AD patients were significantly diminished relative to the control group, which also indicates the neuronal loss along with the AD progression (32). Brain tissues from patients with AD are commonly characterized with extracellular accumulation of amyloid plaques that are composed of beta amyloid peptides (Aβ), an aberrant proteolytically cleaved fragment produced from the amyloid precursor protein (APP). Studies have shown that an array of soluble Aβ species causes deleterious effects such as synapse impairment, compromised

axonal transport, cytotoxicity and neuronal death (33). Another neuropathological feature is the intracellular neurofibrillary tangles (NFT), the major component of which is hyperphosphorylated tau protein, a type of microtubule-associated protein (MAP). MAPs are known to contribute to the stability and assembly of the microtubule network, but enhanced phosphorylation of tau proteins disrupts the microtubule assembly, leading to impaired axoplasmic flow, synaptic loss, and ultimately, neuronal demise (34). The Aβ plaque and NFT formation processes are illustrated in Figure 2.3.

The representative AD symptoms include memory loss, reduced ability to learn new information, confusion with time and place, difficulty in understanding, judgment and communication, and changes in personality and emotions (1). As the AD progresses, these symptoms worsen and patients become bedbound, requiring assistance from their caregivers in virtually all aspects of daily life. Regarding the severity of the symptoms, there seems to be a connection between the symptomatic indication and the prevalence of neuropathological hallmarks to a certain extent. For example, Savva et al. conducted a study with postmortem brain tissues where they found that the neocortical cerebral atrophy showed a strong relationship between the age and dementia in both 75-year-old subjects and 95-year-old subjects (35). However, the relationship between the neocortical neuritic plaques and dementia was reduced for the 95-year-old group compared to the 75-year group, indicating that certain neuropathological features may not translate directly to clinical manifestation. Indeed, it has been well known that brain changes occur approximately one to two decades earlier than the emergence of the first AD signs (36). Even though the accumulation of amyloid plaques and hyperphosphorylated tau neurofibrillary tangles may create a condition for AD onset, it

may not be sufficient to result in clinical symptoms of AD considering that the asymptomatic period spans multiple years. The magnitudes of AD biomarkers, brain atrophy and cognitive impairment along the disease progression are shown in Figure 2.4.

2.4.4 Molecular mechanisms of AD pathogenesis

Throughout the last three decades, studies have considerably broadened our understanding about the molecular and cellular mechanisms associated with neurodegenerative disorders. Nonetheless, the exact mechanism that directs AD development has not been fully clarified with the exception of familial cases of AD triggered by known genetic mutations such as those in APP, presenilin 1 (PS1), and presenilin 2 (PS2). Regarding the cause for AD development, researchers have proposed three central hypotheses: cholinergic hypothesis, amyloid hypothesis, and tau hypothesis. Although the precise mechanism for the AD initiation and symptomatic deterioration remains vastly unknown, the amyloid hypothesis has gained much more scientific strength in the AD research field.

According to the amyloid cascade hypothesis, the accumulation of amyloid plaques has a primary role for initiating AD pathology (37). This hypothesis is largely bolstered by studies that have shown the link between the genetic mutations in APP, PS1, and PS2 genes and clinical manifestations of early onset familial AD (EOFAD) (38,39). These Aβ peptide production-related genetic alterations result in Aβ accumulation in the brain and eventually the loss of neurons and decline in cognitive abilities. Aβ peptides, the key component of amyloid plaques are produced from the sequential cleavage of APP by two proteases: β-secretase and γ-secretase. The β-secretase cleaves the extracellular domain of APP and the γ-secretase sequentially cuts the transmembrane domain of APP

releasing the Aβ peptide fragment (40). The γ-secretase may cut varying sites on the APP transmembrane domain producing Aβ fragments with different numbers of amino acids (Aβ37, Aβ38, Aβ40, Aβ42, Aβ43) and distinct biophysical properties (33,41). All of these species are found in both healthy individuals and AD patients, but to different extents. In contrast to others, Aβ42 is the most fibrillogenic, thus, forming amyloid deposits that cause interruption of synaptic transmission, neuronal damage, and eventually AD development (42). Despite evidences proving the neurotoxicity of Aβ peptide, the amyloid hypothesis has a controversial element in that the level of Aβ aggregates in brain tissues with AD does not necessarily correlate to the degree of cognitive symptoms. Rather, the soluble, invisible form of Aβ was found to serve as a better predictor for the neurodegeneration (43). This indicates that the symptomatic exacerbation may be a consequence of complex molecular and cellular processes involving other factors aside from Aβ plaques.

The tau hypothesis states that the hyperphosphorylated tau protein is the critical pathological substrate for AD. The hyperphosphorylated form of tau proteins form paired helical filaments (PHF) and straight filaments (SF), which are major components of the neurofibrillary tangles (44). Studies have shown that there is a high correlation between the cognitive impairment and the level of NFTs in the affected brain region, as well as the hyperphosphorylated tau protein concentration in cerebrospinal fluids from AD patients (45,46). In addition, multiple studies have demonstrated the reduction of tau proteins protect brain cells from the Aβ-mediated neurotoxicity *in vivo* as well as *in vitro.* This suggests the important role of tau for the Aβ-induced neurodegeneration (47-49). On the contrary, there is evidence showing that Aβ directs the tau-mediated toxic effects.

For example, a study reported that Aβ activates glycogen synthase kinase-3β (GSK-3β), which is responsible for producing phosphorylated tau protein, the neurotoxic form of tau. Moreover, a postmortem assessment revealed that Aβ accumulation significantly precedes tau formation, at least in the frontal cortex of AD patients (50). Though the general consensus from the field is weighed more on the amyloid hypothesis, it is also evident that there is a close relationship between tau pathology and Aβ-mediated neurotoxicity.

The cholinergic hypothesis states that the lack of acetylcholine, a type of neurotransmitter, leads to the neurodegenerative condition and cognitive decline. This was supported from the finding that there is an association between the loss of cholinergic neurons in the cerebral cortex and the memory deficit of the AD patients (51). However, it is now apparent that the acetylcholine deficit has rather an indirect effect on the memory function (52). In fact, cholinomimetic agents or cholinesterase inhibitors do not prevent AD progression, but provide limited cognitive benefits.

Other cellular processes that are associated with neurodegeneration in brain tissues with AD include reactive oxygen species (ROS)-mediated oxidative stress, programmed cell death, glial cell activation, protein misfolding and proteasomal malfunction which leads to abnormal protein aggregates (53). Among these, oxidative stress has been highlighted as pivotal in all of these cellular events. In addition, Aβ-associated free radical formation was observed both *in vitro* and *in vivo*, implying the key role of oxidative stress in Aβ-mediated neurotoxicity in AD brain tissues (54). Another study reported that metal-catalyzed oxidation facilitates the formation of Aβ deposits in AD pathology (55). Although it is still uncertain whether oxidative stress is a direct

cause for the neurodegeneration or just a consequence of the disease process, findings from numerous studies indicate that oxidative stress is at least closely interlinked with those cellular events leading to the neuronal damage and death, which rationalizes the attempts for antioxidant therapy to NDD patients.

2.5 Current AD medicines

The AD diagnosis requires physicians to perform a comprehensive medical assessment that includes patient's medical history, mental status exam, physical exam, neurological exam, blood tests and brain imaging. Depending on the severity of the cognitive symptoms, Dr. Barry Reisberg classified the disease state into seven stages: stage 1: no impairment; stage 2: very mild decline; stage 3: mild decline; stage 4: moderate decline; stage 5: moderately severe decline; stage 6: severe decline; and stage 7: very severe decline (56). Currently, the medications prescribed for AD patients at varied stages are largely categorized into two classes: acetylcholinesterase inhibitors (AChEI) and N-methyl-D-aspartate (NMDA) receptor antagonists.

AChEIs are chemical drugs that suppress the acetylcholinesterase activity, thereby preventing the degradation of acetylcholine and maintaining the postsynaptic cholinergic activity. The medicines in this category are Tacrine (Cognex), Donepezil (Aricept), Rivastigmine (Exelon), and Galantamine (Razadyne). Tacrine was discontinued due to its potential risk of causing liver enzyme elevation (57). These AChEI drugs have shown a significant cognitive decline delaying effect in AD patients from multiple clinical studies (58,59). However, it is generally accepted that AChEI drugs do not provide reliable disease modifying effects in AD treatment (60).

The N-methyl-D-aspartate (NMDA) receptor antagonists, another type of AD

drug, repress the effect of glutamate, a key excitatory neurotransmitter responsible for various cognitive functions (61). It has been known that the overstimulation of glutamate receptors leads to the elevation of post synaptic calcium level causing excitotoxicity to neurons and eventually neurodegenerative conditions (62). Clinical studies showed the treatment of memantine, a type of NMDA receptor antagonist, resulted in beneficial outcome in cognitive and behavioral symptoms of moderate-to-severe AD patients (63,64). As opposed to these results, other clinical studies suggest that the efficacy of memantine for attenuating AD symptoms has a lack of evidence with no significant difference in clinical outcome between the placebo and the drug treatment group (65,66). These study results indicate that the propagation of the neurodegeneration process is not intervened merely by modulating the neurotransmitters, demanding further clarification for underlying mechanisms of neurodegeneration.

2.6 AD medicines under laboratory and clinical investigations

According to a recent report, the failure rate of AD drug development between 2002 and 2012 was 99.6% (67). This unacceptably high failure rate also discourages the pharmaceutical industry from investment in this high risk project, as is evidenced by relatively fewer drug candidates and clinical trials for AD treatment compared to the oncology drugs. Despite this gloomy record, researchers have been continuously investigating various AD drugs that focus on Aβ plaques, tau pathology, neuropsychiatric symptoms, neuroprotection, etc. Selected ongoing clinical trials for AD are listed in Table 2.1.

2.6.1 Immunotherapy

Propelled by numerous studies that propose Aβ plaques as an initial disease triggering factor in AD pathogenesis, a number of clinical trials have tested anti-amyloid strategies in the form of immunotherapy. The immunotherapies for AD are largely classified into two different modes: active vaccination and passive vaccination. The active vaccination approach is to inject Aβ peptide-derived fragments into patients, thereby stimulating the production of anti-Aβ antibody. Alternatively, the passive vaccination approach is to administer the ready-made antibodies against Aβ to the AD patients. Both approaches were conceived to clear the Aβ plaques from the brain tissues via antibody-mediated phagocytic clearance mechanism (68). In the active vaccination approach, there are three peptide vaccines under clinical investigations: ACC-001 (Pfizer), CAD-106 (Novartis), and Affitope (AFFiRiS AG). These peptides are composed of a carrier protein fused with the Aβ(1-6) fragment that acts as a B-cell epitope. Following the phase I studies where the safety and tolerability of these drugs were confirmed, phase II studies with early or mild-to-moderate AD patient groups are now under evaluation. Regarding the passive vaccination approach, humanized antibodies prepared from different parts of Aβ peptide have been investigated. These include Bapineuzemab (Pfizer), Solanezumab (Eli Lilly and Company), Gantenerumab (Hoffmann-La Roche), and Crenezumab (Genentech). Although there have been promising reports about anti-Aβ antibodies in reducing the Aβ level in brain tissues (69,70), no remarkable success from clinical studies has been announced yet. In fact, Bapineuzumab failed to show significant disease-modifying effects on cognitive abilities in AD patients and the study was terminated (71). Solanezumab, another humanized

antibody was also unsuccessful in proving its therapeutic effectiveness in cognitive functions of mild-to-moderate AD patients (72). These recent failures imply that the attempts to clear the Aβ deposits may not be opportune enough to stop the disease progression. In this context, pharmaceutical companies are now redirecting their focus on preventive medicines or early initiation of treatments. As an example, Crenezumab, another Aβ-targeting antibody, is being investigated in individuals bearing PS1 mutation. This population does not display noticeable cognitive symptoms at the time of treatment. The study will examine whether early treatment using Crenezumab can prevent AD onset for people at high risk (73).

2.6.2 BACE inhibitors

Another approach to fight against Aβ plaques is to use the drugs that prevent the production of the Aβ peptide from APP protein upstream. The β-secretase 1 encoded in the BACE1 gene was identified as an enzyme that cleaves the extracellular domain of the APP, releasing the neurotoxic Aβ fragments (74). Therefore, it is conceivable that inhibiting BACE1 activity will prevent Aβ accumulation. Indeed, Roberds et al. reported that the primary cortical culture from BACE1 knockout transgenic mice displayed a significantly lower level of Aβ peptide as well as β-secretase 1 activity below the limit of detection (75). The therapeutic effect of a BACE1 inhibitor is also under clinical investigation. A recent report from Merck showed a promising effect of MK-8931, a BACE inhibitor, in reducing Aβ level in cerebrospinal fluid of AD patients (76). The more upstream anti-Aβ approach provides anticipation for better therapeutic outcomes, especially for patients in the early stages of disease course.

2.6.3 Tau kinase inhibitors

Along with amyloid plaques, the hyperphosphorylated tau protein has also been considered a prime disease trigger for AD (77). To tackle the tauopathy, studies have tested the inhibition of protein kinases responsible for tau phosphorylation. Noble et al. showed that lithium chloride successfully suppressed the activity of glycogen synthase kinase-3 (GSK-3), a tau protein kinase, and significantly reduced the insoluble tau aggregation (78). Moreover, another study reported that lithium chloride treatment reduces Aβ accumulation in APP transgenic mice, suggesting that the inhibition of tau phosphorylation could be a promising strategy for effective treatment of AD (79). The clinical investigation on Tideglusib/NP-12 (Noscira), a GSK-3 inhibitor, is ongoing with mild-to-moderate AD patients after a phase I study confirmed no relevant adverse issues involved with the treatment.

2.6.4 Repositioning of the existing drugs

Rather than starting over, researchers have suggested the idea of repositioning the existing drugs (80). The medicines for other indications may have beneficial effects in slowing AD progression. In this case, remarkable time and cost can be saved compared to the new drug development process and the validated pharmacotoxicological profiles of the existing drugs relieve safety concerns. One example is the use of selective serotonin reuptake inhibitors (SSRI) that were originally prescribed for treatment of major depressive disorder. According to one report, the activation of serotonin receptors facilitates α-secretase-mediated APP processing which produces nonamyloidogenic soluble Aβ fragments (81). Therefore, SSRIs may help divert the neurotoxic Aβ form generating pathway in AD progression. Recently, citalopram, a type of SSRI was found

to be effective in reducing Aβ production in AD transgenic mice and healthy individuals, supporting the potential capacity of SSRIs for AD prevention (82).

2.6.5 Further effort for AD drug development

There have been a number of hopeful reports about the potential efficacy of AD treatments. However, we still do not have a single effective cure that can prevent or even considerably delay progression of the disease. It is imperative to expend persistent efforts to develop an effective drug for AD treatment. In the meantime, more strategic plans should be contemplated to improve the therapeutic outcome in clinical studies. Recent failures of amyloid plaque targeting antibodies in clinical studies teach us that the therapeutics solely focused on the amyloid hypothesis may not be a sufficient solution to holding AD propagation. Extensive laboratory research shows that Aβ deposits can be both a disease-causative agent and a consequence of AD progression. To tackle the AD pathogenesis beyond Aβ, there should be more research using other approaches that eliminate hyperphosphorylated tau proteins or ameliorate the neuroinflammatory conditions in brain tissues, for example (83).

The other lesson from recent failures is that treatment at later stages of the disease process come too late to attain desirable therapeutic benefits. The AD brain undergoes distinct biochemical changes along with the course of disease progression, such that the treatment strategies should be tailored to the altered gene or protein expression profile (84). The development of early diagnosis technology is also required, as it allows physicians to begin earlier treatment on patients at the presymptomic stage, which is more likely to produce better therapeutic outcomes. Recently, Mapstone et al. reported a promising blood-based test that can predict MCI or AD development of cognitively

normal individuals within a 2-3 year timeframe with high and reliable accuracy (85). They identified 10 lipid metabolites that are depleted in plasma from individuals who are predestined to develop cognitive decline within 2-3 years. A blood-based biomarker test is advantageous over the cerebrospinal fluid analysis, which involves an invasive lumbar puncture procedure. Such diagnostic tools that detect the alteration of AD-relevant biomarkers, possibly at early stages, will greatly improve clinical results.

2.7 RNAi therapy as a promising NDD treatment option and potential targets

2.7.1 Brief overview of RNAi

RNA interference (RNAi), one of the most notable discoveries in biology, has received attention in the biomedical research field due to the utility of specific modulation of disease-associated genes under pathological conditions (86). The mechanism of RNAi is as shown in Figure 2.5. Briefly, the pri-miRNAs transcribed from the genome are processed by an enzyme complex to generate pre-miRNAs, which are ~60 to 70 nucleotide-long hairpin RNAs. These pre-miRNAs are subsequently transported to the cytosol where they are cleaved by Dicer, an RNase type III enzyme, into small double-stranded RNA fragments, known as mature miRNA duplexes. These are then bound to the RNA-induced silencing complex (RISC), which cuts out the passenger strand of miRNA and brings the guide strand to its complementary mRNA species. The specific binding of miRNA to the target mRNA leads to the degradation of the mRNA, thereby silencing the expression of the corresponding gene (87). The specific gene silencing mechanism of RNAi can be advantageous in manipulating particular cellular processes, especially those linked to many human diseases. In contrast to small

molecule drugs, proteins, and antibody drugs, the identification and synthesis process of lead RNAi sequences can also be rapidly completed (88). Davis et al. reported successful results from a clinical investigation where they observed the systemic administration of siRNA-loaded nanoparticles led to significant target gene knockdown in solid-tumor bearing patients (89). This promising announcement stimulated the RNAi therapy development for various pathological conditions. Regarding the NDD treatment, the RNAi approach may also be a promising mode of therapy tackling the genes associated with NDD pathology. The potential RNAi targets for NDDs are listed in Table 2.2.

2.7.2 RNAi targets for Alzheimer's disease (AD)

According to the amyloid cascade hypothesis, the key pathological incident in AD onset is the formation of insoluble Aβ aggregates. As overviewed previously, the neurotoxic form of Aβ fragments is generated when amyloid precursor proteins (APP) are proteolytically cleaved by β-secretase 1 (BACE1) and γ-secretase. To curtail the Aβ level in the brain tissues, an RNAi approach may be applied to APPs. Although the exact physiological roles of APP are not fully understood, the increased expression of APP is known to elevate the risk of AD development indicating that mild knockdown of APP may provide clinical benefit in AD prevention (90,91). Another conceivable target is the BACE1 gene, which encodes β-secretase, a major contributor for Aβ production. A postmortem analysis of brain tissues with AD showed significantly elevated BACE-1 activity, which was also correlated to Aβ production in AD brain (92). Therefore, this suggests that the suppression of the BACE1 expression may prevent the overproduction and accumulation of toxic Aβ fragments reducing the likelihood of Aβ plaque buildup.

The hyperphosphorylated tau protein, another pathological feature of AD, should

also be considered for the application of RNAi therapy. As the hyperphosphorylated form of tau is known as a predominant component of intracellular NFTs, clinical efforts have been made on the development of small molecule inhibitors of tau protein kinases such as mitogen-activated protein kinase 1 (MAPK1), cyclin-dependent kinase 5 (CDK5), and glycogen synthase kinase 3 (GSK3) (93). The RNAi technology targeting these genes would also repress the extent of tau phosphorylation, slowing the formation of intracellular tangles. Indeed, the viral vector-aided RNAi against CDK5 gene resulted in reduction of tau phosphorylation in brain tissues of AD transgenic mice (94).

In addition to these targets, the oxidative stress associated pathways can also be a target for RNAi therapy, as virtually all neurodegenerative disorders display extensive oxidative stress in affected brain regions (95). One example is the Nrf2 (NF-E2-related factor 2)-ARE(antioxidant responsive element) pathway. The Nrf2, which normally exists in the cytosol, translocates to nucleus in response to oxidative stress and binds to the ARE activating the expression of various detoxifying and antioxidant genes (96-99). However, the Nrf2 activity is suppressed by Kelch-like ECH associating protein 1 (Keap1), which sequesters Nrf2 in the cytoplasm and eventually directs it to proteasomal degradation (100,101). To enhance the endogenous antioxidant capacity against oxidative stress, the Keap1 gene can be a subject for the RNAi approach. Keap1 silencing was also shown to provide neuroprotection against MPTP (1-methyl-4-phenyl-1,2,3,6-tetrahydropyridine)-induced dopaminergic damage, which suggests that the Keap1 gene is a plausible RNAi target for NDD treatment (102).

2.7.3 RNAi targets for other types of NDDs

Parkinson's disease (PD) is the second most common NDD characterized by progressive death of dopamine-producing neurons in the substantia nigra, which results in movement-related symptoms (103). The key neuropathological feature of PD is that neurons contain Lewy bodies that are formed from the enhanced aggregation of α-synuclein proteins (104). While the physiological role of α-synuclein remains elusive, the first RNAi trial against the α-synuclein gene showed promising neuroprotective effects against neurotoxin N-methyl-4-phenylpyridinium (MPP+) *in vitro* without affecting the cell viability. This suggests that the RNAi approach targeting the α-synuclein gene can be a possible mode of PD treatment (105).

Huntington's disease (HD) is a hereditary neurodegenerative disorder, symptoms of which include cognitive decline, disorientation, and other behavioral abnormalities (106). It is caused by dominant mutations in the Huntington gene (HD) that contains trinucleotide CAG repeats in varying lengths. The abnormally expanded CAG repeats produce polyglutamine (poly Q)-containing proteins, which form cytoplasmic poly Q aggregates leading to neurodegeneration (107). As the Huntington gene is known to have essential functions for brain development (108), RNAi therapy needs to be designed for allele-specific silencing of the mutant poly Q protein in order to maintain the normal copy of the HD gene.

Amyotrophic lateral sclerosis (ALS) is another type of NDD, the representative symptom of which is muscle atrophy caused by progressive loss of motor neurons (109). One of the major disease triggering factors for ALS is the mutations in the superoxide dismutase 1 (SOD1) gene, whose loss of function produces toxic effects on various

organs as well as the nervous system (110). Therefore, RNAi therapy targeting the mutant SOD1 genes may be advantageous to relieve deleterious effects from mutant gene products. However, the RNAi construct should be carefully customized to specifically target individual mutation types considering that more than 100 point mutations have been identified so far in the SOD1 gene.

Regarding the actual application of RNAi therapy for any target, a thorough consideration of the extent of gene silencing should be included because the essential biological functions, if any, of the target gene product can be substantially compromised by RNAi. Therefore, refinement of the dose and the duration of the RNAi treatment are very important steps to accomplish the optimal therapeutic benefit without serious side effects. One can also think of a combinatorial approach targeting multiple genes to maximize the therapeutic effect. Strategically schemed combinatorial RNAi therapy may exert an additive or synergistic effect in attenuating neuropathological and clinical symptoms of NDDs.

2.8 RNAi delivery strategies

2.8.1 Limitations of RNAi for clinical application

RNAi technology can be a powerful therapeutic intervention for various human diseases because of its highly specific target gene silencing mechanism. The synthetic small interfering RNA (siRNA), which contains a target mRNA complementary sequence of 21-25 nucleotides in length, has been commonly applied for downregulation of pathology-associated genes. However, siRNAs lack druggable properties described by Lipinski's rule of five (111). The negatively charged phosphate backbone of siRNAs makes them highly hydrophilic in the physiological environment such that it becomes a

daunting task for siRNAs to interact with cell membranes. The relatively high molecular weight (~14 kD) and the bulky size also make them unfavorable for cellular uptake. Importantly, siRNAs are vulnerable to serum nucleases and reticuloendothelial system (RES)-mediated clearance, which poses another challenge in its application for living systems (88). RNAi therapy, particularly for neurological diseases, is even more difficult largely because of the highly restrictive properties of the BBB. As reviewed previously, the brain microvascular endothelial cells do not allow hydrophilic and large molecules to pass across them. Understandably, it is apparent that there should be additional tactics that assist siRNA delivery to brain tissues. Generally, strategies for brain-targeted siRNA delivery should be capable of the following key aspects: to protect siRNA in biological fluid, to bypass or get across the BBB, to deliver bioactive siRNA to the brain cells, and to produce reliable target gene silencing effect. Additionally, the siRNA delivery strategies should not involve any serious adverse effects caused by non-specific uptake of other organs, immunogenicity of the delivery vehicles, and perturbation of normal cellular processes resulting from the RISC machinery saturation. The examples of RNAi delivery methods that have been attempted in rodent models are listed in Tables 2.3 and 2.4.

2.8.2 RNAi delivery methods

2.8.2.1 Viral delivery

The RNAi can be achieved by short hairpin RNAs (shRNA), or artificial microRNAs (amiRNA) that are typically delivered in a viral vector form. The target sequence-containing constructs are embedded in the viral vector of choice such as adeno-associated viruses (AAVs) or lentiviruses. In particular, AAV are suitable for lasting

RNAi effects in nondividing cells such as neurons because AAV vectors exist episomally. The AAV vectors are not integrated to the host genome where the insertional mutagenesis is unlikely to occur. Alternatively, lentivirus-delivered transgene can be integrated into the host genome and it can be advantageous for sustained RNAi effect in dividing cells. However, the genomic integration may also cause the activation of oncogenes or inactivation of tumor suppressor genes (112). Many preclinical animal studies have tested viral delivery of RNAi into nervous systems. Xia et al. conducted intracerebellar administration of recombinant AAV vectors containing shRNA against spinocerebellar ataxia type 1 (SCA1) into SCA1 transgenic mice. They found that the AAV-mediated RNAi was successfully achieved *in vivo*, resulting in the improvement of motor performance of the SCA1 mice (113). Singer et al. used a lentiviral system to deliver BACE1 targeting siRNA via intracranial injection into the hippocampus of the APP transgenic mice. They showed that lentiviral vector mediated-BACE1 RNAi significantly reduced the BACE1 expression and the Aβ production ameliorating behavioral abnormalities of the AD mice (114). Recently, Foust et al. reported that AAV9-mediated RNAi against the SOD1 gene substantially reduced the mutant SOD1 expression in the ALS mouse model throughout their lifespan and attenuated the progression of neurodegeneration, extending the survival period as well (115). Even with multiple promising results from preclinical animal studies, there should be extreme caution when extrapolating preclinical results for clinical applications to humans because of the differences in brain anatomy and physiology between rodent animal models and humans. In addition, it is difficult to estimate the exact dose and effective duration of the virally delivered RNAi; this adds a potential risk of interrupting the endogenous RNAi

process and producing toxicity issues (88,116). Generally, viral delivery in animal studies has been achieved by local administration such as intracerebral injection or intracerebroventricular injection. However, it may not be readily feasible to apply those invasive procedures to human patients. Moreover, it is possible that patients need to receive multiple injections of the therapeutic RNAi containing viral vectors for desired therapeutic outcome. Apparently, each injection might involve a risk of hemorrhage, edema, bacterial infection, or immune responses (117).

2.8.2.2 Nonviral delivery

In contrast to viral delivery, nonviral RNAi delivery is more favorable for controlled dosing of therapeutic siRNA. However, the duration of the RNAi effect is transient; it may not be a plausible choice for treatment of chronic pathology, which demands long-lasting RNAi effect. As overviewed previously, naked siRNAs are highly susceptible to serum nuclease-mediated degradation and they cannot penetrate into the cell membrane without the assistance provided by delivery vehicles. To address these issues, researchers have conceived a range of siRNA delivery strategies for *in vivo* application (Figure 2.6). Particularly for brain-targeted siRNA delivery, chemically modified siRNAs, liposomes and exosomes, a cell-penetrating peptide-based system, antibody-fused system, and other types of cationic nanoparticles have been investigated.

Chemically modified siRNAs such as cholesterol conjugated siRNAs, siRNAs containing partial phosphorothoiate linkages, 2'-O-methyl sugar modified siRNAs have shown a better pharmacological profile with improved stability against serum nucleases (118). Nakajima et al. administered chemically modified Accell siRNA (Dharmacon) into rats via intracerebroventricular (icv) injection using a microinfusion pump (119). In

this study, they showed that a single icv injection (5 µg of Accell siRNA/rat) was sufficient to achieve significant target gene downregulation 4 days after the injection without any signs of neuroinflammation. The target gene knockdown was observed in diverse brain regions including the cortex, striatum, hippocampus, midbrain and cerebellum. Another study showed that the intravenous administration of cholesterol conjugated siRNAs incorporated into high-density lipoprotein (HDL) resulted in successful target gene downregulation in brain capillary endothelial cells (BCEC) *in vivo* (120). In this work, they did not intend to deliver siRNA to the brain compartment, but to the brain endothelial cells; for this purpose, cholesterol is an optimal molecule, as it does not get into the brain (121) while lipoprotein mixture can be endocytosed via lipoprotein receptors on BCECs. These studies indicate that chemically modified siRNA can be a promising mode of RNAi, particularly due to its enhanced stability compared to the naked siRNA. However, chemically modified siRNAs may not exert satisfactory silencing effects depending on the modified position (122). Moreover, it should be directly injected to the brain via local administration unless they are equipped with brain-targeting moieties.

Liposomal formulation of siRNA is another strategy for efficient siRNA delivery into the cells *in vivo.* Tao et al. encapsulated siRNAs into the core of polyethylene glycol (PEG)-coated liposomes that are decorated with the rabies virus glycoprotein (RVG) peptide as a brain-targeting moiety (123). The RVG peptide is known to bind to the acetylcholine receptors (AchR), which are extensively expressed on brain cells as well as brain endothelial cells. The intravenous injection of RVG-liposomes into mice demonstrated its ability to reach the brain compartment with preferential accumulation in

mouse brain up to 24 hr after injection while displaying relatively lower distribution in other peripheral organs. Although they did not mention the actual *in vivo* siRNA delivery, target gene silencing effect in mice, or any RVG-liposome associated toxicity, this study proposes that the targeted liposomal formulation has a promising potential for brain-targeted siRNA delivery. Another study showed that liposome-siRNA-nine arginine fused RVG peptide (RVG-9R) complex (LSPCs) can deliver siRNA to the brain cells in significant amounts, leading to the substantial knockdown of the target protein expression 48 hr after the tail vein injection into the mice (124). The ability of RVG-9R to deliver siRNA to the mouse brain *in vivo* has already been demonstrated by Kumar et al. (125). This group suggests that additional liposomal formulation to the RVG-9R enhances the siRNA protection against the serum proteins thereby improving the siRNA delivery to the brain compartment.

Instead of using exogenous lipid components, the host-derived nanosized vesicles, namely exosomes, can be used to transport siRNA to the brain cells. A research group used self-derived dendritic cells that were engineered to produce RVG peptide-fused exosomal proteins (126). The exosomes obtained from these dendritic cells were electroporated with siRNAs and intravenously administered to the same mice. In contrast to the naked siRNA, exosome-loaded siRNA were preferentially accumulated in brain tissues resulting in significant target gene knockdown 3 days after a single injection of 150 μg of siRNA. Exosome-mediated RNAi can be an advantageous approach particularly because the self-derived exosomes are unlikely to cause immunological toxicity issues. However, the exosome production procedure, which includes the isolation of dendritic cells, transfection of the targeting peptide expressing plasmids and

purification of the engineered exosomes may be time and labor intensive. Also, the final yield of exosomes needs to be ensured to achieve effective treatment.

Cell-penetrating peptide (CPP)-based systems are also useful vehicles for siRNA delivery. Most CPPs contain positively charged residues such as arginines and lysines at such physiological pH that it facilitates the electrostatic interaction with the negatively charged plasma membrane possibly leading to the internalization of CPPs or CPP-conjugated drugs into the cells (127). Due to the powerful properties of CPPs, it has been vastly utilized to transport drugs such as plasmid DNA (pDNAs), siRNAs, peptides and proteins, small molecule drugs along with diverse nanoparticle drug delivery vehicles. Particularly, the positively charged cationic domain not only confers the ability to readily enter the cells across the cellular membranes, but also serves for siRNA condensation via electrostatic interaction. Kumar et al. combined nine arginine repeats with RVG peptide (RVG-9R) for brain-targeted siRNA delivery *in vivo* (125). They conducted multiple intravenous injections of the GFP targeting siRNAs complexed with RVG-9R peptides into the GFP expressing transgenic mice for 3 consecutive days, which resulted in 30-40% of GFP silencing effect in brain tissues 2 days after the last injection. This result indicates that RVG-9R crosses the BBB and successfully delivers bioactive siRNA into brain tissues. However, it is still unclear how the siRNAs are released from the RVG-9R system once they are internalized into the cells. The incorporation of intracellular pH-responsive amino acid sequences into this CPP system may improve the siRNA detachment from the delivery system. In addition, exogenous peptide sequences should be carefully examined to rule out the possibility of host immune system stimulation.

To achieve effective brain targeting, siRNA carriers can be linked to antibodies

that bind to the receptors on the brain endothelium. Xia et al. used biotinylated siRNAs that are bound to monoclonal transferrin receptor (TfR) antibody-conjugated streptavidin (128). They showed that a single intravenous administration of luciferase targeting 5'-biotinylated siRNA into tumor bearing rats effectively downregulated the luciferase activity (69%) in a luciferase expressing intracranial brain tumor 48 hr after the injection. It is a promising result supporting the use of targeting antibodies for brain-targeted siRNA delivery vehicles. However, the TfRs are ubiquitously expressed on other peripheral organs aside from the brain endothelium (129). Although TfR has been one of the most popularly exploited brain-targeting receptors, it may also bind to other organs and produce nonspecific adverse effects. They used the siRNA containing 2-nucleotide 2'-deoxythymidine overhangs to avoid exonuclease attack in serum (130), but the structure of this system still exposes siRNA to the outer environment that the siRNA stability may be more affected compared to other encapsulating systems.

Cationic polymer-based nanoparticles are another approach for effective siRNA delivery to the cells. Recently, Kozielski et al. reported that linear poly (β-amino esters)s (PBAEs) containing disulfide bonds can be a promising siRNA delivery vehicle ensuring effective siRNA delivery as well as functional cytoplasmic release of siRNA (131). These bioreducible siRNA loaded nanoparticles produced a remarkable knockdown of the target gene expression (97%) in a human primary glioblastoma cell line (GBM 319) without displaying adverse effects, which demonstrates the utility of PBAEs as an effective and safe siRNA carrier. Despite their exciting results, the lack of *in vivo* data give uncertainty about the actual brain-targeted RNAi effect in a living system. To prove the clinical utility, the efficacy and safety of this system should be thoroughly examined

in an animal model. Moreover, this approach does not have brain-targeting ability. To achieve therapeutic RNAi effect in brain tissues, the carrier may need to incorporate a proper brain-targeting moiety or the local administration should be employed for *in vivo* application.

2.8.3 Alternative RNAi delivery strategies

Various RNAi delivery vehicles have notably improved the bioavailability and target gene silencing efficacy of RNAi drugs in multiple *in vivo* preclinical studies. However, the inherent limitations in RNAi should be addressed further, particularly for brain-targeted RNAi delivery. Except for a few types of siRNA delivery vehicles that have brain-targeting moieties, other RNAi delivery systems with no neurotargeting modules are not suited for systemic administration, mainly because of the poor brain accumulation of the RNAi drugs. These delivery systems may be redesigned to additionally accommodate a brain homing group of choice. Studies have identified the peptide or ligands that bind to receptors expressed on the brain endothelium and neuronal cells. These receptors include transferrin receptors (132), insulin receptors (133), low density lipoprotein receptors (134), acetylcholine receptors (135), leptin receptors (136), etc. However, these receptors are not exclusively found in brain tissues. To improve the brain-targeted RNAi delivery and reduce nonspecific adverse effects, further studies are required to discover brain-specific receptors and ligands that bind to those receptors with high affinity.

For those not having the brain-targeting ability, a direct injection into the brain compartment would be desired to bypass the BBB and deliver RNAi to the brain. Local administrations such as intracerebral injections or intracerebroventricular injections

ensure immediate RNAi delivery and robust therapeutic outcome with reduced dose requirement compared to systemic administration. A recent study reported that siRNA-encapsulated cationic lipid nanoparticles (LNP-siRNA) were able to induce significant target gene downregulation in both cases of intracerebral injection and intracerebroventricular injection (137). In this study, more direct and efficient gene silencing effects were observed from the intracortical injection into the specific brain region while the intracerebroventricular injection resulted in a more widespread and diffuse effect. However, these types of direct injections may not be feasible for practical clinical application. Patients may need to receive multiple injections to reach sufficient RNAi effect and these injections may involve highly invasive and risky procedures. In case the pathological condition requires long lasting suppression of the target gene, implantable pumps that continuously infuse RNAi drugs into the brain parenchyma or cerebrospinal fluid would be a conceivable option. Preclinical studies have shown a robust gene silencing effect in rodent brain tissues with implantable osmotic pumps for sustained release of therapeutic siRNAs to the brain (138,139), suggesting the possible use of implantable pumps for clinical application. Alternatively, researchers have investigated intranasal administration for brain-targeted siRNA delivery (140,141). Intranasal administration is an advantageous approach, particularly for CNS therapeutics as the drugs can be delivered to brain tissues while circumventing the BBB and the therapeutics are local acting, which eliminates concerns about potential adverse effects from systemic administration (142). However, siRNA-loaded nanoparticles still need to survive in the mucous layer that covers the olfactory epithelium for effective siRNA delivery (143).

In all cases of diverse RNAi delivery methods and alternative routes of administration, RNAi drugs should establish a reliable efficacy and safety profile to move forward to clinical application. The important criteria for viable RNAi drugs include: 1) effective target gene knockdown, 2) predictable biodistribution of RNAi drugs, 3) safe clearance of delivery vehicles after RNAi performance, and 4) no apparent toxicity issues. Regarding the therapeutic effect, the level of pathology-associated biomarkers, such as CSF concentration of Aβ(1-42) and phosphorylated tau proteins for AD (144), should be closely monitored during therapy to adjust the dosage and treatment duration and to ultimately achieve desirable therapeutic outcomes.

2.9 Concluding remarks

Current AD treatments lack disease-modifying effects. Researchers have investigated drugs that directly combat the culprits accounting for AD pathogenesis. Despite numerous failures, many are under investigation in preclinical studies and clinical trials with a hope to prevent the onset or the progression of AD. The RNAi approach is also a promising therapeutic option for NDDs as it modulates the genes associated with NDD pathological processes. Researchers have attempted a wide variety of siRNA delivery modes to achieve the brain-targeted siRNA delivery and desired target gene knockdown effect while surmounting the BBB. Many have shown impressive data in preclinical studies, but it appears that we need more thorough validation prior to clinical application for patients with NDDs. Along with our current ability to harness diverse delivery strategies, efforts for further refinement of the siRNA carrier design should be continued to accomplish robust RNAi effects in the physiological environment. Furthermore, the development of early diagnosis tools as well as timely initiation of the

therapy would contribute immensely to the improvement of therapeutic outcomes. Because the neurodegeneration process is irreversible and it takes years before noticeable symptoms emerge, researchers generally agree that early treatments or preventive medicines would be beneficial to stop or delay disease progression. Together with the development of novel and potent NDD drugs, precise and reliable diagnosis techniques and adequate preventive therapies would significantly lower incidence of NDDs and ameliorate the quality of life for patients with NDDs.

Table 2.1. Selected investigational AD drugs under current clinical trials.

ClinicalTrials.gov Identifier	Sponsoring group	Subjects	Drug intervention	Study phase	Outcome variables
NCT 01998841	Genentech	Asymptomatic subjects with PS1 E280A mutation, age of 30 to 60 years	Crenezumab (a humanized monoclonal antibody against Aβ)	Phase 2	Scores of multiple cognitive tests, mean cerebral fibrillar Aβ accumulation, cerebral metabolic rate of glucose, structural MRI, tau-based CSF biomarker
NCT 01760005	Dominantly Inherited Alzheimer Network (DIAN)	Asymptomatic subjects at-risk for familial AD (mutations in APP, PS1, and PS2), within -15 to +10 years of predicted AD onset	Gantenerumab and Solanezumab (a humanized monoclonal antibodies against Aβ)	Phase 2 Phase 3	Amount of fibrillar amyloid deposition, concentration of CSF Aβ species, rate of brain atrophy, clinical dementia rating, minimental status exam
NCT 02008357	Eli Lilly and Company	Elderly subjects with evident brain amyloid pathology	Solanezumab (a humanized monoclonal antibody against Aβ)	Phase 3	Free and cued selective reminding test, the logical memory IIa, digit symbol and minimental state exam, changes in CSF tau, Aβ concentration, structural MRI
NCT 01739348	Merck Sharp & Dohme Corp.	Subjects with mild to moderate AD, age of 55 to 85 years	MK-8931 (a BACE1 inhibitor)	Phase 2 Phase 3	Changes in ADAS-Cog score (cognitive function assessment) and ADCS-ADL score (functional performance assessment), changes in brain Aβ load, CSF total tau, total hippocampal volume
NCT 01807026	Eli Lilly and Company	Healthy subjects not taking any concomitant medications, age of 18 years or older	LY2886721 (a BACE1 inhibitor)	Phase 1	Pharmacokinetic parameters (AUC and C_{max} of plasma LY2886721, AUC and C_{max} of CSF LY2886721), Aβ level in plasma and CSF
NCT 01350362	Noscira SA	Subjects with mild to moderate AD, age of 50 to 85 years	Tideglusib (a small molecule non-ATP-competitive GSK3 inhibitor)	Phase 2	Changes in ADAS-Cog score and ADCS-ADL score, tau and phosphorylated tau level in CSF, Aβ level in CSF, structural MRI
NCT 02161458	University of Pennsylvania	Cognitively normal older adults, age of 65 to 85 years	Escitalopram (s-enantiomer of citalopram, an antidepressant of the SSRI class)	Phase 4	Change in the level of Aβ peptides (Aβ 42 and Aβ 40) in the CSF
NCT 00876863	Ceregene	Subjects with mild to moderate AD, age of 55 to 80 years	CERE-110 (adeno-associated virus delivery of NGF)	Phase 2	Changes in ADAS-Cog and ADCS-ADL, minimental state exam

ADAS-Cog, Alzheimer's Disease Assessment Scale- Cognitive Subscale; ADCS-ADL, Alzheimer's Disease Co-operative Study — Activities of Daily Living Inventory; ADCS–PACC, Alzheimer's Disease Cooperative Study–Preclinical Alzheimer's Cognitive Composite; APP, amyloid precursor protein; ATP, adenosine triphosphate; AUC, area under the curve; BACE1, β-secretase I; C_{max}: maximum concentration; CSF, cerebrospinal fluid; GSK3, glycogen synthase kinase 3; MRI, magnetic resonance imaging; NGF, nerve growth factor; PET, positron emission tomography; PS, presenilin; SSRI, selective serotonin reuptake inhibitor. Partly adapted from Becker et al. (145).

Table 2.2. Potential RNAi targets for NDDs.

NDD Type	RNAi target	Pathological function	Ref.
Alzheimer's disease	Swedish variant of APP (amyloid precursor protein)	Abnormal production and accumulation of the toxic Aβ peptides	(91)
	BACE1 (β-secretase)	Increased β-secretase activity leads to the accumulation of toxic Aβ peptides	(114)
	Missense mutations in presenilin 1 (PS1) and presenilin 2 (PS2)	Affects the APP processing and leads to the elevated levels of toxic Aβ peptides	(146)
Parkinson's disease	Single point mutations in the α-synuclein gene, gene duplication and triplication	Forms intracellular aggregates (Lewy bodies) and results in neurodegenerative synucleinopathies	(147)
Huntington's disease	Mutant huntingtin protein (mHTT)	Aberrant extension of polyglutamine repeats	(148)
Amyotrophic lateral sclerosis	Mutations in superoxide dismutase 1 (SOD1)	Progressive motor neuron death	(115)
Spinocerebellar ataxia	Mutant ataxin-1	Toxic gain of function on ataxin-1 due to the polyglutamine expansion	(113)

Table 2.3. Examples of *in vivo* brain-targeted RNAi via viral delivery in rodent models.

Types of RNAi carrier	Target genes	Routes of administration	Dosage regimen	Knockdown effect	Ref.
shRNA expressing recombinant AAV system	Mutated human ataxin-1	Intracerebellar injection	1 μL injected into three separate sites (1×10^{12} genome copies/mL) at 7 weeks of age	From weeks 11 to 21, significant improvement in motor performance of SCA1 mice	(113)
shRNA expressing recombinant AAV system	Mutant huntingtin (mHtt)	Intrastriatal injection	2 μL injection (1 to 5×10^{13} genome copies/mL)	24.5% to 38% decreased expression of mHtt protein in the mHtt transgene and delayed onset of the rear paw clasping phenotype in the R6/1 transgenic HD mice	(150)
shRNA expressing recombinant AAV system	Tyrosine hydroxylase (TH)	Intracranial injection to the substantia nigra	0.4 μl of purified virus suspended in PBS was injected	30% reduction in tyrosine hydroxylase expression 2 weeks after the injection and a motor performance deficit and reduced response to a psychostimulant in C57BL/6J mice	(151)
shRNA expressing lentiviral system	BACE1	Intracranial injection into hippocampus	2 μL of the lentiviral preparations (1.5×10^{7} transduction units) into the hippocampus	> 2-fold decrease in BACE1 protein in hippocampus, reduced Aβ production and relieved behavioral deficits of APP transgenic mice	(114)
shRNA expressing lentiviral system	Enhanced green fluorescent protein (EGFP)	Intracranial injection	2 μL injection (10^{8} pg of p24 /mL) with polybrene (4 mg/mL)	98% reduction in EGFP expression in adult C57BL/6 mice that were co-injected with EGFP expressing lentiviral system	(149)

Table 2.4. Examples of *in vivo* brain-targeted RNAi via nonviral delivery in rodent models.

Types of RNAi carrier	Target genes	Routes of administration	Dosage regimen	Knockdown effect	Ref.
Chemically modified Accell siRNA	Cyclophilin-B and GAPDH	Intracerebro-ventricular injection	Single injection 5 μg of Accell siRNA/rat	Knockdown of cyclophilin-B (38-61%) and GAPDH (23-34%) in cortex, caudate subregion of striatum, and CA1 subregion of hippocampus of adult rat brain at 4 days postinjection	(119)
Cholesterol conjugated siRNAs with high-density lipoprotein	Organic anion transporter 3 (OAT3)	Intravenous injection	Three injections of 1.0, 3.3, or 10 mg/kg with 12 hr intervals	50% reduction of OAT3 mRNA in brain capillary endothelial cells 6 hr after the last injection in female wild-type C57BL/6J mice	(120)
PEG-coated liposomes decorated with rabies virus glycoprotein (RVG)	None	Intravenous injection	Single injection of 100 μL containing 0.1 mg total lipid	Significant accumulation in brain tissues of nude mice at 24 hr postinjection	(123)
Liposome-siRNA-nine arginine fused RVG peptide (RVG-9R) complex (LSPCs)	Cellular prion protein (PrP^C)	Intravenous injection	Single injection of 4 nmoles of siRNA formulated with 4 nmoles of liposomes and 40 nmoles of RVG-9R	Reduced PrP^C expression to approximately 75±11% at 24 hr postinjection	(124)
RVG peptide-fused exosomes	BACE1	Intravenous injection	A single injection of exosomes loaded with 150 μg of siRNA	Significant knockdown (~5%) in brain cortices of C57BL/6 male mice at 3 days postinjection	(126)
RVG peptide (RVG-9R)	GFP	Intravenous injection	Three injections with 24 h intervals (50 μg of siRNA/injection)	30-40% of GFP silencing effect in brain tissues of GFP expressing transgenic mice 2 days after the last injection	(125)
Biotinylated siRNAs bound to TfR antibody-conjugated streptavidin	Luciferase	Intravenous injection	A single injection of 5'-biotinylated siRNA (80 μg/rat) conjugated to the TfRMAb/SA (736 μg/rat)	Reduced luciferase activity (69%) in luciferase expressing intracranial brain tumor-bearing male fischer CD344 rats 48 h after the injection	(128)
siRNA-encapsulated cationic lipid nanoparticles (LNP-siRNA)	Phosphatase and tensin homolog 1 (PTEN 1)	Intracranial & Intracerebro-ventricular injection	5 nL of 5 mg siRNA/mL for intracranial injection, 2 μL of 5 mg siRNA/mL for intracerebroventricular injection	PTEN reduced by 91% in brain cortex from intracranial injection. PTEN reduced by 55.8% in hippocampus and 51.2% in striatum from intracerebroventricular injection in Sprague–Dawley rats at 5 days postinjection	(137)
TAT-conjugated modified poly (ethylene glycol) and poly (ε-caprolactone) (MPEG-PCL-Tat carrier)	FAM-labeled siRNA with no target gene	Intranasal administration	MPEG-PCL-Tat/FAM-siRNA (FAM-siRNA: 0.5 mg/mL) delivered in 5-10 μL drops, alternating every 2-3 min. A total volume of 80 μL was administered over a 30 min	Significantly higher fluorescence intensity in brain tissues than intravenously injected group and naked siRNA delivered group at 1 hr postdelivery	(141)

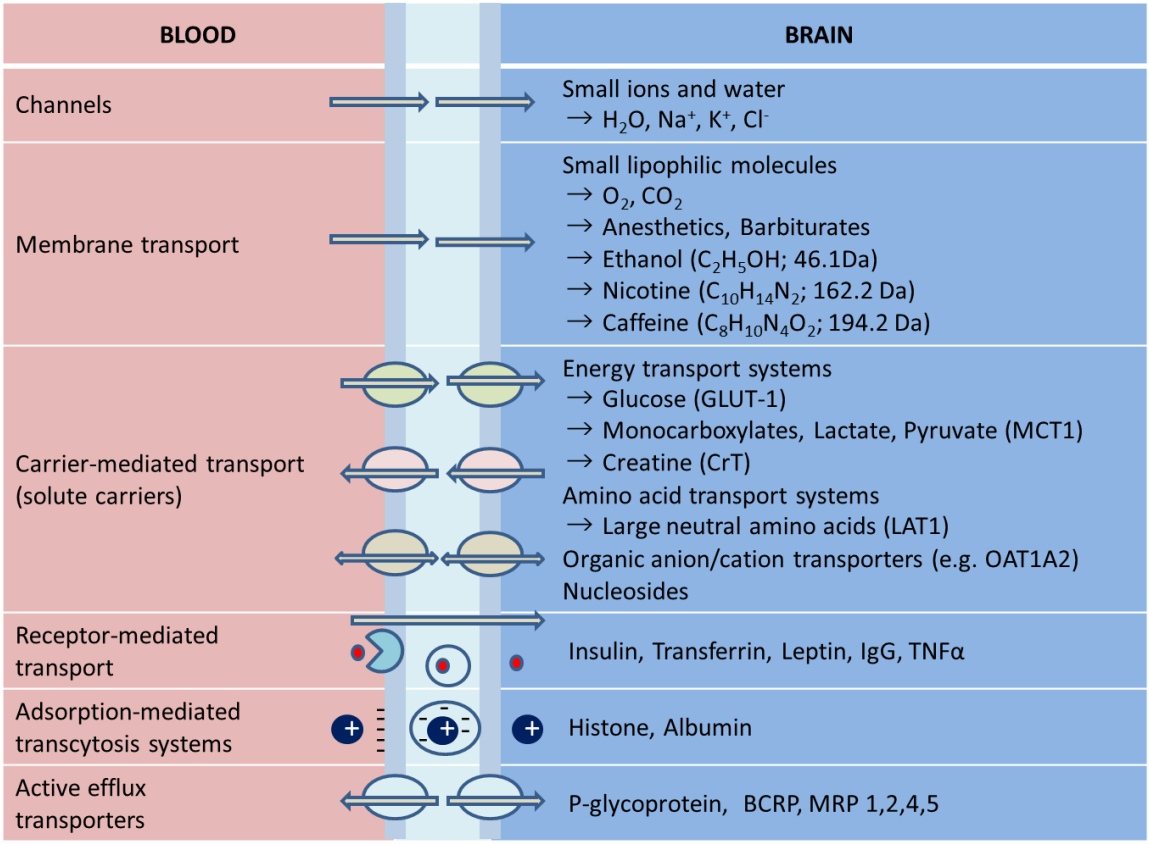

Figure 2.1. Transport systems at the blood-brain barrier. Small ions and water penetrate into the brain via ion channels. Small lipophilic molecules can cross the BBB through the cell membrane. Hydrophilic molecules that are crucial for normal brain function are transported by carrier-mediated transport system. Other molecules can be actively transported into the brain compartment via carrier-mediated transporters, receptor-mediated transporters, adsorption-mediated transcytosis, or efflux pumps. Adapted from (152).

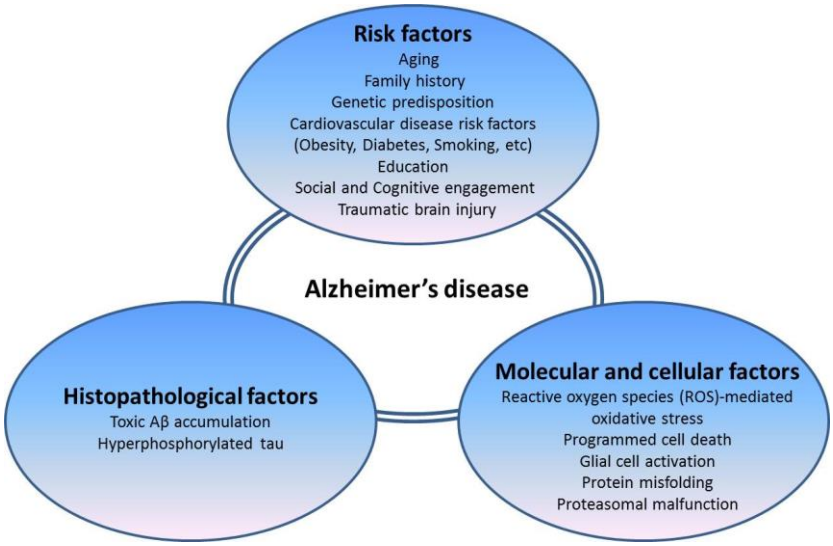

Figure 2.2. Factors associated with Alzheimer's disease pathogenesis.

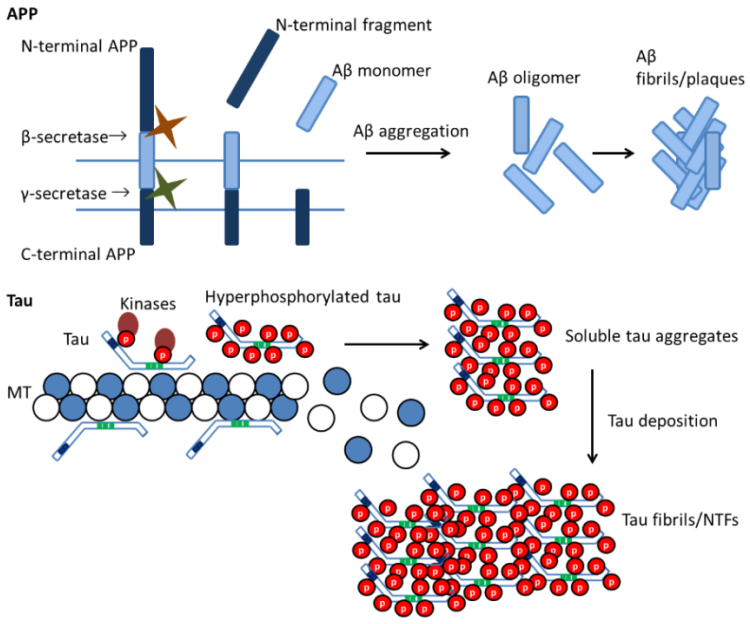

Figure 2.3. APP processing and tau phosphorylation. The Aβ fragment is generated by proteolytic cleavage from the amyloid precursor protein, APP. β-secretase and γ-secretase cleave, respectively, the extracellular domain and the transmembrane domain of the APP to produce the Aβ fragment. The fibrillogenic Aβ species form oligomeric aggregates and further clump to Aβ plaques. The microtubule (MT)-associated protein tau is hyperphosphorylated by multiple kinases under pathological condition. Hyperphosphorylated tau proteins dissociate from microtubules and form aggregates. Further accumulation of tau aggregates eventually form neurofibrillary tangles (NTFs). Adapted from (153).

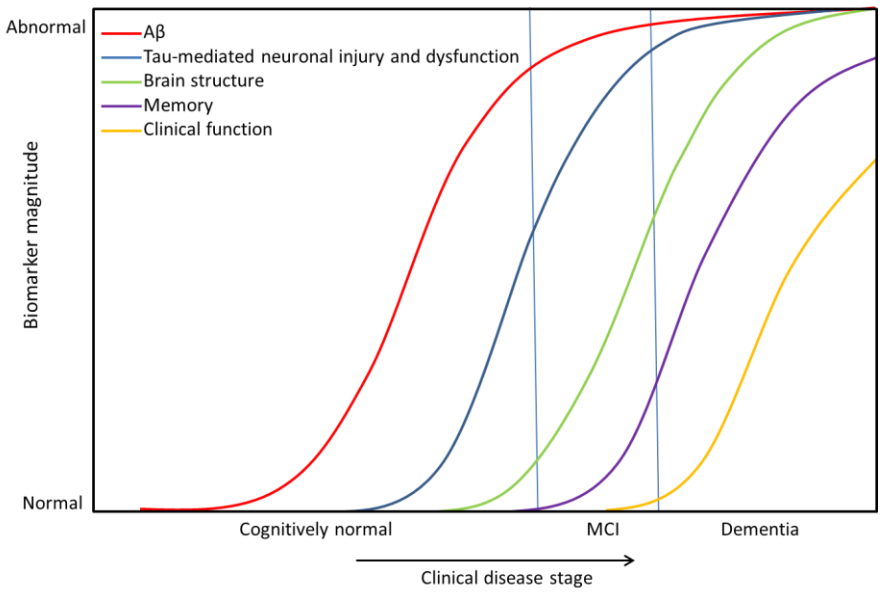

Figure 2.4. Dynamic biomarkers of the Alzheimer's pathological cascade. Aβ is identified by CSF Aβ42 or PET amyloid imaging. Tau-mediated neuronal injury and dysfunction is identified by CSF tau or fluorodeoxyglucose-PET. Brain structure is measured by structural MRI. MCI, mild cognitive impairment. Adapted from (154).

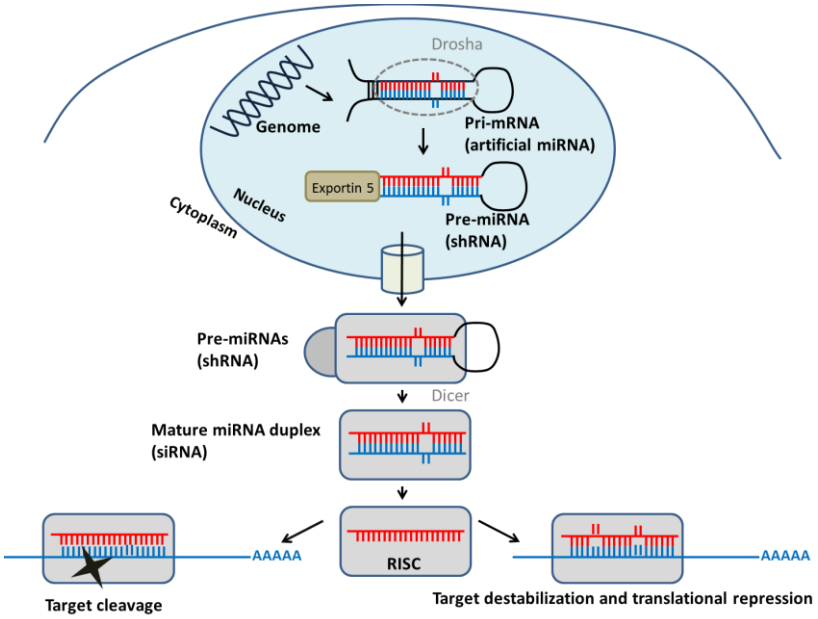

Figure 2.5. Diagram of the endogenous RNAi pathway. The single stranded RNA processed from the RISC binds to its target mRNA species. Depending on the level of sequence complementarity, different modes of the gene silencing mechanism are operated; nearly complete base-pairing leads to the target cleavage while incomplete base-pairing results in translational repression. Adapted from (155).

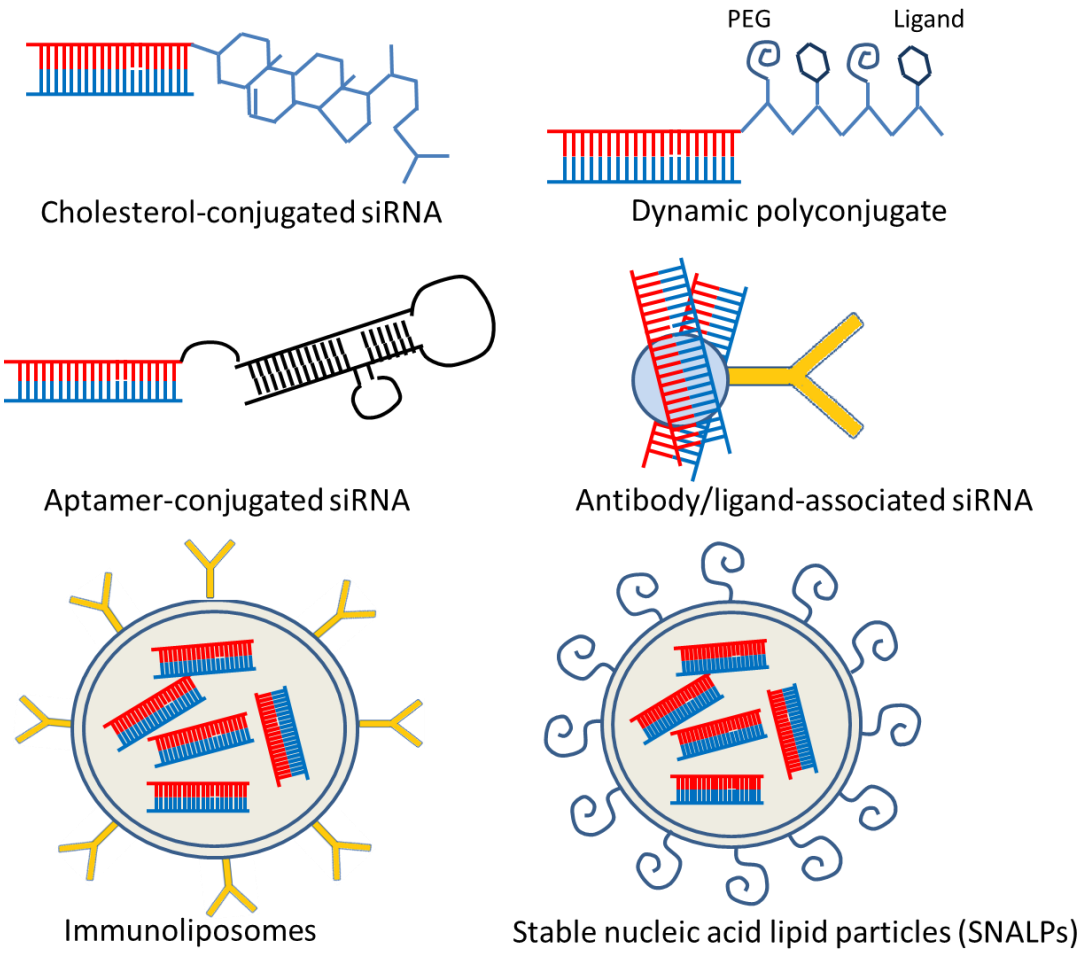

Figure 2.6. Strategies for the siRNA delivery *in vivo*. Diverse approaches have been undertaken for siRNA delivery *in vivo*. The siRNA can be directly conjugated to ligands, polymers or aptamers for targeting purpose. The negatively charged siRNAs can form complexes with positively charged peptide or protein linked to an antibody or a ligand. The siRNAs can also be encapsulated into liposomes or polymer nanoparticles. Adapted from (156).

2.10 References

1. Alzheimer's Association. 2013 Alzheimer's disease facts and figures. Alzheimers Dement 2013;9:208-45.

2. Banks WA. Drug delivery to the brain in Alzheimer's disease: consideration of the blood–brain barrier. Adv Drug Deliver Rev 2012;64:629-39.

3. Lares MR, Rossi JJ, Ouellet DL. RNAi and small interfering RNAs in human disease therapeutic applications. Trends Biotechnol 2010;28:570-79.

4. Ehrlich P. Das sauerstoff-bedürfniss des organismus. August Hirschwald; 1885.

5. Lewandowsky M. Zur lehre der cerebrospinalflussigkeit. Z klin Med 1900;40:l900.

6. Hawkins BT, Davis TP. The blood-brain barrier/neurovascular unit in health and disease. Pharmacol Rev 2005;57:173-85.

7. Pardridge WM. Drug and gene delivery to the brain: the vascular route. Neuron 2002;36:555-58.

8. Tsuji A, Tamai I. Carrier-mediated or specialized transport of drugs across the blood–brain barrier. Adv Drug Deliver Rev 1999;36:277-90.

9. Löscher W, Potschka H. Blood-brain barrier active efflux transporters: ATP-binding cassette gene family. NeuroRx 2005;2:86-98.

10. Stamatovic SM, Keep RF, Andjelkovic AV. Brain endothelial cell-cell junctions: how to "open" the blood brain barrier. Curr Neuropharmacol 2008;6:179-92.

11. Pardridge WM. CNS drug design based on principles of blood-brain barrier transport. J Neurochem 1998;70:1781-92.

12. Pajouhesh H, Lenz GR. Medicinal chemical properties of successful central nervous system drugs. NeuroRx 2005;2:541-53.

13. Christine C, Starr P, Larson P, Eberling J, Jagust W, Hawkins R, et al. Safety and tolerability of putaminal AADC gene therapy for Parkinson disease. Neurology 2009;73:1662-69.

14. Farkas A, Szatmári E, Orbók A, Wilhelm I, Wejksza K, Nagyőszi P, et al. Hyperosmotic mannitol induces Src kinase-dependent phosphorylation of β-catenin in cerebral endothelial cells. J Neurosci Res 2005;80:855-61.

15. Pardridge WM. Brain drug targeting: the future of brain drug development. Cambridge University Press; 2001.

16. Wei K-C, Chu P-C, Wang H-YJ, Huang C-Y, Chen P-Y, Tsai H-C, et al. Focused ultrasound-induced blood–brain barrier opening to enhance temozolomide delivery for glioblastoma treatment: a preclinical study. PloS One 2013;8:e58995.

17. Cloughesy TF, Black KL. Pharmacological blood-brain barrier modification for selective drug delivery. J Neuro-Oncol 1995;26:125-32.

18. Zhou L, Yang B, Wang Y, Zhang HL, Chen RW, Wang YB. Bradykinin regulates the expression of claudin-5 in brain microvascular endothelial cells via calcium-induced calcium release. J Neurosci Res 2014;92:597-606.

19. Gabathuler R. Approaches to transport therapeutic drugs across the blood-brain barrier to treat brain diseases. Neurobiol Dis 2010;37:48-57.

20. Prince M, Prina M, Guerchet M. World Alzheimer report 2013: journey of caring: an analysis of long-term care for dementia. London: Alzheimer's Disease International 2013.

21. Thies W, Bleiler L. Alzheimer's Association report: 2012 Alzheimer's disease facts and figures. Alzheimers Dement 2012;8:131-68.

22. Lopez OL, Jagust WJ, DeKosky ST, Becker JT, Fitzpatrick A, Dulberg C, et al. Prevalence and classification of mild cognitive impairment in the cardiovascular health study cognition study: part 1. Arch Neurol 2003;60:1385-89.

23. Lautenschlager N, Cupples L, Rao V, Auerbach S, Becker R, Burke J, et al. Risk of dementia among relatives of Alzheimer's disease patients in the MIRAGE study: what is in store for the oldest old? Neurology 1996;46:641-50.

24. Mahley RW. Apolipoprotein E: cholesterol transport protein with expanding role in cell biology. Science 1988;240:622-30.

25. Hatters DM, Peters-Libeu CA, Weisgraber KH. Apolipoprotein E structure: insights into function. Trends Biochem Sci 2006;31:445-54.

26. Brecht WJ, Harris FM, Chang S, Tesseur I, Yu G-Q, Xu Q, et al. Neuron-specific apolipoprotein E4 proteolysis is associated with increased tau phosphorylation in brains of transgenic mice. J Neurosci 2004;24:2527-34.

27. Corder E, Saunders A, Strittmatter W, Schmechel D, Gaskell P, Small G, et al. Gene dose of apolipoprotein E type 4 allele and the risk of Alzheimer's disease in late onset families. Science 1993;261:921-23.

28. Lee EB. Obesity, leptin, and Alzheimer's disease. Ann N Y Acad Sci 2011;1243:15-29.

29. Fitzpatrick AL, Kuller LH, Lopez OL, Diehr P, O'Meara ES, Longstreth W, et al. Midlife and late-life obesity and the risk of dementia: cardiovascular health study. Arch Neurol 2009;66:336-42.

30. Ott A, Slooter A, Hofman A, van Harskamp F, Witteman J, Van Broeckhoven C, et al. Smoking and risk of dementia and Alzheimer's disease in a population-based cohort study: the Rotterdam Study. Lancet 1998;351:1840-43.

31. Gómez-Isla T, Price JL, McKeel Jr DW, Morris JC, Growdon JH, Hyman BT. Profound loss of layer II entorhinal cortex neurons occurs in very mild Alzheimer's disease. J Neurosci 1996;16:4491-500.

32. Jack CR, Petersen RC, Xu YC, Waring SC, O'Brien PC, Tangalos EG, et al. Medial temporal atrophy on MRI in normal aging and very mild Alzheimer's disease. Neurology 1997;49:786-94.

33. Benilova I, Karran E, De Strooper B. The toxic A [beta] oligomer and Alzheimer's disease: an emperor in need of clothes. Nat Neurosci 2012;15:349-57.

34. Köpke E, Tung Y-C, Shaikh S, Alonso AdC, Iqbal K, Grundke-Iqbal I. Microtubule-associated protein tau. Abnormal phosphorylation of a non-paired helical filament pool in Alzheimer disease. J Biol Chem 1993;268:24374-84.

35. Savva GM, Wharton SB, Ince PG, Forster G, Matthews FE, Brayne C. Age, neuropathology, and dementia. New Engl J Med 2009;360:2302-09.

36. Morris JC, Price JL. Pathologic correlates of nondemented aging, mild cognitive impairment, and early-stage Alzheimer's disease. J Mol Neurosci 2001;17:101-18.

37. Hardy J, Selkoe DJ. The amyloid hypothesis of Alzheimer's disease: progress and problems on the road to therapeutics. Science 2002;297:353-56.

38. Bird TD. Genetic aspects of Alzheimer disease. Genet Med 2008;10:231-39.

39. Goate A, Chartier-Harlin M-C, Mullan M, Brown J, Crawford F, Fidani L, et al. Segregation of a missense mutation in the amyloid precursor protein gene with familial Alzheimer's disease. Nature 1991;349:704-06.

40. Sisodia SS, St George-Hyslop PH. γ-Secretase, notch, Aβ and alzheimer's disease: where do the presenilins fit in? Nat Rev Neurosci 2002;3:281-90.

41. Kamenetz F, Tomita T, Hsieh H, Seabrook G, Borchelt D, Iwatsubo T, et al. APP processing and synaptic function. Neuron 2003;37:925-37.

42. Jarrett JT, Berger EP, Lansbury Jr PT. The carboxy terminus of the beta amyloid protein is critical for the seeding of amyloid formation: implications for the pathogenesis of Alzheimer's disease. Biochemistry 1993;32:4693-97.

43. Lue L-F, Kuo Y-M, Roher AE, Brachova L, Shen Y, Sue L, et al. Soluble amyloid β peptide concentration as a predictor of synaptic change in Alzheimer's disease. Am J Pathol 1999;155:853-62.

44. Crowther R. Straight and paired helical filaments in Alzheimer disease have a common structural unit. P Natl Acad Sci 1991;88:2288-92.

45. Ghoshal N, García-Sierra F, Wuu J, Leurgans S, Bennett DA, Berry RW, et al. Tau conformational changes correspond to impairments of episodic memory in mild cognitive impairment and Alzheimer's disease. Exp Neurol 2002;177:475-93.

46. Buerger K, Ewers M, Pirttilä T, Zinkowski R, Alafuzoff I, Teipel SJ, et al. CSF phosphorylated tau protein correlates with neocortical neurofibrillary pathology in Alzheimer's disease. Brain 2006;129:3035-41.

47. Roberson ED, Scearce-Levie K, Palop JJ, Yan F, Cheng IH, Wu T, et al. Reducing endogenous tau ameliorates amyloid ß-induced deficits in an Alzheimer's disease mouse model. Science 2007;316:750-54.

48. Rapoport M, Dawson HN, Binder LI, Vitek MP, Ferreira A. Tau is essential to β-amyloid-induced neurotoxicity. P Natl Acad Sci 2002;99:6364-69.

49. Ittner LM, Ke YD, Delerue F, Bi M, Gladbach A, van Eersel J, et al. Dendritic function of tau mediates amyloid-β toxicity in Alzheimer's disease mouse models. Cell 2010;142:387-97.

50. Näslund J, Haroutunian V, Mohs R, Davis KL, Davies P, Greengard P, et al. Correlation between elevated levels of amyloid β-peptide in the brain and cognitive decline. JAMA 2000;283:1571-77.

51. Bartus RT, Dean RL, Beer B, Lippa AS. The cholinergic hypothesis of geriatric memory dysfunction. Science 1982;217:408-14.

52. Babic T. The cholinergic hypothesis of Alzheimer's disease: a review of progress. J Neurol Neurosurg Psychiatry 1999;67:558-58.

53. Andersen JK. Oxidative stress in neurodegeneration: cause or consequence? Nat Rev Neurosci 2004;5:S18–S25.

54. Yatin S, Varadarajan S, Link C, Butterfield D. *In vitro* and *in vivo* oxidative stress associated with Alzheimer's amyloid ß-peptide (1–42). Neurobiol Aging 1999;20:325-30.

55. Dyrks T, Dyrks E, Hartmann T, Masters C, Beyreuther K. Amyloidogenicity of beta A4 and beta A4-bearing amyloid protein precursor fragments by metal-catalyzed oxidation. J Biol Chem 1992;267:18210-17.

56. Alzheimer's association, http://www.alz.org/alzheimers_disease_stages_of alzheimers.asp, accessed Aug. 20, 2014.

57. Watkins PB, Zimmerman HJ, Knapp MJ, Gracon SI, Lewis KW. Hepatotoxic effects of tacrine administration in patients with Alzheimer's disease. JAMA 1994;271:992-98.

58. Mohs RC, Doody R, Morris J, Ieni J, Rogers S, Perdomo C, et al. A 1-year, placebo-controlled preservation of function survival study of donepezil in AD patients. Neurology 2001;57:481-88.

59. Rogers S, Farlow M, Doody R, Mohs R, Friedhoff L. A 24-week, double-blind, placebo-controlled trial of donepezil in patients with Alzheimer's disease. Neurology 1998;50:136-45.

60. Schneider LS, Sano M. Current Alzheimer's disease clinical trials: methods and placebo outcomes. Alzheimers Dement 2009;5:388-97.

61. Orrego F, Villanueva S. The chemical nature of the main central excitatory transmitter: a critical appraisal based upon release studies and synaptic vesicle localization. Neuroscience 1993;56:539-55.

62. Epstein FH, Lipton SA, Rosenberg PA. Excitatory amino acids as a final common pathway for neurologic disorders. New Engl J Med 1994;330:613-22.

63. Tariot PN, Farlow MR, Grossberg GT, Graham SM, McDonald S, Gergel I, et al. Memantine treatment in patients with moderate to severe Alzheimer disease already receiving donepezil: a randomized controlled trial. JAMA 2004;291:317-24.

64. Reisberg B, Doody R, Stöffler A, Schmitt F, Ferris S, Möbius HJ. Memantine in moderate-to-severe Alzheimer's disease. New Engl J Med 2003;348:1333-41.

65. Schneider LS, Dagerman KS, Higgins JP, McShane R. Lack of evidence for the efficacy of memantine in mild Alzheimer disease. Arch Neurol 2011;68:991-98.

66. Fox C, Crugel M, Maidment I, Auestad BH, Coulton S, Treloar A, et al. Efficacy of memantine for agitation in Alzheimer's dementia: a randomised double-blind placebo controlled trial. PloS One 2012;7:e35185.

67. Cummings JL, Morstorf T, Zhong K. Alzheimer's disease drug-development pipeline: few candidates, frequent failures. Alzheimers Res Ther 2014;6:37.

68. Lambracht-Washington D, Rosenberg RN. Advances in the development of vaccines for Alzheimer's disease. Discov Med 2013;15:319.

69. Adolfsson O, Pihlgren M, Toni N, Varisco Y, Buccarello AL, Antoniello K, et al. An effector-reduced anti-β-amyloid (Aβ) antibody with unique Aβ binding

properties promotes neuroprotection and glial engulfment of Aβ. J Neurosci 2012;32:9677-89.

70. Ostrowitzki S, Deptula D, Thurfjell L, Barkhof F, Bohrmann B, Brooks DJ, et al. Mechanism of amyloid removal in patients with Alzheimer disease treated with gantenerumab. Arch Neurol 2012;69:198-207.

71. Salloway S, Sperling R, Fox NC, Blennow K, Klunk W, Raskind M, et al. Two phase 3 trials of bapineuzumab in mild-to-moderate Alzheimer's disease. New Engl J Med 2014;370:322-33.

72. Doody RS, Thomas RG, Farlow M, Iwatsubo T, Vellas B, Joffe S, et al. Phase 3 trials of solanezumab for mild-to-moderate Alzheimer's disease. New Engl J Med 2014;370:311-21.

73. Garber K. Genentech's Alzheimer's antibody trial to study disease prevention. Nat Biotechnol 2012;30:731-32.

74. Sinha S, Anderson JP, Barbour R, Basi GS, Caccavello R, Davis D, et al. Purification and cloning of amyloid precursor protein β-secretase from human brain. Nature 1999;402:537-40.

75. Roberds SL, Anderson J, Basi G, Bienkowski MJ, Branstetter DG, Chen KS, et al. BACE knockout mice are healthy despite lacking the primary β-secretase activity in brain: implications for Alzheimer's disease therapeutics. Hum Mol Genet 2001;10:1317-24.

76. Merck Newsroom, http://www.mercknewsroom.com/press-release/alzheimers-disease/merck-presents-findings-phase-1b-study-investigational-bace-inhibit, accessed Aug. 19, 2014.

77. Arriagada PV, Growdon JH, Hedley-Whyte ET, Hyman BT. Neurofibrillary tangles but not senile plaques parallel duration and severity of Alzheimer's disease. Neurology 1992;42:631-31.

78. Noble W, Planel E, Zehr C, Olm V, Meyerson J, Suleman F, et al. Inhibition of glycogen synthase kinase-3 by lithium correlates with reduced tauopathy and degeneration *in vivo*. P Natl Acad Sci 2005;102:6990-95.

79. Phiel CJ, Wilson CA, Lee VM-Y, Klein PS. GSK-3α regulates production of Alzheimer's disease amyloid-β peptides. Nature 2003;423:435-39.

80. Corbett A, Pickett J, Burns A, Corcoran J, Dunnett SB, Edison P, et al. Drug repositioning for Alzheimer's disease. Nat Rev Drug Discov 2012;11:833-46.

81. Robert SJ, Zugaza JL, Fischmeister R, Gardier AM, Lezoualc'h F. The human serotonin 5-HT4 receptor regulates secretion of non-amyloidogenic precursor protein. J Biol Chem 2001;276:44881-88.

82. Sheline YI, West T, Yarasheski K, Swarm R, Jasielec MS, Fisher JR, et al. An antidepressant decreases CSF Aβ production in healthy individuals and in transgenic AD mice. Sci Transl Med 2014;6:236re4-36re4.

83. Selkoe DJ. Preventing Alzheimer's disease. Science 2012;337:1488-92.

84. Citron M. Alzheimer's disease: strategies for disease modification. Nat Rev Drug Discov 2010;9:387-98.

85. Mapstone M, Cheema AK, Fiandaca MS, Zhong X, Mhyre TR, MacArthur LH, et al. Plasma phospholipids identify antecedent memory impairment in older adults. Nat Med 2014;20:415-18.

86. Fire A, Xu S, Montgomery MK, Kostas SA, Driver SE, Mello CC. Potent and specific genetic interference by double-stranded RNA in Caenorhabditis elegans. Nature 1998;391:806-11.

87. Pecot CV, Calin GA, Coleman RL, Lopez-Berestein G, Sood AK. RNA interference in the clinic: challenges and future directions. Nat Rev Cancer 2011;11:59-67.

88. Bumcrot D, Manoharan M, Koteliansky V, Sah DW. RNAi therapeutics: a potential new class of pharmaceutical drugs. Nat Chem Biol 2006;2:711-19.

89. Davis ME, Zuckerman JE, Choi CHJ, Seligson D, Tolcher A, Alabi CA, et al. Evidence of RNAi in humans from systemically administered siRNA via targeted nanoparticles. Nature 2010;464:1067-70.

90. Sleegers K, Brouwers N, Gijselinck I, Theuns J, Goossens D, Wauters J, et al. APP duplication is sufficient to cause early onset Alzheimer's dementia with cerebral amyloid angiopathy. Brain 2006;129:2977-83.

91. Rodríguez-Lebrón E, Gouvion CM, Moore SA, Davidson BL, Paulson HL. Allele-specific RNAi mitigates phenotypic progression in a transgenic model of Alzheimer's disease. Mol Ther 2009;17:1563-73.

92. Holsinger R, McLean CA, Beyreuther K, Masters CL, Evin G. Increased expression of the amyloid precursor β-secretase in Alzheimer's disease. Ann Neurol 2002;51:783-86.

93. Brunden KR, Trojanowski JQ, Lee VM-Y. Advances in tau-focused drug discovery for Alzheimer's disease and related tauopathies. Nat Rev Drug Discov 2009;8:783-93.

94. Piedrahita D, Hernández I, López-Tobón A, Fedorov D, Obara B, Manjunath B, et al. Silencing of CDK5 reduces neurofibrillary tangles in transgenic alzheimer's mice. J Neurosci 2010;30:13966-76.

95. Barnham KJ, Masters CL, Bush AI. Neurodegenerative diseases and oxidative stress. Nat Rev Drug Discov 2004;3:205-14.

96. Motohashi H, Yamamoto M. Nrf2-Keap1 defines a physiologically important stress response mechanism. Trends Mol Med 2004;10:549-57.

97. Melo A, Monteiro L, Lima RMF, de Cerqueira MD. Oxidative stress in neurodegenerative diseases: mechanisms and therapeutic perspectives. Oxid Med Cell Longev 2011;2011:Article ID 467180.

98. Calkins MJ, Johnson DA, Townsend JA, Vargas MR, Dowell JA, Williamson TP, et al. The Nrf2/ARE pathway as a potential therapeutic target in neurodegenerative disease. Antioxid Redox Sign 2009;11:497-508.

99. Element AR. An important role of Nrf2-ARE pathway in the cellular defense mechanism. J Biochem Mol Biol 2004;37:139-43.

100. Itoh K, Wakabayashi N, Katoh Y, Ishii T, Igarashi K, Engel JD, et al. Keap1 represses nuclear activation of antioxidant responsive elements by Nrf2 through binding to the amino-terminal Neh2 domain. Gene Dev 1999;13:76-86.

101. Kobayashi M, Yamamoto M. Molecular mechanisms activating the Nrf2-Keap1 pathway of antioxidant gene regulation. Antioxid Redox Sign 2005;7:385-94.

102. Chen PC, Vargas MR, Pani AK, Smeyne RJ, Johnson DA, Kan YW, et al. Nrf2-mediated neuroprotection in the MPTP mouse model of Parkinson's disease: critical role for the astrocyte. P Natl Acad Sci 2009;106:2933.

103. Jankovic J. Parkinson’s disease: clinical features and diagnosis. J Neurol Neurosurg Psychiatry 2008;79:368-76.

104. Spillantini MG, Schmidt ML, Lee VM-Y, Trojanowski JQ, Jakes R, Goedert M. α-synuclein in Lewy bodies. Nature 1997;388:839-40.

105. Fountaine TM, Wade-Martins R. RNA interference-mediated knockdown of α-synuclein protects human dopaminergic neuroblastoma cells from MPP+ toxicity and reduces dopamine transport. J Neurosci Res 2007;85:351-63.

106. Walker FO. Huntington's disease. Lancet 2007;369:218-28.

107. Paulson HL, Bonini NM, Roth KA. Polyglutamine disease and neuronal cell death. P Natl Acad Sci 2000;97:12957-58.

108. Cattaneo E, Rigamonti D, Goffredo D, Zuccato C, Squitieri F, Sipione S. Loss of normal huntingtin function: new developments in Huntington's disease research. Trends Neurosci 2001;24:182-88.

109. Kiernan MC, Vucic S, Cheah BC, Turner MR, Eisen A, Hardiman O, et al. Amyotrophic lateral sclerosis. Lancet 2011;377:942-55.

110. Bruijn LI, Miller TM, Cleveland DW. Unraveling the mechanisms involved in motor neuron degeneration in ALS. Annu Rev Neurosci 2004;27:723-49.

111. Lipinski CA, Lombardo F, Dominy BW, Feeney PJ. Experimental and computational approaches to estimate solubility and permeability in drug discovery and development settings1. Adv Drug Deliver Rev 2001;46:3-26.

112. Davidson BL, McCray PB. Current prospects for RNA interference-based therapies. Nat Rev Genet 2011;12:329-40.

113. Xia H, Mao Q, Eliason SL, Harper SQ, Martins IH, Orr HT, et al. RNAi suppresses polyglutamine-induced neurodegeneration in a model of spinocerebellar ataxia. Nat Med 2004;10:816-20.

114. Singer O, Marr RA, Rockenstein E, Crews L, Coufal NG, Gage FH, et al. Targeting BACE1 with siRNAs ameliorates Alzheimer disease neuropathology in a transgenic model. Nat Neurosci 2005;8:1343-49.

115. Foust KD, Salazar DL, Likhite S, Ferraiuolo L, Ditsworth D, Ilieva H, et al. Therapeutic AAV9-mediated suppression of mutant SOD1 slows disease progression and extends survival in models of inherited ALS. Mol Ther 2013;21:2148-59.

116. van Gestel M, van Erp S, Sanders L, Brans M, Luijendijk M, Merkestein M, et al. shRNA-induced saturation of the microRNA pathway in the rat brain. Gene Ther 2014;21:205-11.

117. Ojala DS, Amara DP, Schaffer DV. Adeno-associated virus vectors and neurological gene therapy. Neuroscientist 2014:1073858414521870.

118. Soutschek J, Akinc A, Bramlage B, Charisse K, Constien R, Donoghue M, et al. Therapeutic silencing of an endogenous gene by systemic administration of modified siRNAs. Nature 2004;432:173-78.

119. Nakajima H, Kubo T, Semi Y, Itakura M, Kuwamura M, Izawa T, et al. A rapid, targeted, neuron-selective, *in vivo* knockdown following a single intracerebroventricular injection of a novel chemically modified siRNA in the adult rat brain. J Biotechnol 2012;157:326-33.

120. Kuwahara H, Nishina K, Yoshida K, Nishina T, Yamamoto M, Saito Y, et al. Efficient *in vivo* delivery of siRNA into brain capillary endothelial cells along with endogenous lipoprotein. Mol Ther 2011;19:2213-21.

121. Pfrieger F. Cholesterol homeostasis and function in neurons of the central nervous system. Cell Mol Life Sci 2003;60:1158-71.

122. Chiu Y-L, Rana TM. siRNA function in RNAi: a chemical modification analysis. RNA 2003;9:1034-48.

123. Tao Y, Han J, Dou H. Brain-targeting gene delivery using a rabies virus glycoprotein peptide modulated hollow liposome: bio-behavioral study. J Mater Chem 2012;22:11808-15.

124. Pulford B, Reim N, Bell A, Veatch J, Forster G, Bender H, et al. Liposome-siRNA-peptide complexes cross the blood-brain barrier and significantly decrease PrPC on neuronal cells and PrPRES in infected cell cultures. PloS One 2010;5:e11085.

125. Kumar P, Wu H, McBride JL, Jung KE, Kim MH, Davidson BL, et al. Transvascular delivery of small interfering RNA to the central nervous system. Nature 2007;448:39-43.

126. Alvarez-Erviti L, Seow Y, Yin H, Betts C, Lakhal S, Wood MJ. Delivery of siRNA to the mouse brain by systemic injection of targeted exosomes. Nat Biotechnol 2011;29:341-45.

127. Koren E, Torchilin VP. Cell-penetrating peptides: breaking through to the other side. Trends Mol Med 2012;18:385-93.

128. Xia CF, Zhang Y, Boado RJ, Pardridge WM. Intravenous siRNA of brain cancer with receptor targeting and avidin–biotin technology. Pharm Res 2007;24:2309-16.

129. Qian ZM, Li H, Sun H, Ho K. Targeted drug delivery via the transferrin receptor-mediated endocytosis pathway. Pharmacol Rev 2002;54:561-87.

130. Elbashir SM, Harborth J, Lendeckel W, Yalcin A, Weber K, Tuschl T. Duplexes of 21-nucleotide RNAs mediate RNA interference in cultured mammalian cells. Nature 2001;411:494-98.

131. Kozielski KL, Tzeng SY, Hurtado De Mendoza BA, Green JJ. Bioreducible cationic polymer-based nanoparticles for efficient and environmentally triggered cytoplasmic siRNA delivery to primary human brain cancer cells. ACS nano 2014;8:3232-41.

132. Visser CC, Voorwinden LH, Crommelin DJ, Danhof M, de Boer AG. Characterization and modulation of the transferrin receptor on brain capillary endothelial cells. Pharm Res 2004;21:761-69.

133. Banks WA. The source of cerebral insulin. Eur J Pharmacol 2004;490:5-12.

134. Bertrand Y, Currie JC, Demeule M, Régina A, Ché C, Abulrob A, et al. Transport characteristics of a novel peptide platform for CNS therapeutics. J Cell Mol Med 2010;14:2827-39.

135. Lafon M. Rabies virus receptors. J Neurovirol 2005;11:82-87.

136. Banks WA, Niehoff ML, Martin D, Farrell CL. Leptin transport across the blood–brain barrier of the Koletsky rat is not mediated by a product of the leptin receptor gene. Brain Res 2002;950:130-36.

137. Rungta RL, Choi HB, Lin PJ, Ko RW, Ashby D, Nair J, et al. Lipid nanoparticle delivery of siRNA to silence neuronal gene expression in the brain. Mol Ther Nucleic Acids 2013;2:e136.

138. Thakker DR, Natt F, Hüsken D, Maier R, Müller M, van der Putten H, et al. Neurochemical and behavioral consequences of widespread gene knockdown in the adult mouse brain by using nonviral RNA interference. P Natl Acad Sci 2004;101:17270-75.

139. Gondi CS, Lakka SS, Dinh DH, Olivero WC, Gujrati M, Rao JS. RNAi-mediated inhibition of cathepsin B and uPAR leads to decreased cell invasion, angiogenesis and tumor growth in gliomas. Oncogene 2004;23:8486-96.

140. Malhotra M, Tomaro-Duchesneau C, Saha S, Prakash S. Intranasal, siRNA delivery to the brain by TAT/MGF tagged PEGylated chitosan nanoparticles. J Pharmaceutics 2013;2013: ID 812387.

141. Kanazawa T, Akiyama F, Kakizaki S, Takashima Y, Seta Y. Delivery of siRNA to the brain using a combination of nose-to-brain delivery and cell-penetrating peptide-modified nano-micelles. Biomaterials 2013;34:9220-26.

142. Hanson LR, Frey WH. Intranasal delivery bypasses the blood-brain barrier to target therapeutic agents to the central nervous system and treat neurodegenerative disease. BMC Neurosci 2008;9:S5.

143. Illum L. Is nose-to-brain transport of drugs in man a reality? J Pharm Pharmacol 2004;56:3-17.

144. Fagan AM, Xiong C, Jasielec MS, Bateman RJ, Goate AM, Benzinger TL, et al. Longitudinal change in CSF biomarkers in autosomal-dominant Alzheimer's disease. Sci Transl Med 2014;6:226ra30.

145. Becker RE, Greig NH, Giacobini E, Schneider LS, Ferrucci L. A new roadmap for drug development for Alzheimer's disease. Nat Rev Drug Discov 2014;13:156-56.

146. Borchelt DR, Ratovitski T, van Lare J, Lee MK, Gonzales V, Jenkins NA, et al. Accelerated amyloid deposition in the brains of transgenic mice coexpressing mutant presenilin 1 and amyloid precursor proteins. Neuron 1997;19:939-45.

147. Sapru MK, Yates JW, Hogan S, Jiang L, Halter J, Bohn MC. Silencing of human α-synuclein *in vitro* and in rat brain using lentiviral-mediated RNAi. Exp Neurol

2006;198:382-90.

148. Dufour BD, Smith CA, Clark RL, Walker T, McBride JL. Intra-jugular vein delivery of AAV9-RNAi prevents neuropathological changes and weight loss in Huntington's disease mice. Mol Ther 2014;22:797-810.

149. Van den Haute C, Eggermont K, Nuttin B, Debyser Z, Baekelandt V. Lentiviral vector-mediated delivery of short hairpin RNA results in persistent knockdown of gene expression in mouse brain. Hum Gene Ther 2003;14:1799-807.

150. Rodriguez-Lebron E, Denovan-Wright EM, Nash K, Lewin AS, Mandel RJ. Intrastriatal rAAV-mediated delivery of anti-huntingtin shRNAs induces partial reversal of disease progression in R6/1 Huntington's disease transgenic mice. Mol Ther 2005;12:618-33.

151. Hommel JD, Sears RM, Georgescu D, Simmons DL, DiLeone RJ. Local gene knockdown in the brain using viral-mediated RNA interference. Nat Med 2003;9:1539-44.

152. Wong AD, Ye M, Levy AF, Rothstein JD, Bergles DE, Searson PC. The blood-brain barrier: an engineering perspective. Front Neuroeng 2013;6:Article 7.

153. Götz J, Ittner LM. Animal models of Alzheimer's disease and frontotemporal dementia. Nat Rev Neurosci 2008;9:532-44.

154. Jack Jr CR, Knopman DS, Jagust WJ, Shaw LM, Aisen PS, Weiner MW, et al. Hypothetical model of dynamic biomarkers of the Alzheimer's pathological cascade. Lancet Neurol 2010;9:119-28.

155. Boudreau RL, Rodríguez-Lebrón E, Davidson BL. RNAi medicine for the brain: progresses and challenges. Hum Mol Genet 2011;20:R21-R27.

156. Dominska M, Dykxhoorn DM. Breaking down the barriers: siRNA delivery and endosome escape. J Cell Sci 2010;123:1183-89.

CHAPTER 3

A MYRISTOYLATED CELL-PENETRATING PEPTIDE BEARING A TRANSFERRIN RECEPTOR-TARGETING SEQUENCE FOR NEUROTARGETED SIRNA DELIVERY [1]

3.1 Abstract

Many neurodegenerative disorders (NDDs) are characterized by aggregation of aberrant proteins and extensive oxidative stress in brain cells. As a treatment option for NDDs, RNA interference (RNAi) is a promising approach to suppress the activation of abnormal genes and negative regulators of antioxidant genes. Efficient neurotargeted siRNA delivery requires a delicate optimization of nucleic acid carriers, quite distinct from putative pDNA carriers in regard to stable condensation and serum protection of siRNA, blood-brain barrier (BBB) bypass, effective siRNA delivery to brain cells, and functional release of bioactive siRNA at therapeutic levels. Here, we propose that a myristic acid conjugated, cell-penetrating peptide (transportan; TP), equipped with a transferrin receptor-targeting peptide (myr-TP-Tf) will lead to stable encapsulation of siRNA and targeted delivery of siRNA to brain cells overcoming the BBB. Myr-TP-Tf was successfully prepared by solid-phase peptide synthesis with high purity. Myr-TP-

[1] Reprinted with permission from *Molecular Pharmaceutics*, Pilju You, Yizhe Chen, and Darin Y. Ferguson, A myristoylated cell-penetrating peptide bearing a transferrin receptor-targeting sequence for nuerotargeted siRNA delivery, 2014;11(2):486-95.

Tf:siRNA complex formulated at 20:1 (peptide:siRNA) molar ratio provided prolonged siRNA stability against serum and ribonuclease treatment. Fluorescence images clearly indicated that siRNA uptake was successfully achieved by myr-TP-Tf complex in both a murine brain endothelioma and a human glioma cell line. The luciferase assay and the human placental alkaline phosphatase (hPAP) reporter assay results demonstrated the functional gene silencing effect of myr-TP-Tf:siRNA complex in a human glioma cell line, as well as in primary murine neurons/astrocytes, which are supportive of successful release of bioactive siRNA into the cytosol. Finally, the transcytosis assay revealed that favorable siRNA transport via receptor-mediated transcytosis was mediated by myr-TP-Tf complex. In summary, these data suggest that myr-TP-Tf peptides possess promising properties as a vehicle for neurotargeted siRNA delivery. We will further study this peptide *in vitro* and *in vivo* for transport mechanism kinetics and to validate its capability to deliver siRNA to the brain, respectively.

3.2 Introduction

Today, neurodegenerative disorders (NDDs) are a critical, rising major health concern across the globe, a burgeoning pandemic of dementia encompassing Alzheimer's disease (AD), Parkinson's disease (PD), amyotrophic lateral sclerosis (ALS), and Huntington's disease (HD). Based on the growing trend of the aging population, it is estimated that approximately 115 million people will suffer from NDDs by 2050 (1). The health care cost for the treatment of NDDs is estimated to reach $1.1 trillion by 2050 in the US alone (2). Despite increasing incidences and enormous economic, social, and emotional burdens of NDDs, relatively few NDD therapeutics are clinically viable. This disparity is due in large part to the difficulties of drug delivery across the blood-brain

barrier (BBB), which has prompted many pharmaceutical companies to abandon their neuropharmaceutical programs (3,4). Typically, the defensive brain vasculature allows passage of only small, hydrophobic compounds across the BBB because of the regulation provided by tight junction proteins found between endothelial cells. Hence, there is an acute need for drug delivery vehicles and/or biotherapeutic formulations to cross the BBB with favorable PK/PD (5,6).

Many NDDs are characterized by accumulation of abnormal proteins such as beta amyloid peptide (Aβ) and tau proteins found in AD (7), alpha-synuclein in PD (8), and polyglutamine repeats in HD (9). Along with these protein aggregates, the elevated oxidative stress is also considered a key pathological factor for the onset and progression of NDDs (10). As a therapeutic option for NDDs, an RNA interference (RNAi) approach has the potential to suppress the abnormally regulated genes or any negative regulators of endogenous antioxidant genes. For instance, the Nrf2 (NF-E2-related factor 2)-Keap1(kelch-like ECH-associated protein) pathway is a promising target as Nrf2 activates the expression of detoxifying and antioxidant genes, which relieves oxidative stress (10-13). Because Nrf2 activity is normally restricted by Keap1, which sequesters Nrf2 in the cytoplasm and directs it to the proteasomal degradation pathway (14,15), it is expected that downregulation of the Keap1 protein using an RNAi approach will result in liberation and translocation of Nrf2 and subsequent expression of antioxidant genes, thereby providing cytoprotection to brain cells.

However, drug delivery, let alone neurotargeted siRNA delivery, remains a daunting task. First, the negatively charged backbone of siRNA presents a hurdle for favorable cell membrane association. Plus, naked siRNA has a short period of stability

due to its susceptibility to serum nucleases (16,17). More crucially, the vascular endothelium of the BBB does not allow free passage from the systemic circulation to brain parenchyma. Therefore, successful brain-targeted siRNA transport requires formulations that fully condense siRNA *in vitro* and remain stable *in vivo*, and delivery vehicles that deposit a bioactive, therapeutic level of siRNA without undue toxicity at the targeted site. Diverse siRNA delivery platforms have been attempted including: chemically modified siRNA (18), polymeric nanoparticles (19,20), liposomes or exosomes (21,22), antibody-fusion molecules (23), and cholesterol-conjugated siRNA (24). For clinical application, however, currently investigated siRNA vehicles still require optimization regarding physiological stability, BBB-targeting ability, and functional RNAi effect.

To overcome the above listed obstacles, studies have indicated that cationic peptide repeats effectively encapsulate siRNA through electrostatic interactions (25-28) and also facilitate cellular uptake of nucleic acid (29,30). Thus, it is conceivable that siRNA carriers comprised of a cationic domain fused with a BBB-targeting group should be capable of siRNA condensation and delivery across the BBB. Kumar et al. presented transvascular delivery of siRNA to neurons using synthetic oligo-arginine peptides linked with a rabies virus glycoprotein (RVG)-derived domain that binds to acetylcholine receptors on neuronal cells (31). This finding provided an encouraging basis for the development of neurotargeted, peptide-based siRNA carriers. In a recent study, various cell-penetrating peptides were characterized and evaluated in regard to effective siRNA delivery to tumor cells; the myristoylated transportan peptide was identified as the most suited showing a two-fold higher fitness in knockdown efficiency than the TAT (trans-

activator of transcription) cell penetrating peptide (32). Myristolyation of the cell-penetrating peptide is also a beneficial strategy for carrier design, as it is known to enhance the peptide affinity for the cellular membrane (33-35). Another study showed that myristoylated poly-arginine peptides mediated efficient siRNA internalization to brain cells *in vitro* (36), but the physiological performance *in vivo* may not be ensured without an adequate neuro-targeted moiety.

In the current work, we designed a BBB-targeting siRNA carrier exploiting the N-terminally myristoylated transportan peptide as a cell-penetrating and siRNA condensation domain and a transferrin receptor-targeting 12 amino acid sequence (THRPPMWSPVWP)(37,38) as a BBB-targeting domain. We hypothesized that a myristic acid conjugated, cell-penetrating peptide (transportan) equipped with a transferrin receptor-targeting peptide (myr-TP-Tf) would enable the stable condensation of siRNA and facilitate targeted delivery of siRNA to brain cells through receptor-mediated transcytosis, as illustrated in Figure 3.1A. The data from *in vitro* studies confirmed that the myr-TP-Tf peptide formed stable peptide:siRNA complex and achieved superior siRNA uptake in brain endothelial cells and glioma cells when compared to putative Lipofectamine®:siRNA controls or nontargeted (scrambled) peptide:siRNA controls. In addition, myr-TP-Tf:siRNA complex displayed the functional, reporter protein knockdown without affecting cell viability and favorable siRNA transport across a model, brain endothelial cell monolayer.

3.3 Materials and methods

3.3.1 Peptide synthesis

The myristic acid conjugated, cell-penetrating peptide (transportan) equipped with a transferrin receptor-targeting peptide (myr-TP-Tf) and its nontargeting scrambled control peptide (myr-TP-Scr) were prepared by solid-phase peptide synthesis at Selleckchem (Houston, TX). The peptide sequences for myr-TP-Tf and myr-TP-Scr are as follows: myristic acid-GWTLNSAGYLLGKINLKALAALAKKIL-GGGG-THRPPMWSPVWP and myristic acid-GWTLNSAGYLLGKINLKALAALAKKIL-GGGG-PWRPSHPVWMPT, respectively. The purity (>95%) and the molecular weight (4.5 kDa) of the peptides were confirmed by high-performance liquid chromatography (HPLC) and mass spectrometry analyses upon receipt.

3.3.2 Formulation of siRNA-carrier complex and gel retardation assay

Myr-TP-Tf peptide was mixed with 20 pmol of siRNA at different molar ratios ranging from 1:1, to 10:1, 20:1, and 30:1 (peptide:siRNA) in distilled water. Samples were vortexed for 20 s and incubated for 20 min at room temperature. Each sample was mixed with 6× DNA loading dye (Fermentas, Hanover, MD) and subject to 0.8% agarose gel electrophoresis for 20 min at 100V. Bands were stained with SYBR® Green II RNA gel stain (Invitrogen, Carlsbad, CA) and visualized under UV light.

3.3.3 Transmission electron microscopy

The morphology of the myr-TP-Tf:siRNA complex was examined by transmission electron microscopy (TEM). Briefly, 20 µL of the peptide:siRNA complex solution (20:1 molar ratio, 20 µM of siRNA) was loaded on carbon-coated, copper

electron microscopy grids and air-dried for 1 hr. The peptide:siRNA complex was negatively stained with 2% phosphotungstic acid for 30 s and the excess liquid was wicked away with a tip of filter paper. The grids were then examined by a 120 kV Tecnai 12 TEM (FEI, Hillsboro, OR) at the electron microscopy lab in the University of Utah Health Sciences Center Core Research Facility.

3.3.4 Particle size and zeta potential measurement

The myr-TP-Tf:siRNA complex was prepared in either 10:1 or 20:1 molar ratio in distilled water (100 nM of siRNA). The hydrodynamic diameter and the surface charge of the complex were determined by using a Zetasizer Nano ZS (Malvern Inc., Westborough, MA). All measurements were collected in triplicate and expressed as mean ± standard errors. Each measurement consisted of at least 11 runs.

3.3.5 Examination of siRNA stability fetal bovine serum and ribonuclease A

Naked siRNA and myr-TP-Tf:siRNA complex were incubated in 50% fetal bovine serum at 37°C. Aliquots were collected at 0, 30 min, 4 hr, 8 hr, 24 hr of incubation and frozen for storage. Each sample was then treated with proteinase K (1 mg/mL) at 37°C for 10 min. To evaluate the siRNA protection against RNase A, naked siRNA and myr-TP-Tf:siRNA complex were incubated in RNase A solution (0.04 mg/mL) at 37°C for 0, 30 min, 1 h, 2 h, 4 h, and treated with 2 µL of 10 M NaOH solution to disrupt the complex structures. All samples were mixed with 6× DNA loading dye and subject to 0.8% agarose gel electrophoresis for 20 min at 100V. The gels

were stained with SYBR® Green II RNA gel stain (Invitrogen) to examine the siRNA integrity under UV light.

3.3.6 Cell culture: human glioma U87mg and murine brain endothelioma b.End3 cell lines

Human glioma U87mg cells that constitutively express luciferase were kindly donated by Prof. Randy Jensen (University of Utah; Dept. of Neurosurgery) and maintained in DMEM (Dulbecco's Modified Eagle's Medium, Invitrogen) supplemented with 10% fetal bovine serum, 100 U/mL of penicillin/streptomycin, and 0.5 mg/mL of Geneticin® selective antibiotic (G418 sulfate). During the transfection studies, G418 was not contained in the culture medium. Murine brain endothelioma b.End3 cells were purchased from ATCC (Manassas, VA) and maintained in DMEM supplemented with 10% fetal bovine serum and 100 U/mL of penicillin/streptomycin. The cell cultures were maintained in a humidified atmosphere containing 5% CO_2 at 37 °C.

3.3.7 Cell culture: primary murine ARE:hPAP(+) neurons/astrocytes

ARE:hPAP (antioxidant response element:human placental alkaline phosphatase) (+) transgenic mice were kindly gifted by Prof. Jeffrey Johnson (University of Wisconsin-Madison) and maintained in accordance with University of Utah Institutional Animal Care and Use Committee (IACUC) guidelines. The mice were mated and the mother mice were sacrificed at day 15 of pregnancy to isolate the E15 brain cortices from embryonic mice. The tissues were washed with HBSS (Invitrogen) and digested with 0.05% trypsin for 20 min at 37°C. The cell suspensions were filtered through 70 µm cell strainers (BD Falcon, San Jose, CA) and plated at a density of 10^5 cells/well on 96-well

plates in EMEM supplemented with 10% FBS, 10% horse serum, 2 mM of L-glutamine, and 100 U/mL of penicillin/streptomycin following the protocol established by the Johnson lab (39). On day 2, the medium was replaced with neurobasal medium (Invitrogen) containing B27 supplements, 2 mM of L-glutamine, and 100 U/mL of penicillin/streptomycin. The primary neurons/astrocytes were cultured at 37°C in a humidified trigas chamber (5% CO_2 / 5% O_2 / 90% N_2).

3.3.8 Cell transfection

U87mg-Luc cells were plated on 96-well plates with 10^4 cells/well and grown to 70-80% confluency. The cells were transfected with peptide:luciferase siRNA complex (4 pmol of siRNA/well) in DMEM without serum and antibiotics for 3 hr and then incubated in complete culture medium for an additional 45 hr. Lipofectamine® RNAiMAX Reagent (Invitrogen) was used as the control transfection reagent following the manufacturer's protocol.

3.3.9 Immunocytochemistry for transferrin receptors

U87mg cells and b.End3 cells were grown on 6-well plates up to 70% confluency. The cells were twice washed with ice-cold phosphate buffered saline (PBS) and fixed with 4% paraformaldehyde for 15 min at room temperature. Following three additional rinses of PBS, the cells were incubated with a polyclonal, rabbit antibody to the transferrin receptor (Abcam Inc., Cambridge, MA) in PBS at 4°C overnight. After washing the samples with ice-cold PBS 3 times, 5 min each, the cells were incubated with Alexa Fluor® 488 Goat Anti-Rabbit IgG (Invitrogen) for 1 hr and examined using an Olympus IX71F fluorescence microscope (Scientific Instrument Company, Aurora, CO).

3.3.10 Fluorescence imaging of siRNA uptake

To examine the siRNA uptake by U87mg cells and b.End3 cells, siGLO RNA-induced silencing complex (RISC)-free control siRNA labeled with Dy547 fluorescent dye (Thermo Scientific, Rockford, IL) was used to formulate peptide:siRNA complex. The cells were grown on 6-well plates to 70% confluency and each well subsequently treated with 100 pmol of siRNA in either a naked or a peptide:siRNA complex form in DMEM for 3 hr and were then washed with PBS 3 times. The fluorescence images were acquired by using an Olympus IX71F fluorescence microscope and the red fluorescence color was added to the acquired images by Image J software (NIH Image, Bethesda, MD).

3.3.11 Cellular luciferase assay expression for examination of functional gene silencing effect

Upon 48 hr of incubation after transfecting luciferase siRNA, the U87mg-Luc cells were washed with PBS and lysed in a passive lysis buffer (Promega, Madison, WI) for 15 min. Twenty μL of the lysates were transferred to white 96-well plates and 100 μL of luciferase assay reagent (Promega) was added per well. After 2 min of dark incubation, the luminescence intensity from each well was measured using a PlateLumino Luminometer (Stratec Biomedical Systems, Birkenfeld, Germany). The total protein amount was quantified by a bicinchoninic acid (BCA) assay to correct the luminescence intensity per mg of protein.

3.3.12 Human placental alkaline phosphatase (hPAP) assay

The hPAP assay was performed following the protocol established by Prof. Jeffrey Johnson (University of Wisconsin-Madison) (39). Briefly, the primary

neurons/astrocytes were lysed in TMNC lysis buffer (0.05M Tris, 0.005M $MgCl_2$, 0.1M NaCl, 1% 3-[(3-cholamidopropyl) dimethylammonio]-1-propanesulfonate [CHAPS]) and incubated at 65°C for 30 min in 0.2M diethanolamine buffer. The CSPD® (chemiluminescent substrates for alkaline phosphatase) and Emerald™ (luminescence enhancer) reagents from Applied Biosystems (Bedford, MA) were used as substrates to quantify the hPAP activity and the luminescence intensity was measured using a luminometer. A BCA assay followed to normalize the hPAP activity to total protein.

3.3.13 Cell viability assay

Cell viability was determined by using a tetrazolium salt 3-(4,5-dimethylthiazol-2-yl)-5-(3-carboxymethoxyphenyl)-2-(4-sulfophenyl)-2H-tetrazolium salt (MTS) substrate – as per the cell proliferation kit (Promega) and following the manufacturer's instruction.

3.3.14 Transcytosis assessment

The b.End3 cells were seeded at a density of $6\times10^4/cm^2$ onto 12 mm transwell inserts (polycarbonate membrane, 0.4 μm pore size, Corning, NY) and the cells at day 8 were used for experiments. The inserts were filled with 300 μL of DMEM and the bottom compartments with 500 μL of DMEM. Fifty pmol of peptide:Dy547-labeled siRNA complex was applied onto the b.End3-coated, transwell inserts and incubated in a 37°C CO_2 incubator. To evaluate the siRNA transport, 200 μL of the medium was collected from the abluminal compartment 6 hr postincubation. The fluorescence intensity from the aliquots was measured by using a microplate reader (Bio-Rad, Hercules, CA) with a wavelength setting of 557/570 Ex/Em. The amount of transported

siRNA was calculated from a standard curve generated from the fluorescence intensity of the known amount of Dy547-labeled siRNA. Transendothelial electrical resistance (TEER) was measured before and after the siRNA treatment to ensure the b.End3 cell monolayer integrity. The paracellular barrier integrity was additionally monitored by measuring the permeability coefficient of sodium fluorescein (376.3 Da). Ten μM of sodium fluorescein in Krebs-Ringer buffer was loaded to the insert well and the abluminal medium aliquots were collected every 15 min over an hour to determine the diffused concentration.

3.3.15 Statistical analysis

The data are expressed as mean ± standard errors and were statistically analyzed by conducting a one-way ANOVA, followed by Tukey-Kramer HSD post-hoc analysis. A Student's t-test was performed for the siRNA transport study. Statistical significance is indicated by asterisks (*$p < 0.05$; **$p < 0.01$; ***$p < 0.001$). JMP® v10.0 (SAS Institute Inc., Cary, NC) was used for performing the statistical analyses and the graphs were generated by SigmaPlot 10.0 (Systat, San Jose, CA).

3.4 Results

3.4.1 Characterization of myr-TP-Tf peptide

The myr-TP-Tf peptide was successfully synthesized with high purity and precise molecular weight (data not shown). We first investigated the optimal molar ratio of myr-TP-Tf to siRNA at which the complex would achieve stable electrostatic condensation. The gel retardation assay revealed that the myr-TP-Tf peptide condensed siRNA beginning at a 10:1 molar ratio (Figure 3.1B). The hydrodynamic diameter and the

surface charge were measured for the complex formulated at 10:1 and 20:1 molar ratios (Figure 3.1C). The 10:1 complex (85.5 ± 2.1 nm) displayed a relatively smaller size than the 20:1 complex (100.4 ± 4.8 nm), which may be due to an increased association number (N_A) or number of peptides per complex. Experiments are ongoing to further elucidate this trend. The zeta potential of the 10:1 complex (7.0 ± 0.2 mV) was less than the myr-TP-Tf itself, indicating that the cationic charge of myr-TP-Tf was shielded by the electrostatic interaction with the negatively charged siRNA backbone. The 20:1 complex displayed a higher positive charge range (23.4 ± 3.7 mV) compared to the 10:1 complex, which further substantiates our hypothesis of an increased N_A with complex formation. Molar ratios of 30:1 or higher were not included in this study as the excessive cationic charge induced potent cytotoxicity. The general morphology of the peptide:siRNA (20:1) was examined by transmission electron microscopy (TEM). The representative TEM images show that the complex possesses spherical structures, which was in accordance with expectations (Figure 3.1D). The size of the complex was smaller (~30 nm) in the TEM images than the dynamic laser scattering measurements due to shrinkage under the anhydrous, vacuum environment.

3.4.2 Enhanced siRNA stability

The siRNA instability is a major concern for therapeutic RNAi application *in vivo*. We investigated the siRNA integrity in 50% fetal bovine serum (FBS) and RNase A solution to evaluate the siRNA protection ability of the peptide:siRNA complex. It was observed that the siRNA in the complex form displayed prolonged stability, showing at least partial stability for up to 8 hr in 50% FBS, whereas the naked form of siRNA was nearly untraceable at the 4 hr time-point (Figure 3.2A). The siRNA protection capability

of the complex was more dramatic in the RNase A treatment assay. Over the 4 hr incubation time, the siRNA band intensity of the complex stayed nearly intact while the naked siRNA immediately began to degrade (Figure 3.2B). The literature shows that even chemical modification of siRNA does not necessarily improve the gene silencing effect *in vivo*, despite reported enhanced serum stability (16). From a clinical perspective, it would be imperative to achieve the therapeutic concentration at the target organ within a reasonable timeframe in regard to the half-life of the complex.

3.4.3 Favorable siRNA uptake

It is well-known that brain endothelial cells, neurons, and astrocytes express high levels of TfR proteins for transferrin-mediated iron supply, which is an essential cellular process for normal brain functions (40). Prior to applying the myr-TP-Tf peptide, we completed immunostaining to verify the abundant expression of TfR on murine brain endothelial b.End3 and human glioma U87mg cells used in this study. Representative images support the choice of TfR as a targeting receptor for both cell types (Figure 3.3A and C). However, nonspecific uptake by other organs of the complex is expected upon *in vivo* administration because TfR proteins are ubiquitously expressed to varying extents. It should be noted that brain-targeting may not be exclusively achieved, except preferentially with the high levels of TfR existing on the brain endothelial cells (41). Next, siRNA uptake in b.End3 cells and U87mg cells was examined to evaluate siRNA delivery capability of myr-TP-Tf peptides. To visualize siRNA internalization, Dy547 fluorescent dye-labeled siRNA was used in the peptide:siRNA complex formulation. As shown in Figure 3.3B and D, b.End3 cells and U87mg cells displayed intense red fluorescence after 3 hr of myr-TP-Tf:Dy547 siRNA complex incubation, indicating that

the complex successfully transported siRNA (Figure 3.3B and D) across the cell membrane barrier. To evaluate the targeting effect of the myr-TP-Tf peptide, b.End3 and U87mg cells were treated with either naked Dy547 siRNA or nontargeted, myr-TP-Scr:Dy547 siRNA complex. As anticipated, the naked Dy547 siRNA-treated group did not show detectable red fluorescence (Figure 3.4A and D). It was observed that the nontargeted control (scrambled) peptide complex was able to deliver siRNA to the cells (Figure 3.4B and E). This observation was not surprising because the control peptide also contains the cationic cell-penetrating peptide sequence and therefore has the same ability to condense siRNA. Compared to the targeting complex, however, the extent of internalized siRNA was much less prominent, demonstrating that the enhanced cellular uptake of siRNA is possible when combined with a receptor-mediated pathway (Figure 3.4C and F).

3.4.4 Transfection of a human glioma cell line

Next, we investigated if the internalized siRNA functionally downregulates the target protein in brain cells. To this end, we used human glioma U87mg-Luc cells which constitutively express luciferase. The U87mg-Luc cells were treated with either naked siRNA targeting luciferase mRNA or peptide:luciferase siRNA complex for 3 hr and the luciferase activity was measured 45 hr posttransfection. As shown in Figure 3.5A, the luciferase-specific siRNA was successfully delivered to the U87mg cells by myr-TP-Tf peptide complex (20:1) and effectively silenced the luciferase mRNA, which is implicated in the significantly reduced luminescence intensity. The nontargeting peptide complex (20:1) also resulted in a significant gene silencing effect to a certain degree. However, the extent of luciferase expression downregulation was not comparable to the

levels produced by the targeting peptide, which complied with the different levels of cellular uptake of siRNA (Figure 3.4). The complex prepared at a 10:1 molar ratio did not exert any significant RNAi effect. We hypothesize that the higher cationic surface charge and the multivalent presentation of targeting peptides account for the greater mRNA silencing effect of the 20:1 complex, but we did not attempt higher ratios as we had established that higher molar ratios induce potent cytotoxicity. Throughout the transfection study, no significant cytotoxicity was observed from peptide:siRNA complex treatments (Figure 3.5B).

3.4.5 Transfection of primary murine neurons/astrocytes

Primary cells are often considered generally difficult to transfect. In order to further validate the carrier transfection ability, primary murine neurons/astrocytes were extracted from brain cortices of E15 ARE:hPAP(+) transgenic mice, in which the hPAP reporter gene is inserted downstream of the ARE. As remarked upon in the Introduction, the Keap1-Nrf2 pathway is a promising target for the treatment of NDDs. It is expected that downregulation of Keap1 mRNA, using an RNAi approach, will result in liberation and translocation of Nrf2 to the nuclear ARE with subsequent activation of antioxidant genes, thereby providing cytoprotection to brain cells. ARE:hPAP(+) transgenic mice serve as a useful tool to examine the activation of ARE by analyzing the reporter hPAP activity. Here, primary murine neurons/astrocytes were transfected with myr-TP-TfR:siRNA complex against Keap1 and the hPAP activity measured 48 hr posttransfection. As shown in Figure 3.6A, the myr-TP-Tf:Keap1 siRNA complex significantly induced hPAP activity (Figure 3.6A) as compared to the control groups. Again, the nontargeting peptide complex also exhibited positive transfection ability, but

to a lesser degree. As with the immortalized cell lines, the cell viability assay result indicated no significant cytotoxicity of the primary murine neurons/astrocytes (Figure 3.6B).

3.4.6 siRNA transport assay

The actual transport of the siRNA across brain endothelial cells was examined *in vitro* using a transwell system in which b.End3 cells were grown as a confluent monolayer on inserts. We treated the inserts with 50 pmol of peptide:Dy547-labeled siRNA complex for 6 hr and assessed the transport of Dy547 siRNA by measuring the fluorescence intensity of the medium collected from the bottom compartments. The myr-TP-Tf:siRNA complex treated group clearly showed an enhanced transport profile compared to the scrambled myr-TP-Scr:siRNA (Figure 3.7A). However, the transported siRNA quantity was less than the original amount, indicating that a significant portion of siRNA remained in the b.End3 cells monolayer over the 6 hr. A naked siRNA-treated group was not included as the naked form of siRNA was not visibly uptaken by b.End3 cells. To examine if the b.End3 cell monolayer remained intact during the transcytosis experiment, the TEER values before and after the siRNA treatments were compared and no notable changes were detected (Figure 3.7B). The permeability coefficient of the water soluble sodium fluorescein compound was additionally examined to evaluate the monolayer integrity. Even though it was higher [$(6.8 \pm 0.9)\cdot10^{-6}$ cm/s] than the reported value from other *in vitro* BBB models established with primary rat brain endothelial cells [$(3.5 \pm 0.1)\cdot10^{-6}$ cm/s] (42), the order of magnitude of 10^{-6} cm/s is extremely small and considered an acceptable range for an *in vitro* BBB model (43). Although the transported

siRNA quantity over 6 hr was found less than the loaded amount, it remains encouraging that the myr-TP-Tf complex showed a promising siRNA transport property.

3.5 Discussion

The physicochemical characteristics of the myr-TP-Tf:siRNA complex were, in principle, well-suited for cell-targeted *in vivo* administered RNAi. First, the myr-TP-Tf peptide successfully electrostatically condensed siRNAs with apparently optimal condensation in a reasonable range of peptide:siRNA molar ratios below the cytotoxic line of 30:1 molar ratio. Second, the negative staining images of the peptide:siRNA complex under TEM revealed these complexes formed spherical structures, whereupon supramolecular self-assembly promoted core siRNA encapsulation in a core-shell architecture. The moderately positive surface charge of the complex appeared to enhance complex interactions with brain cells. It should be noted that the excessive cationic charge of nanoparticles normally involves detrimental effects to cells (44), but these peptide:siRNA complexes did not arouse any notable cell viability changes to both the glioma cells and the primary murine brain cells within their measured and transfected surface charge range. Fourth, the particle size of the complex was found to be fairly small considering that the siRNA molecule itself is quite bulky (14 kD). However, the particle size values measured in distilled water may not reflect the actual size in the culture medium or in the bloodstream. Indeed, when formulated in PBS (pH 7.4), the particle size was quite increased (230 ± 27.6 nm) while the surface charge was relatively maintained (28.6 ± 0.9 mV). It is likely that the ionic strength in buffer affects the tightness of the peptide-siRNA interaction, leading to particle expansion (45). Even with the increased diameter, the peptide:siRNA complex did not show micron-sized aggregate

formation. The imaging and the transfection results support that these complexes remain structurally viable for targeted cellular uptake and functional siRNA release in the brain cells.

In addition, the peptide:siRNA complex was advantageous in regard to the siRNA stability in serum. The improved siRNA stability in the complex also indicated that the siRNAs were protectively loaded within the complex structure. However, the *in vitro* serum stability testing may not present an accurate level of stability *in vivo*. This potential instability is a factor of the bloodstream itself, which may contain multiple nucleases in various ranges of concentration, resulting in dissimilar patterns of siRNA degradation kinetics (46). Furthermore, it is plausible for this complex to be entrapped by phagocytic cells and rapidly cleared from the bloodstream. Despite these multiple hurdles, an effective concentration of peptide:siRNA complex should reach the brain, preserving bioactive siRNA integrity within the brain interstitial tissue while awaiting endo-/transcytosis. In depth studies elucidating the physiological stability needs and mechanisms of transport across the BBB are ongoing.

The transferrin receptor-targeting capacity of the complex may raise questions because the nontargeting carrier with a scrambled sequence also showed the ability to deliver siRNA to the brain cells and exert some level of target gene silencing. For our purposes, we hypothesize that not only the targeting moiety, but also the cationic surface charge on the complex, plays a significant role for the cellular uptake of the complex. At a lower molar ratio (10:1), even for the TP-targeted carrier, no significant RNAi effect was observed, which may be the outcome of an insufficient cationic charge to interact with the cell membrane and/or the lack of targeting moieties presented to the cell

receptors. Nevertheless, the targeted complex formulated at a seemingly optimal (20:1) molar ratio showed preferential siRNA uptake and more significant target gene knockdown compared to a nontargeted complex at the same molar ratio. These data suggest that the receptor targeting ability provides an added effect for enhanced siRNA delivery. The siRNA transport results from the transwell system also substantiate the benefit of the TfR-targeting peptide sequence in the siRNA carrier. To achieve the highly selective targeting and thereby avoid the adverse effects from the nonspecific binding, further research efforts are required to find the optimal receptor candidates and identify their ligand binding modes.

In the siRNA transport assay, the targeting complex also showed more favorable siRNA transport to the abluminal compartment compared to the nontargeting complex. However, this result may not be directly translatable to the *in vivo* condition; it should be noted that the *in vitro* BBB model used in our study is limitedly simulating the physiological BBB. Although the b.End3 cells can grow as a monolayer on the transwell insert membrane and express various tight junction proteins, the tightness of the monolayer, usually represented as TEER, never attains the values obtained from the *in vivo* BBB (47). Being aware of the limitation, we conducted the experiments when the b.End3 cells formed a morphologically mature monolayer and the TEER values reached a fairly stable level. To exclude the possibility of any free Dy547 dye existence, HPLC-purified siRNAs were used and the siRNA integrity was further examined on a couple of polyacrylamide gels before any assay. Though the b.End3 cells grown in a transwell system may not be the most desirable surrogate for the physiological BBB, it served as a convenient tool to readily examine the complex's ability to transport siRNA. Again,

further complete examination for the siRNA transport should be followed by testing the complex in animal models.

As our studies were executed only *in vitro*, the *in vivo* performance of the complex is therefore not yet guaranteed, even with its promising properties. One reasonable question is whether this single delivery system will or will not achieve the two, seminal intracellular trafficking processes: (i) receptor-mediated transcytosis across the BBB and (ii) subsequent cytosolic and/or transcytotic release of therapeutic levels of bioactive siRNA in the brain parenchyma. Transport mechanism studies are beyond the scope of this manuscript; however, the data are encouraging and similar peptide-based delivery systems have shown levels of brain-targeted siRNA delivery and RNAi in the mouse brain (31,36). These authors did not provide a detailed explanation of proposed transport mechanisms; however, again, these studies remain encouraging for peptide-mediated siRNA delivery across the BBB. Our goal is to achieve neurotargeted siRNA delivery, following systemic administration of the complex. However, we recognize the established difficulties of peptide-mediated, systemically administered, targeted drug delivery, let alone the complicated issues surrounding the applicability and relevance of RNAi therapy when compared to small molecules therapies. We remain optimistic, as RNAi therapy remains a potent mode of treatment, while continuing to provide exciting challenges for therapeutic efficacy. Systemic administration may be overcome by alternative routes, such as local, intrathecal, or nasal delivery to avoid prolonged serum exposure, RES clearance, and inefficient neurotargeting. Nasal delivery, with its readily accessible pathways to the brain parenchyma is a viable option (48). It would avoid the invasive complications of local delivery. Regardless, stable siRNA complex with cell- or

tissue-targeting capability to deliver bioactive and therapeutic levels of RNAi without compromising cell viability remain the key components in the continued advancement of the RNAi field.

To conclude, the myr-TP-Tf peptide shows stable siRNA condensation and protection capability against serum and RNase A. Moreover, the novel peptide construct successfully delivered siRNA in amounts that significantly reduced reporter luciferase levels beyond that of the established, industrial siRNA-delivery vehicle of Lipofectamine® in immortalized and primary cell lines. When combined, the data present an encouraging basis for continued exploration of the peptide *in vitro* and *in vivo*. In future work, we plan to use a fluorescently labeled peptide to better understand the exact transport mechanism(s) *in vitro* and *in vivo*. It will also elucidate the biodistribution pattern and neurotargeting ability of the peptide in a living system. The successful completion of preclinical studies will ultimately provide a promising strategy for therapeutic siRNA delivery to brain tissues, which may be useful for treating or relieving the symptoms of various NDDs and numerous other brain maladies.

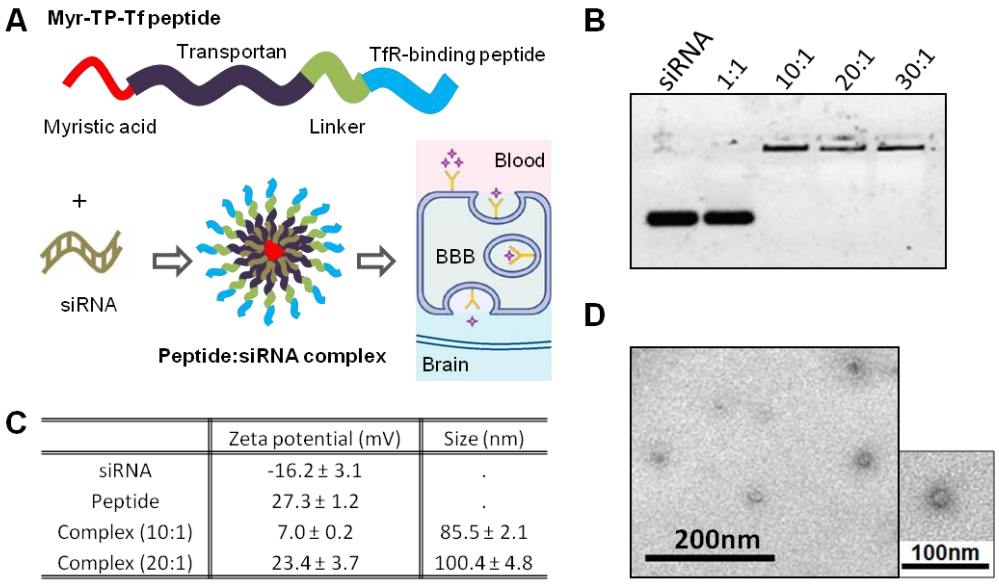

	Zeta potential (mV)	Size (nm)
siRNA	-16.2 ± 3.1	.
Peptide	27.3 ± 1.2	.
Complex (10:1)	7.0 ± 0.2	85.5 ± 2.1
Complex (20:1)	23.4 ± 3.7	100.4 ± 4.8

Figure 3.1. Design and characterization of myristoylated transportan peptide equipped with transferrin receptor targeting short peptide (myr-TP-Tf). (A) Illustration of myr-TP-Tf peptide and its postulated peptide:siRNA complex structure and expected brain-targeted siRNA delivery mechanism; (B) Gel retardation assay. Samples prepared in distilled water were loaded in a 0.8% agarose gel for electrophoresis at 100 V for 20 min in 1× TAE buffer (Tris-Acetate-EDTA) and (C) zeta potential and particle size measurements (n=3/group). Data reported as mean ± standard error; and (D) transmission electron microscopy images of peptide:siRNA complex (20:1 molar ratio).

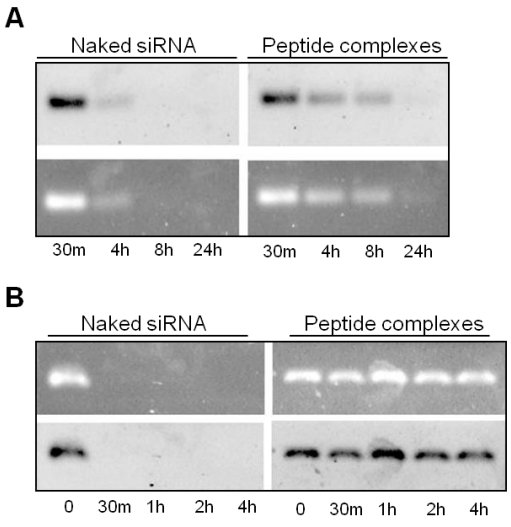

Figure 3.2. Comparison of siRNA stability – naked siRNA vs. siRNA-peptide complex forms. (A) siRNA stability against 50% fetal bovine serum, 0.8% agarose gel electrophoresis at 100V for 20 min in 1× TAE buffer and (B) siRNA stability against ribonuclease A, 0.8% agarose gel electrophoresis at 100V for 20 min in 1× TAE buffer.

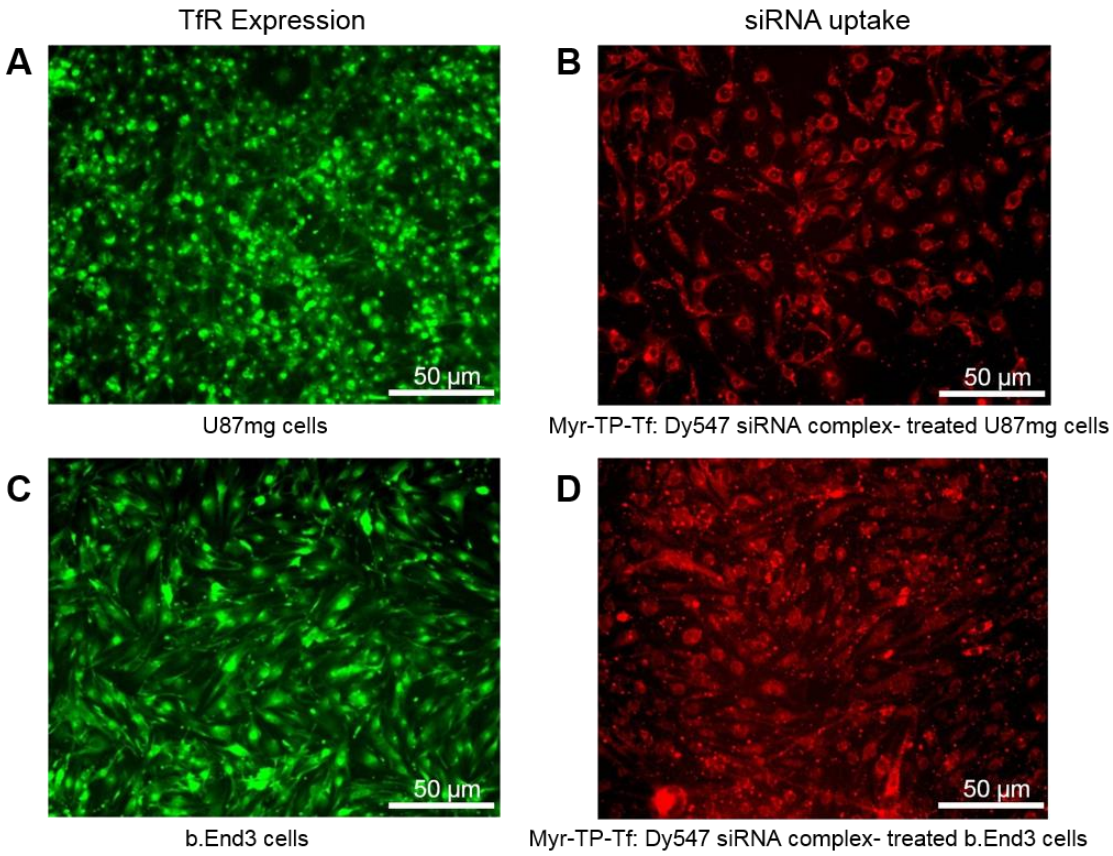

Figure 3.3. Verification of transferrin receptor expression and siRNA uptake in U87mg and b.End3 cells. Immunostaining of TfR on U87mg cells (A) and on b.End3 cells (C) and myr-TP-Tf:Dy547 siRNA complex-treated U87mg cells (B) and b.End3 cells (D).

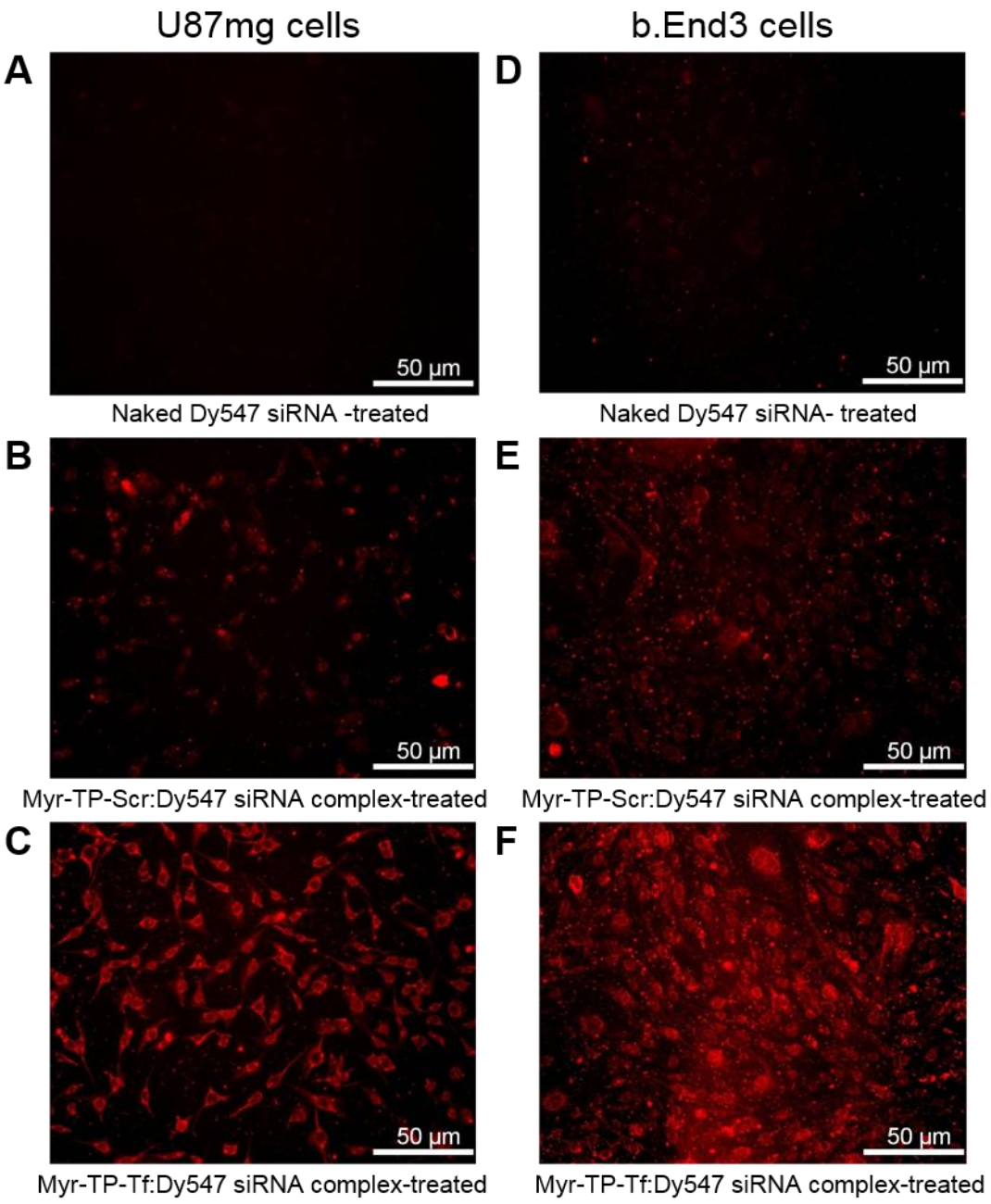

Figure 3.4. Enhanced siRNA uptake mediated by myr-TP-Tf. Naked Dy547-labeled siRNA-treated U87mg (A) and b.End3 cells (D); myr-TP-Scr:Dy547 siRNA complex-treated U87mg (B) and b.End3 cells (E); and myr-TP-Tf:Dy547 siRNA complex-treated U87mg (C) and b.End3 cells (F).

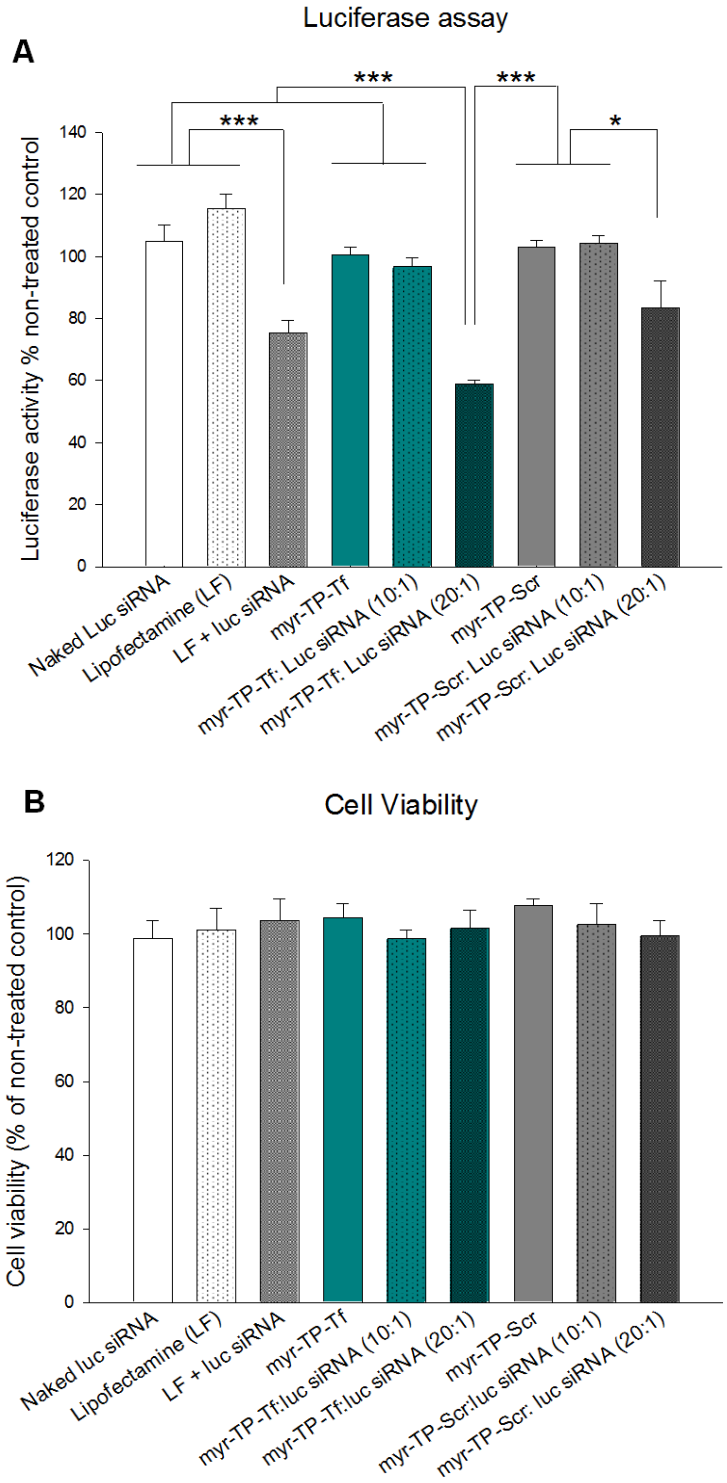

Figure 3.5. Transfection of myr-TP-Tf: Luciferase-siRNA to U87mg-Luc glioma cells. (A) Luciferase assay (n=5-7/group) and (B) cell viability assay (n=5/group) at 48 hr post-transfection. Data reported as mean ± standard error; one-way ANOVA with Tukey-Kramer post-hoc test was performed (*$p < 0.05$; **$p < 0.01$; ***$p < 0.001$).

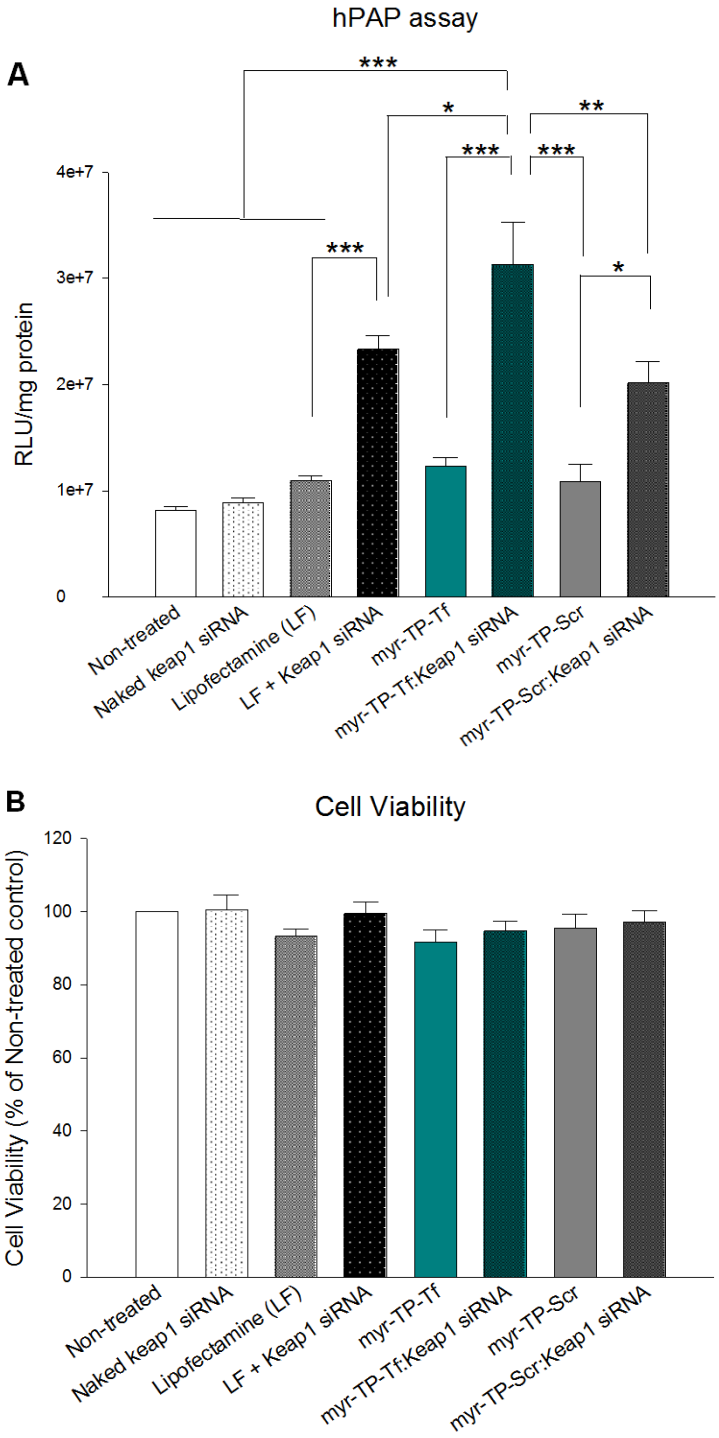

Figure 3.6. Transfection of myr-TP-Tf:Keap1 siRNA complex to primary murine neurons/astrocytes. (A) Human placental alkaline phosphatase (hPAP) assay (n=6/group) and (B) cell viability assay (n=5/group) at 48 hr posttransfection. Data reported as mean ± standard error; one-way ANOVA with Tukey-Kramer post-hoc test was performed (*$p < 0.05$; **$p < 0.01$; ***$p < 0.001$).

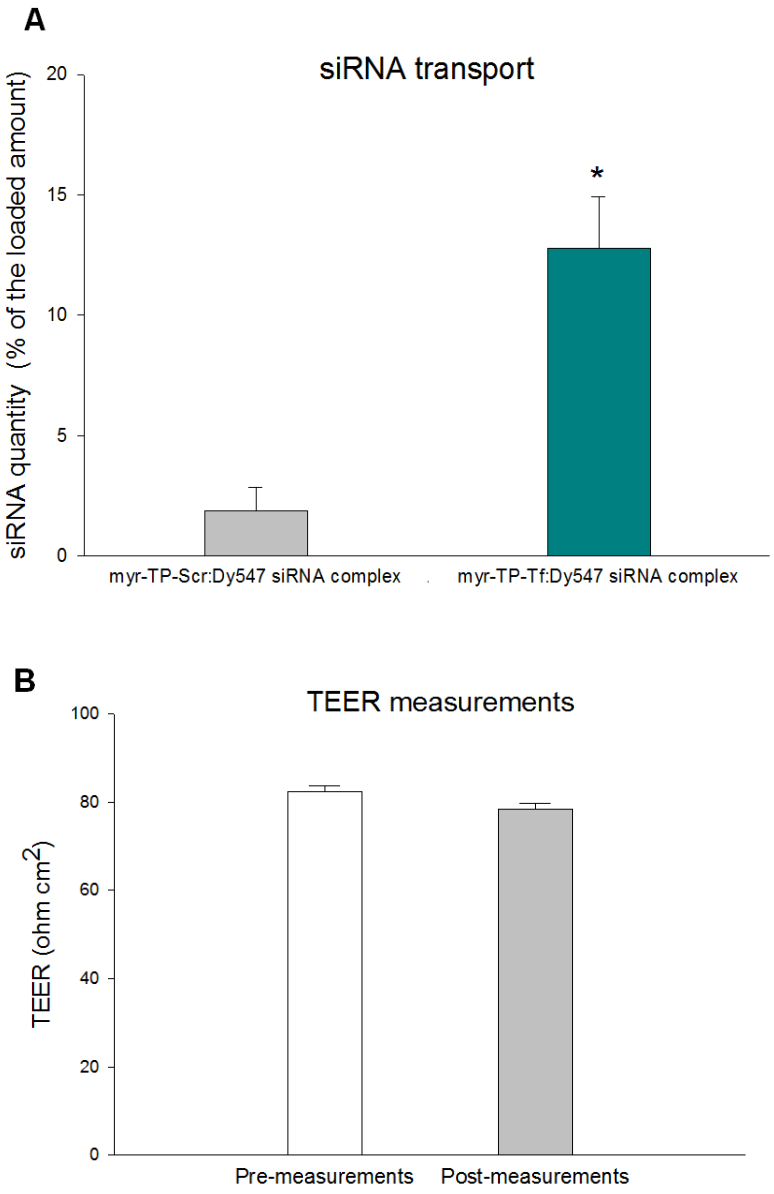

Figure 3.7. Assessment of siRNA transport across the b.End3 monolayer in a transwell system 6 hr after serum-free treatment. (A) Comparison of siRNA transport by myr-TP-Scr peptide:Dy547 siRNA complex vs. myr-TP-Tf:Dy547 siRNA complex (n=6/group). Student's t-test was performed (*$p < 0.05$) and also (B) TEER measurements before and after the transcytosis experiment (n=6/group).

3.6 Supplementary section

To examine the size distribution, the peptides and the siRNA-peptide complexes (100 nM of siRNA) were prepared in distilled water, separately. Samples were vortexed for 20 s and incubated for 20 min at room temperature. The size was measured with Zetasizer Nano ZS (Malvern Inc., Westborough, MA). Both myr-TP-Tf and myr-TP-Scr were found to be quite large (309.5 nm for myr-TP-Tf and 259.6 nm for myr-TP-Scr), which indicated that the peptides themselves may form larger structures or aggregates rather than being suspended as monomers (Figure 3.S1). The siRNA-peptide complexes displayed smaller size than the peptide sample (92.1 nm for siRNA/Myr-TP-Tf complex and 153.6 nm for siRNA/Myr-TP-Scr complex) with relatively narrow size distributions. It appears that the electrostatic interaction between the negatively charged siRNAs and the positively charged peptides contributes to the tight complex formation. The size difference between the siRNA/Myr-TP-Tf complex and the siRNA/Myr-TP-Scr complex was unexpected because the myr-TP-Tf and the myr-TP-Scr are basically the same, but only different in the arrangements of 12 amino acids in the targeting domain. It is thought that the distinct arrangement of the amino acids at the C-terminus may affect the complex size, possibly due to the different intermolecular interaction with the peptides and the aqueous medium. The dispersity (PDI) of the peptides and the complexes were not in the monodisperse range (PDI < 0.1), indicating that the actual hydrodynamic size of the peptides and the complexes can be varied.

To measure the zeta potential, the siRNA, peptides and the siRNA-peptide complexes (1:20) were prepared in distilled water, separately. Samples were vortexed for 20 s and incubated for 20 min at room temperature. The zeta potential was measured

with Zetasizer Nano ZS (Malvern Inc., Westborough, MA). The siRNA displayed a negative surface charge (-18.0 mV) because of its anionic phosphate backbone. Both myr-TP-Tf and myr-TP-Scr peptides showed positive surface charges (32.5 mV for the myr-TP-Tf and 28.0 mV for the myr-TP-Scr), which stem from four lysine residues in the transportan CPP domain and an arginine residue in the targeting domain (Figure 3.S2). The negative charge of the siRNA was shielded by the cationic peptides upon the siRNA-peptide complex formation (29.1 mV for siRNA/Myr-TP-Tf complex and 28.9 mV for siRNA/Myr-TP-Scr complex), which was consistent with the gel retardation assay result (Figure 3.1B).

Similar systems in the literature were looked at in order to understand the hydrodynamic size of the peptide. Ren et al. used a myristoylated cell-penetrating peptide fused with a tumor-targeting sequence as a siRNA delivery system, which displayed the particle size of 343 nm and the zeta potential of 31 mV when it formed siRNA-peptide complex. However, they did not show the particle size data of the peptide itself (49). Another group used a myristoylated polyarginine peptide to deliver siRNA to the cells (50) and Kumar et al. exploited nine arginie repeats linked to the rabies virus glycoprotein as a neurotargeted siRNA delivery system (51). However, both studies did not include any physicochemical characterization data although they showed positive biological effects.

Instead, a study about surfactant-like peptides that contain hydrophobic tails and one or two hydrophilic amino acids was checked (52). In this study, a short peptide composed of ten glycines and two aspartic acids ($G_{10}D_2$) was expected to have a length of 4.7 nm in its extended conformation. As our peptide system is composed of 43 amino

acids with a myristic acid at the N-terminal residue, it is expected that the myr-TP-Tf peptide can be larger than this $G_{10}D_2$ peptide. However, the hydrodynamic diameter of the myr-TP-Tf peptide sample (310 nm) was obviously too large to be considered as individual peptides. The molecular modeling and TEM images of the surfactant-like short peptides showed that they can form bilayer structures such as nanotubes with ~50 nm of diameter and varying ranges of length, and nanovesicles that are ~100 nm in diameter. This led us to think that our peptide system, even without siRNA, may also possibly form such structures that display relatively large size and longer length than the peptide monomer.

Many studies have used peptide amphiphiles that were designed for the anticancer drug delivery. For example, Javali et al. prepared C16 (palmitic acid)-RGD (arginine-glycine-aspartic acid) and C18 (stearic acid)-RGD for active targeting of tumor endothelium (53). We examined this study as our peptide system can also be classified into fatty acid-conjugated peptides. According to their data, these C16-RGD and C18-RGD formed self-assembled peptide amphiphile nanostructures and displayed a particle size of 266 nm and 450 nm, respectively. These relatively large hydrodynamic sizes were similar to what we observed from our peptide system. Although they described these as peptide amphiphile micelles and also showed critical micelle concentrations, the particle sizes were too large to be considered as micelles. We think that these fatty acid-conjugated peptide amphiphiles may possibly form large bilayer structures such as nanotubes and nanovesicles just as the surfactant-like peptides also do.

In a recent study, the Tirrell group investigated the *in vivo* biodistribution and the clearance of peptide amphiphile micelles composed of DSPE (Distearoyl

phosphoethanolamine)-PEG(2000)-CREKA (cysteine–arginine–glutamic acid–lysine–alanine, a fibrin-binding peptide) (54). This amphiphilic peptide formed spherical micelles that showed ~8 nm of hydrodynamic diameter in the DLS measurement. Our peptide system is quite different from this peptide amphiphile in that it has a single fatty acid chain per peptide and a longer amino acid sequence. If it can form micelle-like structures, however, it should still show small hydrodynamic sizes like this amphiphilic peptide. The relatively large particle size of our peptide system (260-310 nm) indicated that myr-TP-Tf peptides exist as large structures instead of micelles in the aqueous environment.

Another group used C16-ARLPRTMVHPKPAQP (Pal-L1), which can bind to hemagglutinin (HA), the surface protein of influenza virus (55). This palmic acid-conjugated peptide showed surfactant-like behaviors and formed micelles with a size of ~7 nm in diameter. Along with this small sized micelles, the DLS measurement showed an additional broad peak in 50-200 nm range. They explained that this Pal-L1 peptide may aggregate to form bigger micelles, rods or cylindrical form. Considering its similar composition with our peptide system, we think that myr-TP-Tf may also have the potential to form micelle structures. Judging from the size measurements (Figure 3.S1), however, it appears that the myr-TP-Tf peptides are more likely to form larger structures which may be similar to the entities found in the secondary peak of the Pal-L1 peptide.

A. Myr-TP-Tf

	Size (d.nm):	% Intensity:	St Dev (d.nm):
Peak 1:	309.5	100.0	29.47
Peak 2:	0.000	0.0	0.000
Peak 3:	0.000	0.0	0.000

PDI= 0.336~0.466

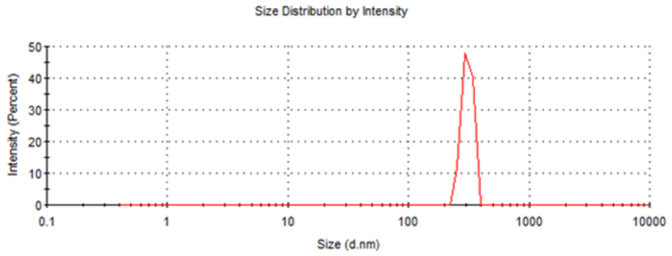

B. siRNA/Myr-TP-Tf complex (1:20)

	Size (d.nm):	% Intensity:	St Dev (d.nm):
Peak 1:	92.13	100.0	13.95
Peak 2:	0.000	0.0	0.000
Peak 3:	0.000	0.0	0.000

PDI= 0.252~0.355

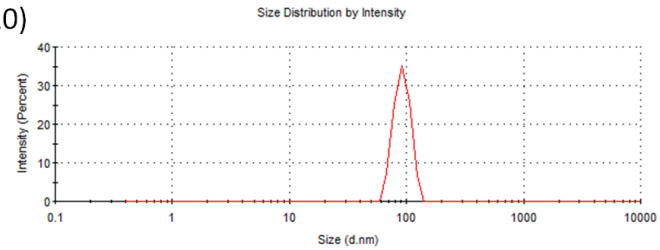

C. Myr-TP-Scr

	Size (d.nm):	% Intensity:	St Dev (d.nm):
Peak 1:	259.6	100.0	43.97
Peak 2:	0.000	0.0	0.000
Peak 3:	0.000	0.0	0.000

PDI= 0.420~0.507

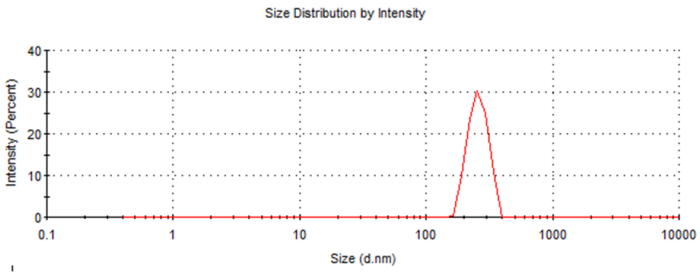

D. siRNA/Myr-TP-Scr complex (1:20)

	Size (d.nm):	% Intensity:	St Dev (d.nm):
Peak 1:	153.6	100.0	21.23
Peak 2:	0.000	0.0	0.000
Peak 3:	0.000	0.0	0.000

PDI= 0.345~0.491

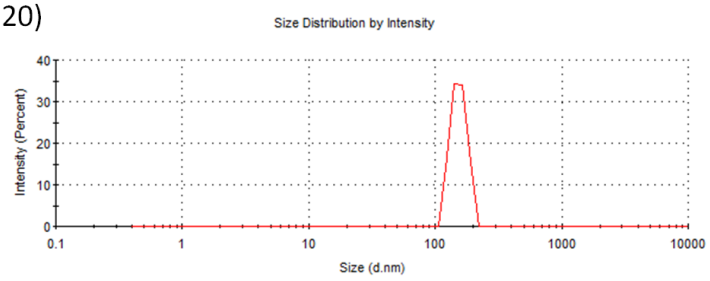

Figure 3.S1. Particle size measurements of the peptides and the siRNA-peptide complexes. (A) Myr-TP-Tf; (B) siRNA/Myr-TP-Tf complex (1:20); (C) Myr-TP-Scr; and (D) siRNA/Myr-TP-Scr complex (1:20).

A. siRNA

	Mean (mV)	Area (%)	St Dev (mV)
Peak 1:	-18.0	100.0	5.15
Peak 2:	0.00	0.0	0.00
Peak 3:	0.00	0.0	0.00

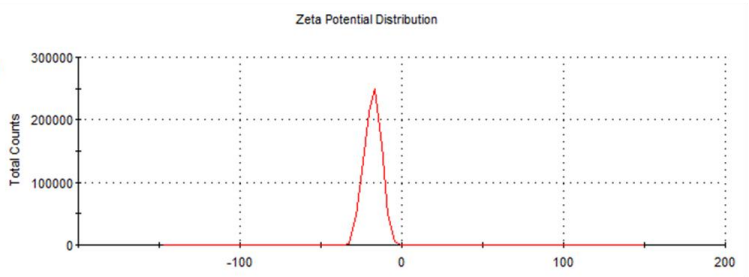

B. Myr-TP-Tf

	Mean (mV)	Area (%)	St Dev (mV)
Peak 1:	32.5	95.0	5.96
Peak 2:	48.5	5.0	1.81
Peak 3:	0.00	0.0	0.00

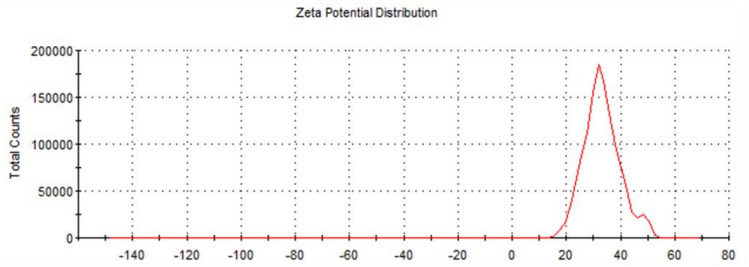

C. siRNA/Myr-TP-Tf complex (1:20)

	Mean (mV)	Area (%)	St Dev (mV)
Peak 1:	29.1	100.0	4.74
Peak 2:	0.00	0.0	0.00
Peak 3:	0.00	0.0	0.00

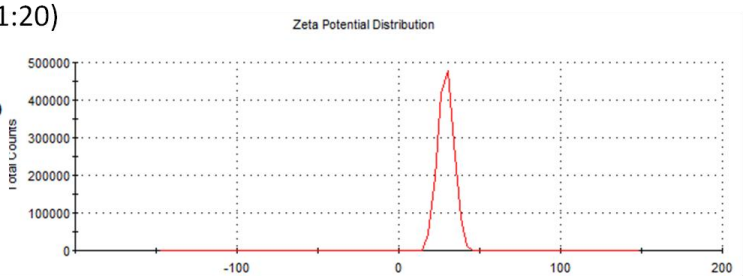

D. Myr-TP-Scr

	Mean (mV)	Area (%)	St Dev (mV)
Peak 1:	28.0	100.0	8.15
Peak 2:	0.00	0.0	0.00
Peak 3:	0.00	0.0	0.00

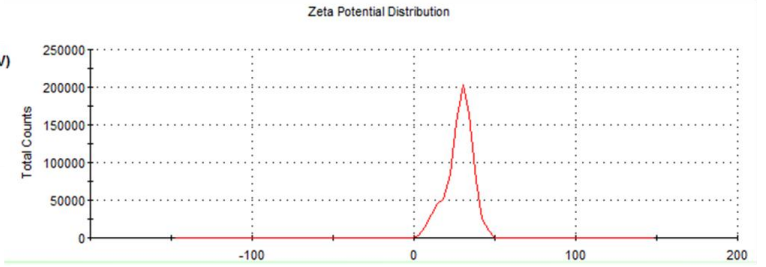

E. siRNA/Myr-TP-Scr complex (1:20)

	Mean (mV)	Area (%)	St Dev (mV)
Peak 1:	28.9	100.0	5.07
Peak 2:	0.00	0.0	0.00
Peak 3:	0.00	0.0	0.00

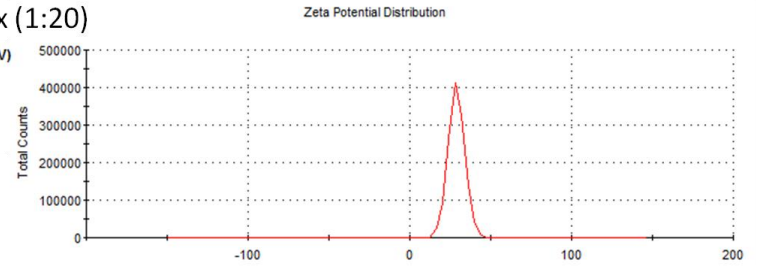

Figure 3.S2. Zeta potential measurements of the siRNA, peptides, and the siRNA-peptide complexes. (A) siRNA; (B) Myr-TP-Tf; (C) siRNA/Myr-TP-Tf complex (1:20); (D) Myr-TP-Scr; and (E) siRNA/Myr-TP-Scr complex (1:20).

3.7 References

1. Batsch NL, Mittelman MS. World Alzheimer report 2012: overcoming the stigma of dementia. London: Alzheimer's Disease International 2012.

2. Alzheimer's Association. 2013 Alzheimer's disease facts and figures. Alzheimers Dement 2013;9:208-45.

3. Abbott NJ, Rönnbäck L, Hansson E. Astrocyte–endothelial interactions at the blood–brain barrier. Nat Rev Neurosci 2006;7:41-53.

4. Pardridge WM. Blood-brain barrier biology and methodology. J Neurovirol 1999;5:556-69.

5. Pavan B, Dalpiaz A, Ciliberti N, Biondi C, Manfredini S, Vertuani S. Progress in drug delivery to the central nervous system by the prodrug approach. Molecules 2008;13:1035-65.

6. Groothuis DR. The blood-brain and blood-tumor barriers: a review of strategies for increasing drug delivery. Neuro-Oncology 2000;2:45-59.

7. Tiraboschi P, Hansen L, Thal L, Corey-Bloom J. The importance of neuritic plaques and tangles to the development and evolution of AD. Neurology 2004;62:1984-89.

8. Braak H, Tredici KD, Rüb U, de Vos RA, Jansen Steur EN, Braak E. Staging of brain pathology related to sporadic Parkinson's disease. Neurobiol Aging 2003;24:197-211.

9. Scherzinger E, Sittler A, Schweiger K, Heiser V, Lurz R, Hasenbank R, et al. Self-assembly of polyglutamine-containing huntingtin fragments into amyloid-like fibrils: implications for Huntington's disease pathology. Proc Natl Acad Sci 1999;96:4604-09.

10. Melo A, Monteiro L, Lima RMF, de Cerqueira MD. Oxidative stress in neurodegenerative diseases: mechanisms and therapeutic perspectives. Oxid Med Cell Longev 2011;2011:Article ID 467180.

11. Motohashi H, Yamamoto M. Nrf2-Keap1 defines a physiologically important stress response mechanism. Trends Mol Med 2004;10:549-57.

12. Barnham KJ, Masters CL, Bush AI. Neurodegenerative diseases and oxidative stress. Nat Rev Drug Discov 2004;3:205-14.

13. Calkins MJ, Johnson DA, Townsend JA, Vargas MR, Dowell JA, Williamson TP, et al. The Nrf2/ARE pathway as a potential therapeutic target in neurodegenerative disease. Antioxid Redox Sign 2009;11:497-508.

14. Itoh K, Wakabayashi N, Katoh Y, Ishii T, Igarashi K, Engel JD, et al. Keap1 represses nuclear activation of antioxidant responsive elements by Nrf2 through binding to the amino-terminal Neh2 domain. Gene Dev 1999;13:76-86.

15. Kobayashi M, Yamamoto M. Molecular mechanisms activating the Nrf2-Keap1 pathway of antioxidant gene regulation. Antioxid Redox Sign 2005;7:385-94.

16. Layzer JMM, A. P.; Tanner, A. K.; Huang, Z.; Kay, M. A.; Sullenger, B. A. *In vivo* activity of nuclease-resistant siRNAs. RNA 2004;10:766-71.

17. Turner JJ, Jones SW, Moschos SA, Lindsay MA, Gait MJ. MALDI-TOF mass spectral analysis of siRNA degradation in serum confirms an RNAse A-like activity. Mol Biosyst 2006;3:43-50.

18. Nakajima H, Kubo T, Semi Y, Itakura M, Kuwamura M, Izawa T, et al. A rapid, targeted, neuron-selective, *in vivo* knockdown following a single intracerebroventricular injection of a novel chemically modified siRNA in the adult rat brain. J Biotechnol 2012;157:326-33.

19. Chen C, Mei H, Shi W, Deng J, Zhang B, Guo T, et al. EGFP-EGF1-conjugated PLGA nanoparticles for targeted delivery of siRNA into injured brain microvascular endothelial cells for efficient RNA interference. PloS One 2013;8:e60860.

20. Malmo J, Sandvig A, Vårum KM, Strand SP. Nanoparticle mediated p-glycoprotein silencing for improved drug delivery across the blood-brain barrier: a siRNA-chitosan approach. PloS One 2013;8:e54182.

21. Alvarez-Erviti L, Seow Y, Yin HF, Betts C, Lakhal S, Wood MJA. Delivery of siRNA to the mouse brain by systemic injection of targeted exosomes. Nat Biotechnol 2011;29:341-45.

22. Tao Y, Han J, Dou H. Brain-targeting gene delivery using a rabies virus glycoprotein peptide modulated hollow liposome: bio-behavioral study. J Mater Chem 2012;22:11808-15.

23. Xia CF, Zhang Y, Boado RJ, Pardridge WM. Intravenous siRNA of brain cancer with receptor targeting and avidin–biotin technology. Pharm Res 2007;24:2309-16.

24. Kuwahara H, Nishina K, Yoshida K, Nishina T, Yamamoto M, Saito Y, et al. Efficient *in vivo* delivery of siRNA into brain capillary endothelial cells along with endogenous lipoprotein. Mol Ther 2011;19:2213-21.

25. Wang YH, Hou YW, Lee HJ. An intracellular delivery method for siRNA by an arginine-rich peptide. J Biochem Bioph Meth 2007;70:579-86.

26. Leng Q, Goldgeier L, Zhu J, Cambell P, Ambulos N, Mixson AJ. Histidine-lysine peptides as carriers of nucleic acids. Drug News Perspect 2007;20:77.

27. Deshayes S, Morris M, Divita G, Heitz F. Cell-penetrating peptides: tools for intracellular delivery of therapeutics. Cell Mol Life Sci 2005;62:1839-49.

28. Gupta B, Levchenko TS, Torchilin VP. Intracellular delivery of large molecules and small particles by cell-penetrating proteins and peptides. Adv Drug Delivery Rev 2005;57:637-51.

29. Wender PA, Mitchell DJ, Pattabiraman K, Pelkey ET, Steinman L, Rothbard JB. The design, synthesis, and evaluation of molecules that enable or enhance cellular uptake: peptoid molecular transporters. Proc Natl Acad Sci 2000;97:13003.

30. Kim WJ, Christensen LV, Jo S, Yockman JW, Jeong JH, Kim YH, et al. Cholesteryl oligoarginine delivering vascular endothelial growth factor siRNA effectively inhibits tumor growth in colon adenocarcinoma. Mol Ther 2006;14:343-50.

31. Kumar P, Wu H, McBride JL, Jung KE, Kim MH, Davidson BL, et al. Transvascular delivery of small interfering RNA to the central nervous system. Nature 2007;448:39-43.

32. Ren Y, Hauert S, Lo JH, Bhatia SN. Identification and characterization of receptor-specific peptides for siRNA delivery. ACS Nano 2012;6:8620–31.

33. Pham W, Kircher MF, Weissleder R, Tung CH. Enhancing membrane permeability by fatty acylation of oligoarginine peptides. Chembiochem 2004;5:1148-51.

34. Galbiati F, Guzzi F, Magee AI, Milligan G, Parenti M. Chemical inhibition of myristoylation of the G-protein Gi1 alpha by 2-hydroxymyristate does not interfere with its palmitoylation or membrane association. Evidence that palmitoylation, but not myristoylation, regulates membrane attachment. Biochem J 1996;313:717-21.

35. Nelson AR, Borland L, Allbritton NL, Sims CE. Myristoyl-based transport of peptides into living cells. Biochemistry 2007;46:14771-81.

36. Ifediba MA, Medarova Z, Ng S-w, Yang J, Moore A. siRNA delivery to CNS cells using a membrane translocation peptide. Bioconjugate Chem 2010;21:803-06.

37. Lee JH, Engler JA, Collawn JF, Moore BA. Receptor mediated uptake of peptides that bind the human transferrin receptor. Eur J Biochem 2001;268:2004-12.

38. Van Kuik-Romeijn P, Platenburg GJ. Molecules for targeting compounds to various selected organs, tissues or tumor cells. US Patent No. 2010/0184947 A12010.

39. Gan L, Johnson DA, Johnson JA. Keap1-Nrf2 activation in the presence and absence of DJ-1. Eur J Neurosci 2010;31:967-77.

40. Rouault TA, Cooperman S. Brain iron metabolism. Semin Pediatr Neurol 2006;13:142-48.

41. Qian ZM, Li H, Sun H, Ho K. Targeted drug delivery via the transferrin receptor-mediated endocytosis pathway. Pharmacol Rev 2002;54:561-87.

42. Shayan G, Choi YS, Shusta EV, Shuler ML, Lee KH. Murine *in vitro* model of the blood-brain barrier for evaluating drug transport. Eur J Pharm Sci 2010;42:148-55.

43. Wilhelm I, Fazakas C, Krizbai IA. *In vitro* models of the blood-brain barrier. Acta Neurobiol Exp (Wars) 2011;71:113-28.

44. Leroueil PR, Berry SA, Duthie K, Han G, Rotello VM, McNerny DQ, et al. Wide varieties of cationic nanoparticles induce defects in supported lipid bilayers. Nano Lett 2008;8:420-24.

45. Kennedy MT, Pozharski EV, Rakhmanova VA, MacDonald RC. Factors governing the assembly of cationic phospholipid-DNA complexes. Biophys J 2000;78:1620-33.

46. Bartlett DW, Davis ME. Effect of siRNA nuclease stability on the *in vitro* and *in vivo* kinetics of siRNA-mediated gene silencing. Biotechnol Bioeng 2007;97:909-21.

47. Brown RC, Morris AP, O'Neil RG. Tight junction protein expression and barrier properties of immortalized mouse brain microvessel endothelial cells. Brain Res 2007;1130:17-30.

48. Hanson LR, Frey WH. Intranasal delivery bypasses the blood-brain barrier to target therapeutic agents to the central nervous system and treat neurodegenerative disease. BMC Neurosci 2008;9:S5.

49. Ren Y, Hauert S, Lo JH, Bhatia SN. Identification and characterization of receptor-specific peptides for siRNA delivery. ACS Nano 2012;6(10):8620–31.

50. Ifediba MA, Medarova Z, Ng S-w, Yang J, Moore A. siRNA delivery to CNS cells using a membrane translocation peptide. Bioconjugate Chem 2010;21(5):803-06.

51. Kumar P, Wu H, McBride JL, Jung KE, Kim MH, Davidson BL, et al. Transvascular delivery of small interfering RNA to the central nervous system. Nature 2007;448(7149):39-43.

52. Santoso S, Hwang W, Hartman H, Zhang S. Self-assembly of surfactant-like peptides with variable glycine tails to form nanotubes and nanovesicles. Nano Lett 2002;2(7):687-91.

53. Javali NM, Raj A, Saraf P, Li X, Jasti B. Fatty acid–RGD peptide amphiphile micelles as potential paclitaxel delivery carriers to αvβ3Integrin overexpressing tumors. Pharm Res 2012;29(12):3347-61.

54. Chung EJ, Mlinar LB, Sugimoto MJ, Nord K, Roman BB, Tirrell M. *In vivo* biodistribution and clearance of peptide amphiphile micelles. Nanomed-Nanotechnol 2014.

55. Hüttl C, Hettrich C, Miller R, Paulke B-R, Henklein P, Rawel H, et al. Self-assembled peptide amphiphiles function as multivalent binder with increased hemagglutinin affinity. BMC Biotechnol 2013;13(1):51.

CHAPTER 4

CYTOPROTECTION AGAINST BETA-AMYLOID (Aβ) PEPTIDE-MEDIATED OXIDATIVE DAMAGE AND AUTOPHAGY BY KEAP1 RNAI IN HUMAN GLIOMA U87MG CELLS [1]

4.1 Abstract

Extensive oxidative stress has been considered one of the primary pathological factors responsible for the onset and/or progression of many neurodegenerative disorders (NDDs). We speculated that the oxidative damage to brain cells can be managed by promoting the endogenous cellular antioxidant defense system through the RNA interference (RNAi) approach against the Keap1 (kelch-like ECH-associated protein) gene. Keap1 acts as a negative regulator of Nrf2 (NF-E2-related factor 2) that represses the activation of the antioxidant responsive element (ARE) and thus endogenous antioxidant transcription. Here, we investigated whether Keap1 knockdown enhances the cellular antioxidant capacity and ultimately provides neuroprotection against oxidative stress from hydrogen peroxide and beta-amyloid (Aβ) peptide in human glioma U87mg cells. We found that the Keap1 siRNA pretreated group displayed higher expression of diverse antioxidant genes and an increased total antioxidant capacity compared to the

[1] Reprinted from *Neuroscience Research*, Pilju Youn, Yizhe Chen, and Darin Y. Furgeson, Cytoprotection against beta-amyloid (Aβ) peptide-mediated oxidative damage and autophagy by Keap1 RNAi in human glioma U87mg cells, Jan.20, 2015, with permission from Elsevier.

control group. Moreover, the Keap1 RNAi exerted a cytoprotective effect against exclusive H_2O_2 treatment. In Aβ peptide treatment experiments, the Keap1 siRNA pretreated groups maintained acceptable cell viability, relatively intact cellular morphology, and controlled oxidative damage levels while the control groups were affected by Aβ peptide-mediated neurotoxicity. Autophagosome staining and immunoblotting for the LC3-II (microtubule-associated protein light chain 3) protein, an autophagy marker, indicated that Keap1 RNAi may attenuate the oxidative stress-mediated autophagy as well. These findings suggest that Keap1 RNAi can serve as a therapeutic strategy for relieving oxidative stress-associated symptoms in many NDDs.

4.2 Introduction

Neurodegenerative disorder (NDD) incidences have been growing steadily on a global scale, making Alzheimer's disease (AD) the most common form of dementia; it is ranked sixth among the leading causes of death in the US as of 2013 (1). Memory robbing AD is typified by progressive loss of neuronal functions and brain shrinkage, with pathogenesis initiated from the accumulation of amyloid plaques, according to the amyloid hypothesis (2). Thus, therapeutic development has focused on clearing the plaques by using amyloid plaque-specific antibodies such as solanezumab and bapineuzumab. However, recent clinical trials of these drugs have failed to show determinative effects on cognitive improvement (3). Currently, crenezumab, another amyloid plaque targeting antibody, is being tested as a preventive medicine for a population with no AD signs, but that are at high risk to develop early onset AD due to the presenilin-1 mutation (4). Instead of targeting the amyloid plaques, beta-secretase 1 (BACE1) inhibitor has been suggested to prevent amyloid plaque formation by

interfering with the enzyme that cleaves the amyloid precursor protein (APP) to generate beta-amyloid (Aβ) (5). A clinical trial with a BACE inhibitor is also in progress with promising news of Aβ level reduction in cerebrospinal fluid (6). Along with amyloid plaques, hyperphosphorylated tau is considered a prime pathogenic contributor for AD (7). Inhibitors for protein kinases such as glycogen synthase kinase-3 have been investigated as a therapeutic intervention against the hyperphosphorylated tau-mediated pathology, and some are under clinical evaluation (8,9). Despite broad research efforts, there remains a critical need for cures or treatments to attenuate AD progression.

Other therapeutic strategies have targeted the extensive oxidative stress commonly observed in many NDDs, including AD. It has been suggested that oxidative stress is highly associated with neurodegeneration as either the cause or the consequence of its pathology (10). In AD, Aβ peptide-mediated oxidative stress has been considered a major contributing factor to neuronal damage (11). Therefore, researchers have attempted the administration of various antioxidants to deactivate the toxic reactive oxygen species (ROS). For example, α-tocopherol (vitamin E) showed a therapeutic effect in lowering amyloid plaque accumulation in a transgenic AD mouse model (12). The recent clinical trial also reported encouraging data that vitamin E slows the cognitive decline in AD patients (13). However, it does not appear to prevent disease progression and the high dosage of vitamin E may increase all-cause mortality (14).

As an alternative approach to exogenous antioxidants, the Nrf2 (NF-E2-related factor 2)-Keap1 (kelch-like ECH-associated protein) pathway has been highlighted for its cytoprotective potential in neurodegenerative conditions (15). Nrf2 is a transcription factor that translocates to the nucleus in response to oxidative stress and binds to the ARE

(antioxidant responsive element), leading to the expression of an array of various antioxidants and detoxification proteins (16). However, Keap1 normally suppresses Nrf2 activity by cytoplasmic sequestration and ubiquitin-mediated degradation (17). Hence, the downregulation of Keap1 through the RNAi approach will rescue Nrf2 activation, which will ultimately provide cellular antioxidant defense against oxidative assault. Indeed, studies have indicated that the knockdown of Keap1 or the overexpression of Nrf2, protected cells from oxidative damage (18,19). In addition, Keap1 RNAi was suggested as a chemoprevention strategy for cancer in which oxidative stress plays a key role for the initiation and promotion of the disease (20). Oxidative stress often induces autophagic signaling pathways, whose prolonged activation can lead to cell death as opposed to its beneficial roles for cell survival (21). It was also reported that the Aβ peptide induces autophagic cell death in U87 cells (22). This finding raised speculation that Keap1 RNAi would relieve oxidative stress through activation of the antioxidant defense system and therefore reduce autophagy-mediated cell death in brain cells.

Brain-targeted siRNA delivery, however, has been a formidable task largely due to the instability of naked siRNA in serum and the tight junctions in the brain vasculature which do not allow bulky and charged molecules, such as siRNA, to move across the BBB (22,23). Previously, we have designed a neurotargeting peptide-based siRNA carrier (myr-TP-Tf) that can protectively load siRNA and deliver bioactive siRNAs to brain cells. This leads to target gene silencing with a potential to cross a brain endothelial cell line monolayer *in vitro*, although the *in vivo* performance is yet to be proven (24). In the current study, we attempted Keap1 siRNA delivery with this carrier to evaluate the therapeutic potential of Keap1 RNAi against Aβ peptide and H_2O_2-

mediated oxidative stress in U87mg cells. As delineated in Figure 4.1, our hypothesis is that Keap1 siRNA delivered as a siRNA-peptide carrier complex will downregulate the Keap1 protein, allowing the nuclear translocation of Nrf2 and the subsequent activation of the ARE. The ensuing upregulation of antioxidant and detoxifying enzymes will protect cells from Aβ peptide and H_2O_2 -mediated oxidative stress. Here, the results showed that Keap1 RNAi enhanced the antioxidant capacity and provided cellular defense against the Aβ peptide and H_2O_2 as manifested by higher viability, relatively managed oxidative damage levels, and the basal autophagy level compared to the control groups. Taken together, the data suggest that Keap1 RNAi possesses the therapeutic potential for relieving the oxidative stress-associated damage in NDDs, which encourages further exploration in *in vivo* studies.

4.3 Materials and methods

4.3.1 Preparation of Keap1 siRNA and a peptide-based siRNA carrier

Human Keap1 siRNA was synthesized and purified at the DNA/Peptide Lab in the University of Utah HSC Core Research Facility. The sequence for each strand is as following; (sense) 5'-GGCCUUUGGCAUCAUGAACTT-3', (antisense) 5'-GUUCAUGAUGCCAAAGGCCTG-3' (20,25). The myristic acid conjugated, cell-penetrating peptide (transportan) equipped with a transferrin receptor-targeting peptide (myr-TP-Tf) was prepared by solid-phase peptide synthesis at Selleckchem (Houston, TX). The peptide sequence for myr-TP-Tf is as follows: myristic acid-GWTLNSAGYLLGKINLKALAALAKKIL-GGGG-THRPPMWSPVWP. The purity (>95%) and the molecular weight (4.5 kDa) of the peptide were confirmed upon receipt.

4.3.2 Cell culture: a human glioma U87mg cell line

Human glioma U87mg cells were maintained in DMEM (Dulbecco's Modified Eagle Medium, Invitrogen, Carlsbad, CA) supplemented with 10% fetal bovine serum and 100 U/mL of penicillin/streptomycin. The cells were cultured in a humidified incubator containing 5% CO_2 at 37 °C.

4.3.3 Formulation and transfection of Keap1 siRNA-peptide complex

Each strand of Keap1 siRNA was dissolved in sterile RNase-free water and annealed together by incubating both strands in an annealing buffer (10 mM Tris, 20 mM NaCl, pH 8.0) at 90 °C for 1 min and then cooling to room temperature. The siRNA solution was mixed with myr-TP-Tf peptide in distilled water at a 20:1 (peptide to siRNA) molar ratio which was determined as an optimal siRNA condensation ratio in our previous study (24). This mixture was vigorously vortexed for 20 s and incubated at room temperature for 20 min to form a siRNA-peptide complex. The U87mg cells were seeded either in 96-well plates or in 6-well plates at a density of 10^4 cells/cm^2 and grown until they reached 70-80% confluency. The cells were transfected with Keap1 siRNA-peptide complex in DMEM without serum and antibiotics for 3 hr and further incubated in a complete culture medium.

4.3.4 cDNA synthesis and quantitative real time PCR (qRT-PCR)

Total RNA of U87mg cells was extracted using Trizol reagent (Invitrogen) according to the manufacturer's instructions. RNA samples with purity of 1.9 or higher and 260/280 absorbance ratio were used to synthesize cDNA. Briefly, 1 μg of RNA was mixed with random primers, dNTPs in the reverse transcription buffer (New England

Biolabs, Beverly, MA), heated for 3 min at 70 °C, and then cooled in ice for 2 min. Subsequently, MMuLV RTase and RNase inhibitor (NEB) were added to make the final volume 20 μL. The cDNA synthesis reaction was conducted at 42 °C for an hour and then an enzyme deactivation step (90 °C for 10 min) was followed in a thermal cycler, after which cDNA samples were stored at -20 °C until use. Dilute cDNA and each gene-specific primer set were added to Express SYBR® GreenER™ qPCR Supermix (Invitrogen) and qRT-PCR was performed on a StepOnePlus™ real-time PCR system (Applied Biosystems, Carlsbad, CA). The reaction was conducted as follows: 50 °C for 2 min and 95 °C for 10 min (denaturation), 40 cycles of 95 °C for 15 s (amplification), and 60 °C for 1 min (elongation). The GAPDH (glyceraldehyde 3-phosphate dehydrogenase) mRNA transcript was included in the analysis as an internal control to determine the relative quantification of individual gene expression levels. The primer sequences are listed in Table 4.1.

4.3.5 Immunoblotting

The cells were washed with ice-cold phosphate buffered saline (PBS) and harvested using a cell lysis buffer (62.5 mM Tris-HCl (pH 6.8), 2% w/v SDS, 10% glycerol, 1% protease inhibitor). The cell lysates were sonicated for 10 s and centrifuged at 13,000 × g for 15 min to remove the cell debris. The supernatants were transferred to fresh tubes and each protein sample was quantified by a bicinchoninic acid (BCA) protein assay kit (Pierce, Rockford, IL) as per the manufacturer's instruction. Twenty μg of protein were loaded on each well of NuPAGE® Novex® 4-12% Bis-Tris gels (Invitrogen) for SDS-PAGE (120 V for 1.5 hr) in NuPAGE® MES SDS running buffer (Invitrogen). The proteins were then transferred to PVDF membranes in NuPAGE®

transfer buffer (Invitrogen) at 30 V for an hour. The membranes were blocked with TBST (Tris-buffered saline with 0.1% Tween-20) buffer containing 5% (w/v) nonfat dry milk for an hour and then washed with TBST buffer 3 times for 5 min each. The membranes were incubated with rabbit polyclonal anti-Keap1 antibody (Abcam Inc., Cambridge, MA, #ab139729), rabbit polyclonal anti-Nrf2 antibody (Santa Cruz Biotechnology, Inc., Dallas, TX, #sc-722), rabbit polyclonal anti-LC3B antibody (Sigma-Aldrich, St. Louis, MO, #L7543), and rabbit polyclonal anti-β actin antibody (Abcam, #ab8227) separately in TBST buffer containing 5% bovine serum albumin (BSA) at 4°C overnight. After rinsing 3 times for 5 min each, the membranes were incubated with goat polyclonal antibody to rabbit IgG conjugated with horseradish peroxidase (HRP) (Abcam, #ab6721) for an hour and then washed 3 times. The protein blots were visualized with WesternBright Quantum HRP substrate (Advansta, Menlo Park, CA) and the chemiluminescent images were acquired by using FluorChem FC2 imaging system (Alpha Innotech, San Leandro, CA).

4.3.6 Total antioxidant capacity (TAC) assay

Endogenous antioxidant activation was examined by measuring the cellular total antioxidant capacity using a TAC assay kit from Cell Biolabs, Inc. (San Diego, CA). This assay is based on the activities of antioxidant enzymes that reduce copper (II) to copper (I) through a single electron transfer mechanism (SET). The resulting copper (I) ions subsequently react with a coupling chromogenic reagent that has maximum absorbance at 490 nm. Briefly, the cells were harvested by trypsinization and washed twice with cold PBS. The cell suspension was sonicated for cell lysis and then centrifuged at 10,000 × g for 10 min at 4°C to remove the debris. The supernatants were

mixed with the assay buffer containing copper ion reagent and incubated for 5 min, after which the absorbance at 490 nm was measured using a microplate reader. The absorbance values were compared with a standard curve prepared with a set of uric acids with known concentrations and the total reductive capacity was normalized to the protein amount determined from a BCA assay.

4.3.7 Hydrogen peroxide (H_2O_2) treatment

Hydrogen peroxide solution (30% w/w in H_2O, Sigma-Aldrich) was diluted in sterile distilled water to prepare the stock solutions with concentrations from 10 mM to 30 mM. These stock solutions were then diluted in the complete culture medium to make cell treatments with concentrations ranging from 0.4 mM to 1.2 mM. The treatment volume was controlled not to exceed 5% of the total media volume and the nontreated control groups were given the equal volume of plain PBS.

4.3.8 Beta-amyloid (Aβ) peptide treatment

Aβ peptide (1-42) fragment was purchased from AnaSpec (San Jose, CA). The purity and the molecular weight of the peptide were confirmed upon receipt. The lyophilized peptide powder was dissolved in sterile distilled water and incubated at 37°C for 4 days to generate oligomeric forms. The peptide concentration was determined by using a NanoDrop™ 2000 spectrophotometer (Thermo Scientific, Wilmington, DE) that calculates the concentration from the absorbance at 280 nm and the parameters including the extinction coefficient (ε=1,280) and the molecular weight (4.51 kDa). Four hundred μM of Aβ peptide stock solution prepared in distilled water was diluted in the complete culture medium for the cell treatments.

4.3.9 Cell viability assay

Cell viability was determined by the cellular dehydrogenase activities that reduce the WST-8 (water soluble tetrazolium salt) to form colorimetric formazan dyes. The yellow colored formazan products are quantified from the absorbance at 450 nm. This assay was performed by using a CCK-8 assay kit (Dojindo, Rockville, MD) as per the manufacturer's instruction.

4.3.10 Malondialdehyde (MDA) assay

Oxidative damage to lipids was evaluated by measuring the MDA level using a lipid peroxidation assay kit (Abcam). Cells were collected by trypsinization and sonicated in MDA lysis buffer, after which the cell lysates were centrifuged at 13,000 × g for 10 min at 4°C. The supernatants were mixed with tribarbituric acid (TBA) solution and incubated at 95 °C for an hour to allow for the MDA-TBA adduct formation, which can be quantified by the absorbance at 532 nm. Samples were then cooled down in ice and placed in a 96-well plate for analysis in a microplate reader. The absorbance values were compared with a standard curve generated with MDA standard solutions. The MDA level was standardized to the protein amount determined from a BCA assay.

4.3.11 Protein carbonyl assay

Oxidative damage to proteins was examined by measuring the protein carbonyl content using a protein carbonyl colorimetric assay kit (Cayman Chemical Company, Ann Arbor, MI) as per the manufacturer's instructions. Briefly, the cells were lysed with sonication and then centrifuged at 10,000 × g for 10 min at 4°C. The supernatants were transferred to two tubes: one for testing samples and the other for serving as controls,

respectively. The 2,4-dinitrophenylhydrazine (DNPH) solution was added to the sample tubes and the 2.5 M hydrochloric acid solution was added to the control tubes. Both were incubated at room temperature in the dark for an hour to allow the reaction between 2,4-dinitrophenylhydrazine (DNPH) and protein carbonyls to form a Schiff base which can be analyzed colorimetrically by absorbance at 360-385 nm. After several steps of rinsing with trichloroacetic acid (TCA) solutions (20% and 10%), ethanol/ethyl acetate solution, the precipitated pellet was finally resuspended in guanidine hydrochloride solution and the protein-hydrozone products were quantified spectrophotometrically in a microplate reader. The resulting values were normalized to protein concentration calculated from a BCA assay.

4.3.12 Autophagy assay

Autophagy was assessed by staining cells with a fluorescent marker for lysosomal/autophagic vacuoles using a Cyto-ID® Autophagy Detection Kit from Enzo Life Sciences Inc. (Farmingdale, NY). Briefly, the cells were washed with the assay buffer and incubated with the Cyto-ID® green and Hoechst 33342 dyes diluted in DMEM containing no phenol red for 30 min. Following several rinses with the assay buffer, the relative autophagy level was determined by the fluorescence intensity measured with a wavelength set of Ex/Em (480 nm / 530 nm). The Hoechst 33342, used for the nuclei counter stain, was read with a wavelength set at 340/480 nm in a microplate reader. Fluorescence images were also acquired to visually examine the extent of autophagosome formation using an Olympus IX71F fluorescence microscope (Scientific Instrument Company, Aurora, CO).

4.3.13 Statistical analysis

The data were expressed as mean ± standard errors of the mean. The statistical analysis was conducted with one-way ANOVA followed by Tukey-Kramer HSD post-hoc analysis of the cell viability, oxidative damage and autophagy assays, and with a Student's t-test for qRT-PCR results. Statistical significance was noted by asterisks (*$p < 0.05$; **$p < 0.01$; ***$p < 0.001$). The graphs were drawn by using SigmaPlot 10.0 (Systat, San Jose, CA) and the statistical analysis was performed with JMP® v10.0 (SAS Institute Inc., Cary, NC).

4.4 Results

4.4.1 Functional downregulation of Keap1 gene and subsequent activation of antioxidant genes via Keap1 siRNA-peptide complex

We examined whether the Keap1 siRNA-peptide complex treatment affects cell viability in U87mg cells. The cells plated in 96-well plates were treated with either the siRNA-peptide complex (a mixture of 4 pmoles of siRNA and 80 pmoles of siRNA carrier peptide/well), or the myr-TP-Tf siRNA carrier itself (80 pmoles of siRNA carrier peptide/well) for 3 hr in serum-free DMEM and then subjected to the CCK-8 assay. The result revealed that neither the siRNA-peptide complex nor the carriers caused any noticeable cytotoxicity issues compared to the control group (Figure 4.2A). The Keap1 siRNA-peptide complex were also able to deliver functional siRNA to the cytosol, leading to the effective downregulation of Keap1 mRNA transcripts (72.2% reduction) at 48 hr posttransfection as shown in the qRT-PCR result (Figure 4.2B). The Keap1 RNAi ultimately downregulated the Keap1 protein expression level as well (> 90% reduction), which was detected from immunoblotting assays (Figure 4.2C and D). The decrease in

Keap1 gene expression level was not significantly different for the prolonged transfection group (72 hr) at the mRNA level, so we chose the 48 hr posttransfection as an optimal Keap1 gene downregulation time-point for the rest of our experiments. The Nrf2 proteins are identified as two bands at 98 kDa and 118 kDa. Along with the Keap1 downregulation, the Nrf2 protein level was increased compared to the control group (Figure 4.2E and F). The qRT-PCR results showed that Keap1 gene silencing did not affect the Nrf2 mRNA expression pattern (Figure 4.3A). However, it did subsequently facilitate the activation of various endogenous antioxidants and detoxifying enzymes under the ARE, such as NQO1 (NAD(P)H dehydrogenase, quinone 1) (3.1-fold, Figure 4.3B), SOD1 (superoxide dismutase 1) (1.8-fold, Figure 4.3C), and GCLM (glutamate-cysteine ligase, modifier subunit) (1.8-fold, Figure 4.3D). This result indicates that the Keap1 RNAi does not alter the basal Nrf2 mRNA expression, but may post-transcriptionally increase the Nrf2 protein level leading to subsequent ARE activation in U87mg cells.

4.4.2 Enhanced antioxidant capacity and cytoprotective effect against H_2O_2-induced oxidative assault

We investigated if Keap1 RNAi-mediated antioxidant upregulation enhances the cellular antioxidant capacity compared to the control group. To test this, the total antioxidant capacity (TAC) was evaluated by measuring the cellular reductive activity that converts the copper ion (I) to copper ion (II) by a single electron transfer mechanism. As anticipated, it was found that the TAC was significantly increased in the Keap1 RNAi group at 48 hr posttransfection (1.7-fold) while making little difference at 24 hr posttransfection (Figure 4.4A). Because the optimal downregulation of the Keap1 gene

was achieved at 48 hr posttransfection, the higher TAC level at 48 hr than at 24 hr posttransfection is possibly explained by the time-point at which the antioxidant genes are effectively activated. The improved antioxidant capacity was further assessed by monitoring the cell viability changes in response to the H_2O_2 treatment for 18 hr. Although both the control group and the Keap1 siRNA-peptide complex pretreated group showed dose-dependent cell death in the range of 0.4 mM to 1.2 mM of H_2O_2 treatment, the Keap1 RNAi groups generally showed better tolerance to the oxidative stress by displaying a bit higher viability than control groups at each concentration, except at 1.2 mM, the highest concentration (Figure 4.4B). In addition, the cells in the Keap1 RNAi group maintained relatively normal morphologies, whereas the control group had more dead cells losing their normal morphology at 0.8 mM of H_2O_2 treatment (Figure 4.4C).

4.4.3 Alleviation of Aβ peptide-induced cytotoxicity

The oligomeric forms of the Aβ (1-42) peptide are known to induce oxidative damage, which plays a key role in the neurodegeneration process in patients with AD (26). We examined whether the Keap1 siRNA-peptide complex pretreatment can provide cellular protection against the Aβ peptide in U87mg cells. The Keap1 siRNA-peptide complex pretreated groups were treated with Aβ peptide at 5 μM and 20 μM for 18 hr along with the control groups and the CCK-8 assay followed. As opposed to the control groups, which showed a dose-dependent decrease in cell viability to the Aβ treatment (~80% viability at 5 μM Aβ and ~57% viability at 20 μM Aβ), the Keap1 RNAi group displayed fairly intact cell viability at both 5 μM and 20 μM of Aβ concentration (Figure 4.5A), supporting our hypothesis that the Keap1 RNAi-mediated antioxidant activation protects cells from Aβ-induced neurotoxicity. The cell images also demonstrated that the

control groups were more vulnerable to the Aβ treatment, as revealed from their unusual cell aggregate formation and somewhat abnormal morphology (Figure 4.5B, upper panel). On the other hand, the Keap1 siRNA-peptide complex pretreated group displayed relatively normal cell shapes with fewer cell clumps (Figure 4.5B, lower panel).

4.4.4 Endogenous antioxidant defense against oxidative damage to cellular components

To ascertain whether the Keap1 RNAi has a neuroprotective effect against oxidative stress, the extent of the oxidative damage to biomolecules such as lipids and proteins was assessed. First, the control group and the Keap1 siRNA-peptide complex pretreated group were treated with 20 μM of Aβ for 18 hr and then cells were assayed. The lipid damage and the protein damage were examined by quantifying the malondialdehyde (MDA) level and the protein carbonyl content, respectively. As shown in Figure 4.6A, the nontreated group had ~30% higher MDA levels after oxidative assault compared to the control group, whereas the Keap1 RNAi group did not show a significant difference in MDA levels with the nontreated group. The protein carbonyl content exhibited even more of a prominent difference between these two groups; the control group had ~ 4-fold increased protein carbonyl content in response to the Aβ treatment while only ~1.5-fold increased protein carbonyl level was observed in the Keap1 RNAi group (Figure 4.6B). These findings corroborated our speculation that the activation of endogenous antioxidant genes elicited a neuroprotective effect against Aβ peptide-mediated oxidative stress.

4.4.5 Controlled autophagy level in U87mg cells

It has been reported that oxidative stress causes autophagy in human glioma cell lines (27). To examine the Keap1 RNAi effect on the autophagy level, we stained the cells with an autophagosome vacuoles-specific fluorescent dye. The fluorescence intensity indicated that the control group had relatively more autophagic activity under oxidative stress while the Keap1 RNAi group displayed similar levels of intensity with the nontreated group (Figure 4.7A). The autophagosomal staining was also visually examined under a fluorescence microscope. As shown in Figure 4.7B, the control groups had more punctate autophagic vacuoles in response to the oxidative stress compared to the Keap1 RNAi group, as in accordance with the fluorescence intensity data. In the non-treated groups, the green fluorescence was dispersed through the cytosol or was rather weak, while its intensity was increased and focused upon oxidative assault. The punctate green fluorescence was also observed in Keap1 RNAi groups under oxidative stress, but to a relatively lesser extent compared to the nontreated control. It is well known that, along with autophagy activation, the LC3-I protein is converted into the LC3-II form which is specifically associated with the autophagosomal membrane (28). Therefore, the amount of LC3-II has served as a good indicator of the autophagic activity. The immunoblotting showed that the control groups had increased LC3-II form in response to the oxidative stress compared to the Keap1 siRNA-peptide complex pretreated group, which relatively maintained its basal level of LC3-II protein (Figure 4.7C). Contrary to our expectation, LC3-I was not decreased along with the LC3-II conversion and showed rather increased band intensity. A report explains that the LC3-II is usually detected with higher sensitivity than LC3-I. Therefore, the comparison of the amount of LC3-II rather

than the LC3-I/II ratio is a more accurate indication of the autophagy (22,29). Considering that the loading was controlled, it seems the increase in the absolute amount of LC3-II indicates autophagy activation upon oxidative stress. These results supported our postulation that the enhanced cellular antioxidant capacity balances the ROS level so that it can protect the cells from autophagy-mediated cell death.

4.5 Discussion

Extensive oxidative stress is highly involved in the pathology of many NDDs, including Alzheimer's disease (AD), Parkinson's disease (PD), Huntington's disease (HD), and amyotrophic lateral sclerosis (ALS) (30). In order to prevent and relieve the detrimental effects of oxidative damage, it seems promising to enhance the intrinsic cellular antioxidant defense system. In this study, we proposed the Keap1 RNAi approach to suppress the Keap1-directed negative regulation on Nrf2 and to eventually activate the Nrf2-ARE pathway for the expression of diverse antioxidants and detoxifying proteins. The results showed that Keap1 downregulation provides cytoprotective effects against Aβ and H_2O_2-mediated oxidative stress in U87mg cells. This demonstrates the therapeutic potential of Keap1 RNAi in brain cells under a pathological oxidative stress environment.

In a recent study, the Keap1 knockdown was attempted in a human colon cancer cell line where it showed relatively less accumulation of 4-HNE (4-hydroxynonenal), a lipid peroxidation indicator, upon oxidative assault compared to the control groups (19). Likewise, we were able to observe that Keap1 downregulation groups were more resistant to oxidative stress in U87mg cells displaying lower levels of MDA and protein carbonyls in Aβ-treated conditions. In H_2O_2 treatment experiments, the cell viability was

generally higher in the Keap1 RNAi groups than in the control groups. However, the Keap1 RNAi groups were still subject to H_2O_2 toxicity, showing a dose-dependent decrease in cell viability and morphological changes. In addition, the Aβ treatment resulted in increased protein carbonyl content in the Keap1 RNAi group as well, although the extent of the increase was much higher in the control groups (Figure 4.6B). It is likely that the oxidative stress beyond the endogenous antioxidant capacity would not be ameliorated properly, leading to oxidative damage and neuronal demise. To maximize cytoprotection, in the RNAi therapy aspect, we may adjust the parameters such as siRNA concentration, transfection duration, and even the siRNA sequences for the potent downregulation of the Keap1 gene.

Although the Keap1 knockdown holds therapeutic potential for oxidative stress-associated pathological conditions, the complete knockout of the Keap1 gene may not be beneficial as learned from a study in which homozygous Keap1 mutant mice did not survive more than 3 weeks after birth even with the constitutive expression of antioxidant proteins and drug metabolizing enzymes (31). This indicates that a certain level of Keap1 activity is required for survival. The siRNA amount used in our *in vitro* experiments was sufficient to significantly downregulate the Keap1 protein while having no harmful effect on cell viability. When the Keap1 RNAi therapy is applied to a living system, it will require a thorough consideration of the dose and the administration intervals of Keap1 siRNA to accomplish the anticipated therapeutic effect with no toxicity issues. Another consideration is that the Keap1 RNAi may not be effective if the Nrf2-ARE pathway is affected by the pathological condition. A study reported that Nrf2 was prominently found in the cytoplasm of the hippocampal neurons in AD patients,

suggesting that the machinery for the nuclear localization of Nrf2 may be impaired in AD (32). In this case, Keap1 knockdown may not be able to change the antioxidant expression status. This suggests that Keap1 RNAi therapy should be applied in the early stage of NDD progression because the treatment may not exert the adequate therapeutic effect due to the dysregulation of the Nrf2-ARE pathway and the excessive ROS generation in advanced NDD.

As Keap1 RNAi is expected to work better as a preventive medicine rather than a treatment for the later stages of NDDs, an earlier diagnosis should be accompanied for desired therapeutic outcomes. Many NDD drugs have failed partly because the treatment usually started after the neurodegeneration had already progressed too far to benefit from the therapeutics (33); this also shows the need for early diagnostic tools. In a recent study, the researchers validated a blood test in which the levels of ten lipids can be used to predict AD onset within 2 to 3 years with high accuracy (34). This early diagnostic is advantageous over current diagnosis techniques, such as lumbar puncture and PET scanning, which are invasive or expensive, and often unreliable. To achieve better clinical benefits from the Keap1 RNAi and other NDD therapeutics in general, it would also be very important to develop early diagnostic tools with high sensitivity and specificity.

Accumulation of the autophagic vacuoles has been commonly found in the postmortem brain tissues from AD patients and also in AD animal models, indicating that the autophagic pathway is highly associated with AD pathology (35,36). Although autophagy is a normal process that breaks down and recycles the unnecessary or damaged cytosolic components for cellular homeostasis (37), its misregulation can result in

pathological conditions and cell death. For example, studies have shown that the modulation of the autophagy process contributes to the accumulation of aberrant proteins and neurodegeneration (36,38). Extensive oxidative stress can also lead to prolonged autophagy, resulting in cell death (21). In this study, we have found that the Aβ and H_2O_2 treated cells displayed higher autophagic activity than the Keap1 RNAi groups, which also supports the view that the oxidative stress activates the autophagic pathway. Though it is not confirmed if the activated autophagy could serve as a survival process or a cell death mechanism, the attenuation of the oxidative stress via Keap1 RNAi seems beneficial for maintaining basal autophagy levels and cell survival.

While the Keap1 RNAi approach is to alleviate oxidative stress, it is still unclear if oxidative stress is the primary cause or the consequence of the neurodegenerative process. It was reported that metal-catalyzed oxidation contributes to the formation of Aβ aggregates in AD pathology (39). On the other hand, aberrant protein aggregates can be a major player that results in oxidative stress and neurodegeneration as evidenced by a study that showed Aβ produces H_2O_2 in brain cell lines and primary rat neuronal cultures (40). Although the underlying pathology for neurodegeneration has not been fully understood, it appears that oxidative stress, abnormal protein aggregates, and other neurodegenerative phenomena are closely linked, not necessarily as a sequential flow but presumably as a cycle of events (41). Thus, in a therapeutic point of view, it is also conceivable to apply a combinatorial approach such as Keap1 RNAi with an amyloid plaque-targeting therapeutic. The expectation of which is that it would manage the oxidative stress and clear the pathological plaques simultaneously, which might be more effective than a single therapy in preventing the debilitating effects on brain cells in AD.

In conclusion, we propose Keap1 RNAi as an NDD treatment for cytoprotection of brain cells against oxidative stress and autophagy-mediated cell death, possibly through the augmentation of the endogenous antioxidant capacity. In order to attain clinically meaningful therapeutic results, there should be more comprehensive considerations which include an appropriate regimen of Keap1 siRNA, a timely treatment with the aid of early diagnostic tools, and combined approaches with an anti-amyloid therapy to maximize the therapeutic benefit. Although it is still preliminary, the results here encourage us to further evaluate the therapeutic potential of Keap1 RNAi in a living system, such as AD animal models.

Table 4.1. Gene-specific primer sequences for qRT-PCR.

Gene	Forward primer	Reverse primer
hGAPDH	5'CCACTCCTCCACCTTTGAC3'	5'ACCCTGTTGCTGTAGCCA3'
hKeap1	5'CAGATTGGCTGTGTGGAGTT3'	5'GCTGTTCGCAGTCGTACTTG3'
hNrf2	5'ATAGCTGAGCCCAGTATC3'	5'CATGCACGTGAGTGCTCT3'
hSOD1	5'GATTCCATGTTCATGAGTTT3'	5'AGGATAACAGATGAGTTAAG3'
hNQO1	5'CAGTGGTTTGGAGTCCCTGCC3'	5'TCCCCGTGGATCCCTTGCAG3'
hGCLM	5'TGAAGGGACACCAGGACAGCC3'	5'GCAGTGTGAACCCAGGACAGC3'

(h: human)

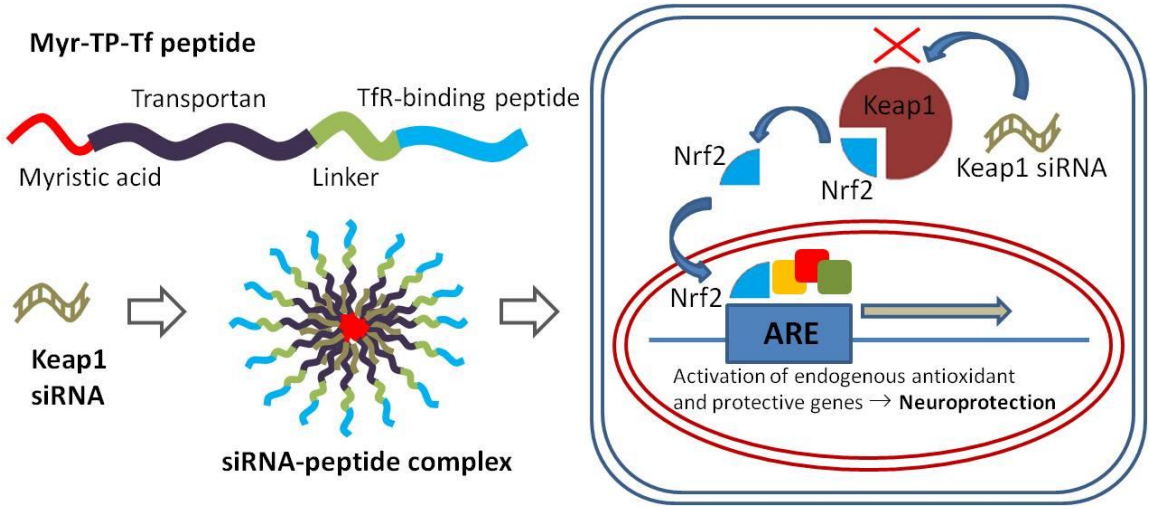

Figure 4.1. Illustration of the siRNA-peptide complex and Keap1 RNAi-mediated neuroprotection against oxidative stress.

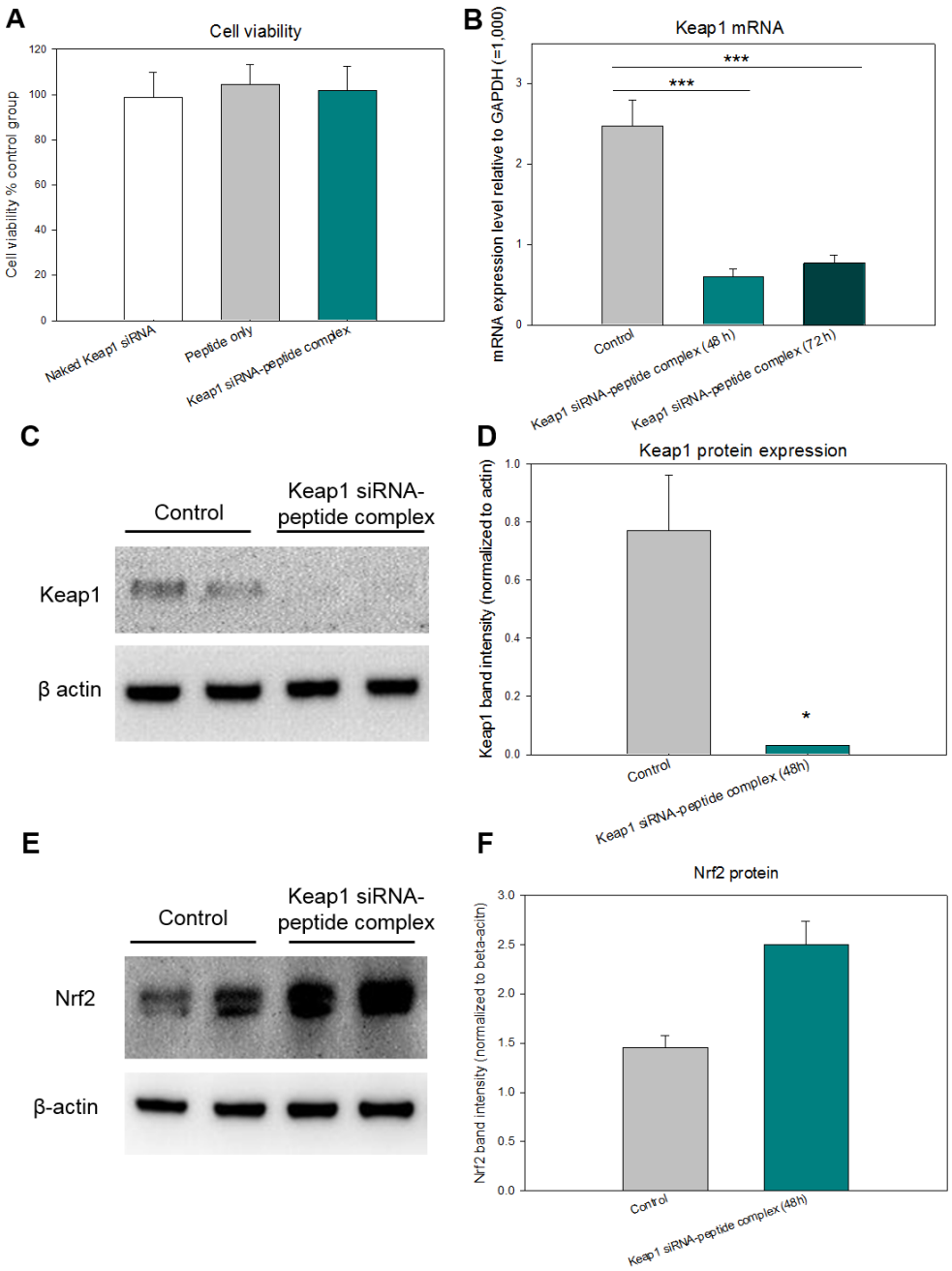

Figure 4.2. The cell viability and the gene regulation of Keap1 and Nrf2 after the treatment of Keap1 siRNA-peptide complex to U87mg cells. U87mg cells were transfected with Keap1 siRNA-peptide complex for 3 hr in a serum-free condition and then further incubated in a complete medium until specific times for assays. (A) Cell viability (n=5/group); (B) qRT-PCR for Keap1 mRNA transcript (n=3/group); (C) immunoblotting for Keap1 protein; (D) Keap1 protein band intensity; (E) immunoblotting for Nrf2 protein; and (F) Nrf2 protein band intensity.

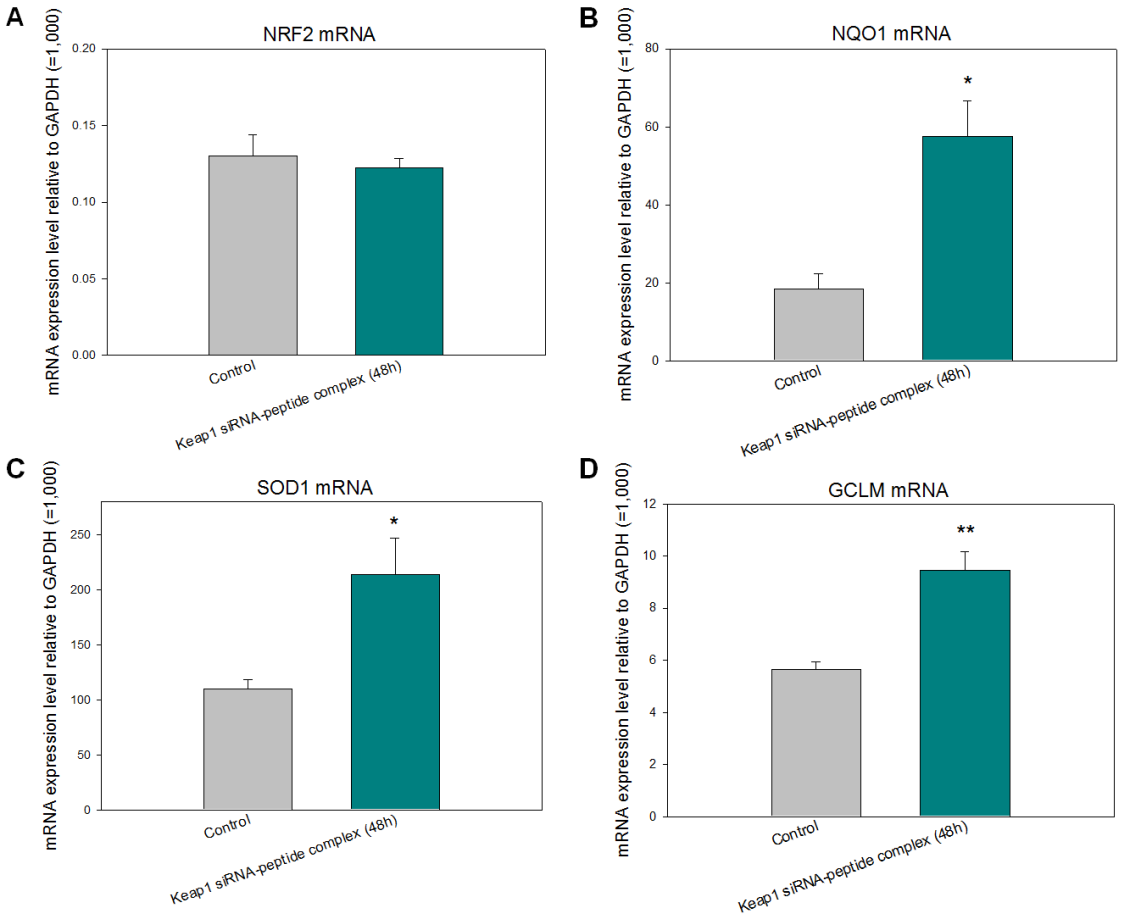

Figure 4.3. Gene regulation of Nrf2 and antioxidant genes under the antioxidant responsive element (ARE) after the treatment of Keap1 siRNA-peptide complex (48 h) in U87mg cells (n=3/group). (A) NRF2 mRNA; (B) NQO1 mRNA; (C) SOD1 mRNA; and (D) GCLM mRNA.

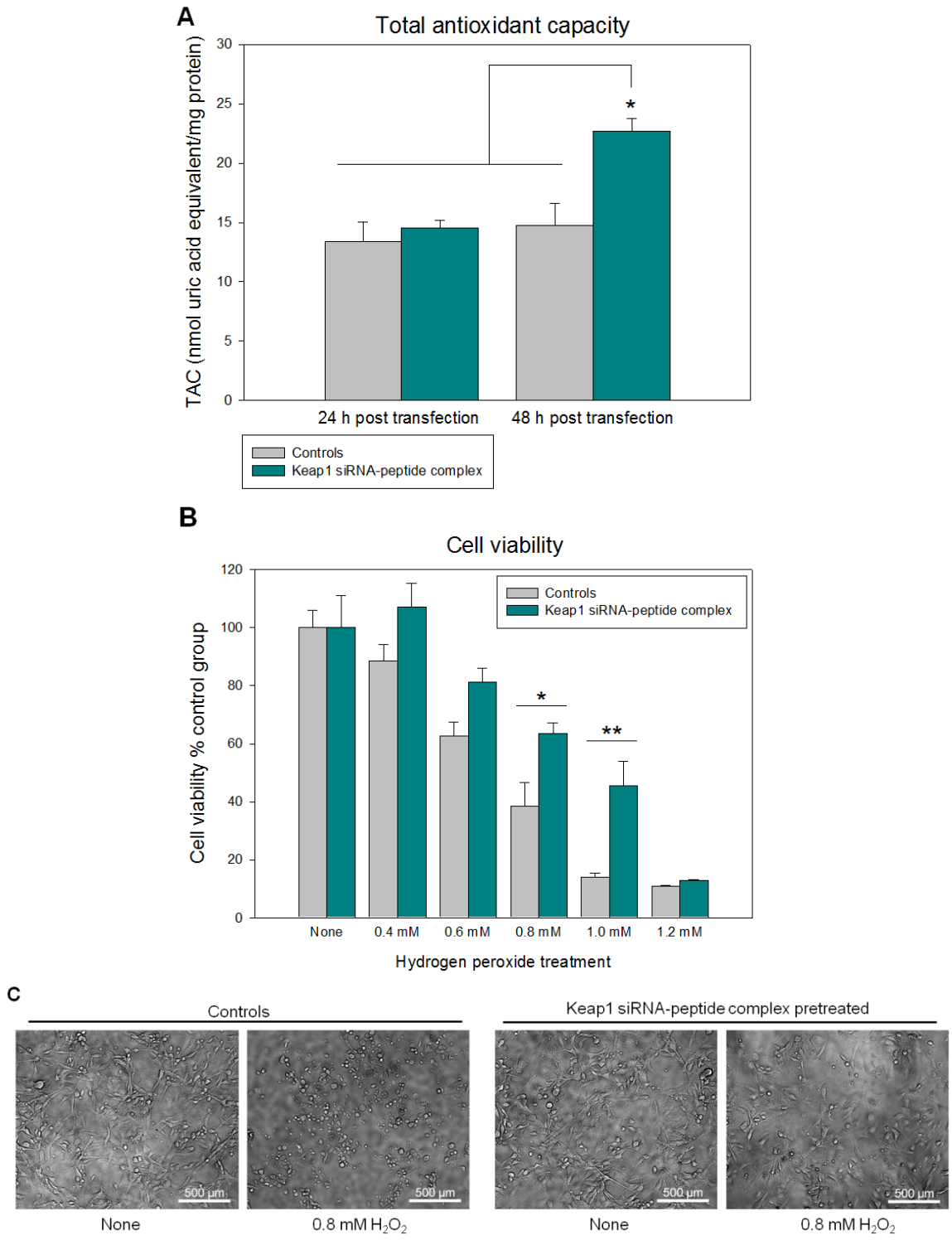

Figure 4.4. Keap1 siRNA-peptide complex treatment enhanced total antioxidant capacity and provided partial protection against hydrogen peroxide-mediated cell death in U87mg cells. (A) Total antioxidant capacity (n=4/group); (B) cell viability (n=4/group); and (C) cell morphology.

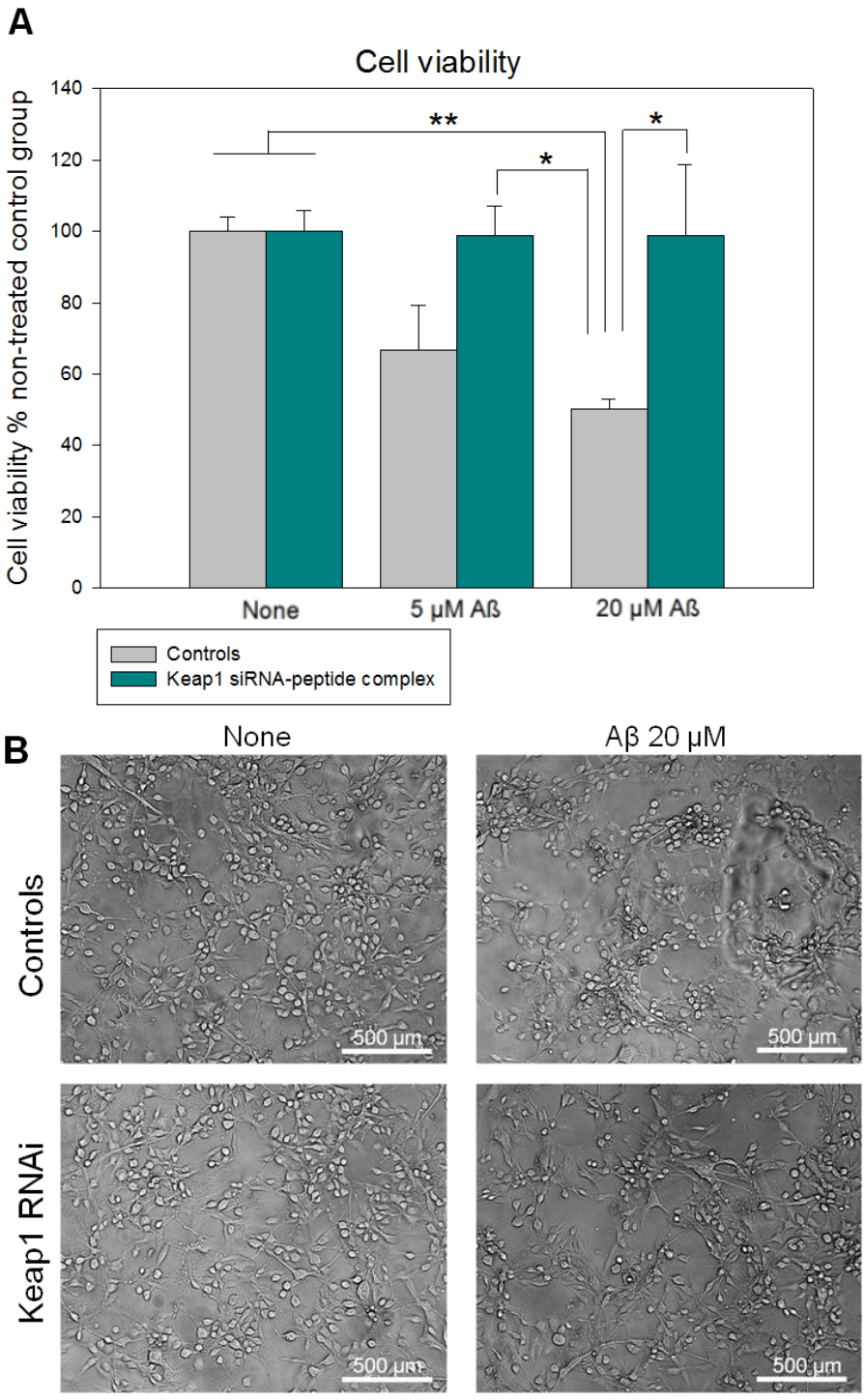

Figure 4.5. Aβ-induced cell stress and cytoprotection with pretreatment of Keap1 siRNA-peptide complex in U87mg cells. The cells were incubated with either 5 µM or 20 µM of Aβ peptide for 18 hr. (A) Cell viability (n=4/group); and (B) cell morphology examination under the light microscope.

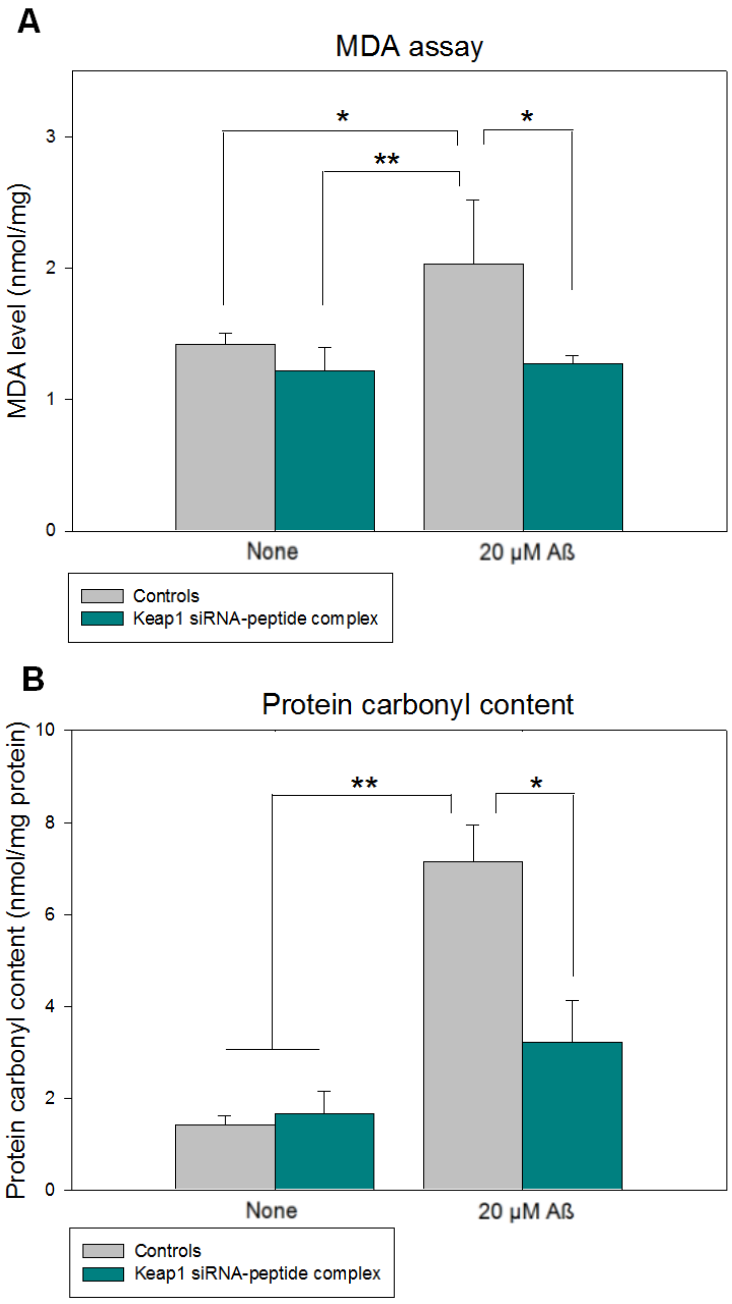

Figure 4.6. Protective effect of Keap1 RNAi against oxidative damage from Aβ peptide. U87mg cells were grown in 6-well plates and transfected with Keap1 siRNA-peptide complex for 3 hr and further incubated for 48 hr. The cells were then incubated with Aβ peptide for 18 hr until reaching specific time-points for oxidative damage assays. (A) Lipid damage (MDA assay, n=3/group); and (B) protein damage (protein carbonyl content assay, n=3/group).

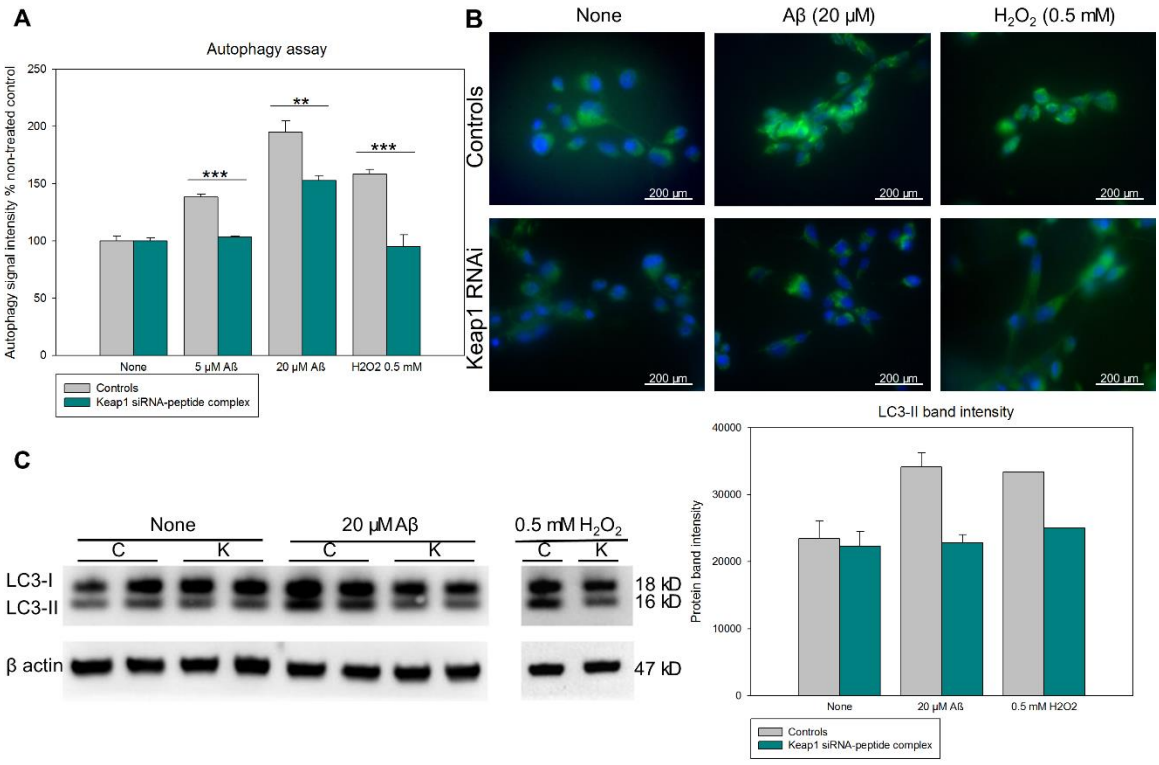

Figure 4.7. Protective effect of Keap1 RNAi against Aβ peptide-induced autophagy. U87mg cells were grown in 6-well plates and transfected with Keap1 siRNA-peptide complex for 3 hr and further incubated for 48 hr. The cells were then incubated with either Aβ (1-42) peptide or H_2O_2 for 18 hr until used for the autophagy assay and immunoblotting for LC3 protein. (A) The fluorescence intensity measured after the autophagic vacuole specific green fluorescent dye staining (n=4/group); (B) fluorescence microscopy images of cells stained with the autophagic vacuole specific green fluorescent dye; and (C) immunoblotting for LC3–I/II proteins and the calculated band intensity.

4.6 References

1. Alzheimer's Association. 2013 Alzheimer's disease facts and figures. Alzheimers Dement 2013;9:208-45.

2. Hardy J, Selkoe DJ. The amyloid hypothesis of Alzheimer's disease: progress and problems on the road to therapeutics. Science 2002;297:353-56.

3. Salloway S, Sperling R, Fox NC, Blennow K, Klunk W, Raskind M, et al. Two phase 3 trials of bapineuzumab in mild-to-moderate Alzheimer's disease. New Engl J Med 2014;370:322-33.

4. Garber K. Genentech's Alzheimer's antibody trial to study disease prevention. Nat Biotechnol 2012;30:731-32.

5. Robert V. BACE1: the beta-secretase enzyme in Alzheimer's disease. J Mol Neurosci 2004;23:105-14.

6. Merck Newsroom, http://www.mercknewsroom.com/press-release/alzheimers-disease/merck-presents-findings-phase-1b-study-investigational-bace-inhibit, accessed Aug. 19, 2014.

7. Arriagada PV, Growdon JH, Hedley-Whyte ET, Hyman BT. Neurofibrillary tangles but not senile plaques parallel duration and severity of Alzheimer's disease. Neurology 1992;42:631-31.

8. Le Corre S, Klafki HW, Plesnila N, Hübinger G, Obermeier A, Sahagún H, et al. An inhibitor of tau hyperphosphorylation prevents severe motor impairments in tau transgenic mice. P Natl Acad Sci 2006;103:9673-78.

9. Noble W, Planel E, Zehr C, Olm V, Meyerson J, Suleman F, et al. Inhibition of glycogen synthase kinase-3 by lithium correlates with reduced tauopathy and degeneration *in vivo*. P Natl Acad Sci 2005;102:6990-95.

10. Barnham KJ, Masters CL, Bush AI. Neurodegenerative diseases and oxidative stress. Nat Rev Drug Discov 2004;3:205-14.

11. Yatin S, Varadarajan S, Link C, Butterfield D. *In vitro* and *in vivo* oxidative stress associated with Alzheimer's amyloid ß-peptide (1–42). Neurobiol Aging 1999;20:325-30.

12. Sung S, Yao Y, Uryu K, Yang H, LEE VM, Trojanowski JQ, et al. Early vitamin E supplementation in young but not aged mice reduces Aβ levels and amyloid deposition in a transgenic model of Alzheimer's disease. Faseb J 2004;18:323-25.

13. Dysken MW, Sano M, Asthana S, Vertrees JE, Pallaki M, Llorente M, et al. Effect of vitamin E and memantine on functional decline in Alzheimer disease:

the TEAM-AD VA cooperative randomized trial. J Am Med Assoc 2014;311:33-44.

14. Miller ER, Pastor-Barriuso R, Dalal D, Riemersma RA, Appel LJ, Guallar E. Meta-analysis: high-dosage vitamin E supplementation may increase all-cause mortality. Ann Intern Med 2005;142:37-46.

15. de Vries HE, Witte M, Hondius D, Rozemuller AJM, Drukarch B, Hoozemans J, et al. Nrf2-induced antioxidant protection: a promising target to counteract ROS-mediated damage in neurodegenerative disease? Free Radical Bio Med 2008;45:1375-83.

16. Itoh K, Chiba T, Takahashi S, Ishii T, Igarashi K, Katoh Y, et al. An Nrf2/small Maf heterodimer mediates the induction of phase II detoxifying enzyme genes through antioxidant response elements. Biochem Bioph Res Co 1997;236:313-22.

17. Kobayashi A, Kang M-I, Okawa H, Ohtsuji M, Zenke Y, Chiba T, et al. Oxidative stress sensor Keap1 functions as an adaptor for Cul3-based E3 ligase to regulate proteasomal degradation of Nrf2. Mol Cell Biol 2004;24:7130-39.

18. Calkins MJ, Johnson DA, Townsend JA, Vargas MR, Dowell JA, Williamson TP, et al. The Nrf2/ARE pathway as a potential therapeutic target in neurodegenerative disease. Antioxid Redox Sign 2009;11:497-508.

19. Jung KA, Kwak MK. Enhanced 4-hydroxynonenal resistance in KEAP1 silenced human colon cancer cells. Oxid Med Cell Longev 2013;2013:Article ID 423965.

20. Devling TW, Lindsay CD, McLellan LI, McMahon M, Hayes JD. Utility of siRNA against Keap1 as a strategy to stimulate a cancer chemopreventive phenotype. P Natl Acad Sci 2005;102:7280-85.

21. Chen Y, McMillan-Ward E, Kong J, Israels S, Gibson S. Oxidative stress induces autophagic cell death independent of apoptosis in transformed and cancer cells. Cell Death Differ 2008;15:171-82.

22. Wang H, Ma J, Tan Y, Wang Z, Sheng C, Chen S, et al. Amyloid-β 1-42 induces reactive oxygen species-mediated autophagic cell death in U87 and SH-SY5Y cells. J Alzheimers Dis 2010;21:597-610.

23. Boudreau RL, Rodríguez-Lebrón E, Davidson BL. RNAi medicine for the brain: progresses and challenges. Hum Mol Genet 2011;20:R21-R27.

24. Youn P, Chen Y, Furgeson DY. A myristoylated cell-penetrating peptide bearing a transferrin receptor-targeting sequence for neuro-targeted siRNA delivery. Mol Pharmaceutics 2014;11:486-95.

25. Li W, Yu S-W, Kong A-NT. Nrf2 possesses a redox-sensitive nuclear exporting signal in the Neh5 transactivation domain. J Biol Chem 2006;281:27251-63.

26. Drake J, Link CD, Butterfield DA. Oxidative stress precedes fibrillar deposition of Alzheimer's disease amyloid β-peptide (1–42) in a transgenic Caenorhabditis elegans model. Neurobiol Aging 2003;24:415-20.

27. Zhang H, Kong X, Kang J, Su J, Li Y, Zhong J, et al. Oxidative stress induces parallel autophagy and mitochondria dysfunction in human glioma U251 cells. Toxicol Sci 2009;110:376-88.

28. Kabeya Y, Mizushima N, Ueno T, Yamamoto A, Kirisako T, Noda T, et al. LC3, a mammalian homologue of yeast Apg8p, is localized in autophagosome membranes after processing. EMBO J 2000;19:5720-28.

29. Mizushima N, Yoshimori T. How to interpret LC3 immunoblotting. Autophagy 2007;3:542.

30. Melo A, Monteiro L, Lima RMF, de Cerqueira MD. Oxidative stress in neurodegenerative diseases: mechanisms and therapeutic perspectives. Oxid Med Cell Longev 2011;2011:Article ID 467180.

31. Wakabayashi N, Itoh K, Wakabayashi J, Motohashi H, Noda S, Takahashi S, et al. Keap1-null mutation leads to postnatal lethality due to constitutive Nrf2 activation. Nat Genet 2003;35:238-45.

32. Ramsey CP, Glass CA, Montgomery MB, Lindl KA, Ritson GP, Chia LA, et al. Expression of Nrf2 in neurodegenerative diseases. J Neuropath Exp Neur 2007;66:75-85.

33. Lang AE. Clinical trials of disease-modifying therapies for neurodegenerative diseases: the challenges and the future. Nat Med 2010;16:1223-26.

34. Mapstone M, Cheema AK, Fiandaca MS, Zhong X, Mhyre TR, MacArthur LH, et al. Plasma phospholipids identify antecedent memory impairment in older adults. Nat Med 2014;20:415-18.

35. Nixon RA, Wegiel J, Kumar A, Yu WH, Peterhoff C, Cataldo A, et al. Extensive involvement of autophagy in Alzheimer disease: an immuno-electron microscopy study. J Neuropath Exp Neur 2005;64:113-22.

36. Yu WH, Cuervo AM, Kumar A, Peterhoff CM, Schmidt SD, Lee J-H, et al. Macroautophagy—a novel β-amyloid peptide-generating pathway activated in Alzheimer's disease. J Cell Biol 2005;171:87-98.

37. Mortimore GE, Schworer CM. Induction of autophagy by amino-acid deprivation in perfused rat liver. Nature 1977;270:176-76.

38. Hara T, Nakamura K, Matsui M, Yamamoto A, Nakahara Y, Suzuki-Migishima R, et al. Suppression of basal autophagy in neural cells causes neurodegenerative disease in mice. Nature 2006;441:885-89.

39. Dyrks T, Dyrks E, Hartmann T, Masters C, Beyreuther K. Amyloidogenicity of beta A4 and beta A4-bearing amyloid protein precursor fragments by metal-catalyzed oxidation. J Biol Chem 1992;267:18210-17.

40. Behl C, Davis J, Lesley R, Schubert D. Hydrogen peroxide mediates amyloid β protein toxicity. Cell 1994;77:817-27.

41. Andersen JK. Oxidative stress in neurodegeneration: cause or consequence? Nat Rev Neurosci 2004;5:S18–S25.

CHAPTER 5

IN VIVO EVALUATION OF A MYRISTOYLATED CELL-PENETRATING PEPTIDE FOR BRAIN-TARGETED SIRNA DELIVERY

5.1 Abstract

RNAi technology holds a therapeutic promise for many neurological diseases. However, brain-targeted siRNA delivery is challenged by restrictive brain vasculature. To obtain access to the brain compartment, we have designed a myristoylated cell-penetrating peptide equipped with a transferrin-receptor targeting short peptide (myr-TP-Tf) as a brain-targeted siRNA delivery system. Our previous work demonstrated that this siRNA-peptide complex system was able to achieve successful neuronal cell uptake and functional target gene silencing effect *in vitro*. Herein, we move forward to an *in vivo* study to examine whether this siRNA-peptide complex shows the brain targeting ability and the target gene downregulation effect in a living system. To compare the effects from local vs. systemic administration, the siRNA-peptide complex was given to adult mice via two different routes of administration: intracranial vs. retrobulbar injections. As expected for the direct administration, the intracranial injection groups displayed strong and persistent siRNA accumulation signals in the brain area and significant target gene silencing effect even at a relatively lower dose. Although the extent of the brain accumulation and the gene downregulation effect were lower than those of the intracranial injection groups, the retrobulbar injection also achieved a certain degree of

brain-targeted siRNA delivery, which produced a significant reporter protein (hPAP; human placental alkaline phosphatase) activity compared to other control groups. The results in this study, albeit limited, suggest that the siRNA/myr-TP-Tf complex system has a promising potential as an RNAi therapy tool for various neurological diseases.

5.2 Introduction

A recent study reported that the clinical trials for Alzheimer's disease (AD) treatments attempted over the last decade (2002-2012) recorded 99.6% failure rate with only five approved drugs, which merely provide temporary symptomatic relief (1). In light of the health and economic effects of AD, more research endeavors are required to develop AD drugs with substantial therapeutic effects. The investigational drugs studied until now include symptomatic agents, disease-modifying small molecules, and disease-modifying immunotherapies (2). While the amyloid deposits and the tau protein have been frequently focused as key pathological causes for neurodegeneration, no agent has been yet validated for these targets in clinical trials. To improve the success rate of AD drug trials, diverse modes of therapeutics with varying mechanisms of action need to be explored.

As one of the promising approaches for neurodegenerative disorders (NDDs), RNAi therapy has also a great therapeutic potential (3,4). The powerful gene silencing mechanism of RNAi can be employed to effectively downregulate the genes associated with the NDD pathogenesis. For instance, the β-secretase 1 (BACE 1), which contributes to the generation of the neurotoxic form of Aβ fragment, can be targeted to suppress the amyloid accumulation in an AD brain (5,6). The hyperphosphorylated tau protein, another putative culprit for AD progression, can be reduced by applying RNAi against

tau protein kinases such as glycogen synthase kinase 3 (GSK3) and cyclin-dependent kinase 5 (CDK5) (7-9). To protect neuronal cells against extensive oxidative stress, a common hallmark found in many NDDs, the RNAi approach could be utilized for the activation of the endogenous antioxidant system. In the Keap1 (kelch-like ECH-associated protein)-Nrf2 (NF-E2-related factor 2) pathway, the Nrf2, which is responsible for the activation of ARE (antioxidant responsive system), is repressed by the Keap1 protein. By downregulating the Keap1 gene, the Nrf2 can translocate to the nucleus where it binds to the ARE and subsequently activates the expression of various antioxidants and detoxifying enzymes (10).

However, the brain entry of large and charged molecules such as siRNA is impeded by the blood-brain barrier (BBB) (11,12). Moreover, siRNAs are susceptible to the serum nuclease-mediated degradation and clearance in the blood stream, raising a challenge for its use *in vivo* application (13-15). Previously, we have sought to overcome this obstacle by using a myristoylated cell-penetrating peptide equipped with a transferrin-receptor targeting sequence (myr-TP-Tf) for brain-targeted siRNA delivery. The siRNA-peptide complex demonstrated its promising properties *in vitro* by showing successful cellular uptake into the brain endothelial cells (b.End3) and primary murine neurons/astrocytes, functional target gene downregulation, and favorable siRNA transport across the b.End3 cell monolayer (16). In this study, the siRNA-peptide complex was further evaluated concerning brain targeting ability and the target gene silencing effect in a living system.

To assess the Keap1 gene RNAi effect, ARE-hPAP transgenic mice that contain the hPAP (human placental alkaline phosphatase) reporter gene in the ARE downstream

were used as an animal model. The siRNA-peptide complex was injected into these mice via two different routes to compare the performance from the local vs. systemic administrations. Although the tail vein injection is the most commonly adopted route for the systemic administration, the hPAP transgenic mice (C57/BL) were not favorable for this method because their dark and thick tail skins made it difficult to locate the veins. As an alternative, retrobulbar injection was attempted as a systemic administration method. It involves little distress to animals when properly executed under anesthesia. In addition, there are multiple veins located at the retrobulbar sinus (superficial temporal vein, supraorbital vein, ocular angle vein, dorsal nasal vein, inferior palpebral vein, and facial vein), which makes retrobulbar injection useful as an alternative route of systemic administration (17,18). As illustrated in Figure 5.1, the siRNA-peptide complex was prepared by mixing the siRNA and the peptide-based carrier at an optimal molar ratio (1:20 of siRNA to peptide), which was determined in the previous study. The siRNA-peptide complex suspension was given to the mice via either intracranial or retrobulbar injections per the dosage regimen described in the scheme. Here, the brain targeting ability of the siRNA-peptide complex was examined in live animals and the target gene knockdown capacity was assessed from brain tissues isolated after the injections.

5.3 Materials and methods

5.3.1 Formulation of the siRNA-peptide complex

The myristic acid conjugated cell-penetrating peptide (transportan) equipped with a transferrin receptor-targeting peptide (myr-TP-Tf) and the nontargeting scrambled peptide (myr-TP-Scr) were prepared by solid-phase peptide synthesis technique at SelleckChem (Houston, TX). The amino acid sequences for myr-TP-Tf and myr-TP-Scr

are as follows: myristic acid-GWTLNSAGYLLGKINLKALAALAKKIL-GGGG-THRPPMWSPVWP (myr-TP-Tf) and myristic acid-GWTLNSAGYLLGKINLKALAA-LAKKIL-GGGG-PWRPSHPVWMPT (myr-TP-Scr). The purity (>95%) and the molecular weight (4.5 kDa) of each peptide were validated in high-performance liquid chromatography (HPLC) and mass spectrometry analysis. The mouse Keap1 siRNA was prepared at the DNA/Peptide Lab in the University of Utah HSC Core Research Facility. The sequence for each strand is as follows: (sense) 5'- GCUAUGACCCGGACAGUGA-UU-3', (antisense), 5'- UCACUGUCCGGGUCAUAGCUU-3'. For the imaging study, the 5' end of the sense strand was labeled with Cy5.5 fluorescent dye. To prepare the siRNA-peptide complex, the siRNA solution was mixed with the peptide carrier in distilled water at a 20:1 (peptide to siRNA) molar ratio following our previous work (16). This mixture was vigorously vortexed for 20 s and incubated at room temperature for 20 min. All siRNA-peptide complex suspensions were freshly prepared before the injection.

5.3.2 Animals: human placental alkaline phosphatase (hPAP) transgenic mice/C57BL

Human placental alkaline phosphatase (ARE-hPAP) (+) transgenic mice were obtained from the Dr. Jeffrey Johnson lab (University of Wisconsin) and maintained in an animal facility according to the protocol approved by IACUC at University of Utah. Mice were genotyped with tail biopsy before weaning to verify the presence of the hPAP reporter gene and allowed to grow until they were 7 to 8 months old. The hPAP(+) mice were allocated for the gene downregulation study and the hPAP (-) mice were used for the imaging study. Both genders were included in this work. The average body weight of the mice was 34.2 ± 6.3 g (males: 40.2 ± 5.5 g; females: 30.7 ± 3.6 g) and none of

them showed any significant body weight change or detectable health issues during the study.

5.3.3 Retrobulbar and intracranial injection of the siRNA-carrier complex

The retrobulbar injection groups received three consecutive injections (50 μg of siRNA suspended in 100 μL of phosphate buffered saline loaded in 30-gauge insulin syringes) through the retrobulbar sinus with 24 hr intervals and were euthanized a day after the last injection for brain isolation. The retrobulbar injection technique was performed following the tips described in the literature (17). The intracranial injection groups also received three consecutive injections (5 μg of siRNA suspended in 5 μL of phosphate buffered saline per injection) into the brain cortices. The intracranial injection groups were prepared as following. The mouse head was shaved to remove the hair and disinfected with povidone-iodine solution. A ~2 to 3 mm incision was made along the midline of the scalp and a ~1 mm hole was made on the skull at a point 2 mm lateral and 1 mm anterior to the bregma by carefully drilling with a 26-gauge needle. The sterilized guide screw was rotated into the hole with a specially devised screwdriver and the incision was closed using tissue adhesives. The mice were placed back to the cages for 3 days to allow the incisions to be healed. The siRNA suspension was loaded into a modified 10 μL syringe (Hamilton Co. Reno, NV) attached to a 26-gauge needle and injected into the brain cortices by placing the needle through the guide screw, which controls the injection site and depth (~3 mm). The siRNA suspension was delivered over a minute and the needle was retained for additional 30 sec to ensure injection. During the injections and the screw insertion procedure, mice were anesthetized by placing the head in a nose cone that supplies vaporized isoflurane (3 %) and oxygen (with a flow rate at 1

liter/min). In the imaging study, the mice received a single injection for each route and were used immediately for taking images. Postprocedural monitoring was accompanied to examine any significant body weight changes or adverse signs during the study.

5.3.4 *In vivo* fluorescence imaging

For the imaging study, Cy5.5-labeled siRNA were used to formulate the siRNA-peptide complex. The PBS control, naked Cy5.5-siRNA-injected, Cy5.5 siRNA/myr-TP-Tf complex-injected, and Cy5.5 siRNA/myr-TP-Scr complex-injected mice were lined up under anesthesia and the near-infrared fluorescence (NIR) images were acquired using an IVIS 200 imaging system (Caliper Life Sciences, Hopkins, MA) at 1 hr, 2 hr, 24 hr, and 48 hr postinjection with a wavelength setting as excitation/emission of 675/694 nm. Both belly-side up and belly-side down positions were taken at each time-point to examine the fluorescence distribution.

5.3.5 Human placental alkaline phosphatase (hPAP) assay

The hPAP assay was performed according to the protocol established by the Dr. Jeffrey Johnson lab (19). Briefly, flash-frozen mouse brain tissues were homogenized in Tris/MgCl2/NaCl/CHAPS (TMNC) lysis buffer (0.05 M Tris, 0.005 M $MgCl_2$, 0.1 M NaCl, 4% 3-[(3-cholamidopropyl) dimethylammonio]-1-propanesulfonate [CHAPS]) and incubated at 65°C for 30 min in 200 mM diethanolamine buffer. The CSPD and Emerald reagents from Applied Biosystems (Bedford, MA) were used as substrates to evaluate the hPAP activity. Samples were placed in a white 96-well plate and the luminescence intensity was measured in a luminometer. Bicinchoninic acid (BCA) protein assay (Pierce, Rockford, IL) was conducted to quantify the protein concentration and the hPAP

activity was normalized to the protein quantity.

5.3.6 cDNA synthesis and quantitative real time PCR (qRT-PCR)

Total RNA of brain tissues was extracted using Trizol reagent (Invitrogen) according to the manufacturer's instructions. RNA samples with purity of 1.9 or higher and 260/280 absorbance ratio were used to prepare cDNA. Briefly, 1 μg of RNA was mixed with random primers, dNTPs in the reverse transcription buffer (New England Biolabs, Beverly, MA), heated for 3 min at 70 °C, and then cooled in ice for 2 min. Subsequently, MMuLV RTase and RNase inhibitor (NEB) were added to the reaction mixtures. The cDNA synthesis was conducted at 42 °C for an hour and then an enzyme deactivation step (90 °C for 10 min) followed. Diluted cDNA and each gene-specific primer set were mixed with EXPRESS SYBR® GreenER™ qPCR Supermix (Invitrogen) and qRT-PCR was performed on a StepOnePlus™ real-time PCR system (Applied Biosystems, Carlsbad, CA). The reaction was conducted as follows: 50 °C for 2 min and 95 °C for 10 min (denaturation), 40 cycles of 95 °C for 15 s (amplification), and 60 °C for 1 min (elongation). The GAPDH (glyceraldehyde 3-phosphate dehydrogenase) was included as an internal control for the relative quantification of each gene expression level. The sequences of the primer sets used in this study are listed in Table 5.1.

5.3.7 Immunoblotting

The flash-frozen mouse brain tissues were homogenized in a lysis buffer (62.5 mM Tris-HCl (pH 6.8), 2% w/v SDS, 10% glycerol, 1% protease inhibitor). The tissue lysates were sonicated for 10 s and centrifuged at 13,000 × g for 15 min to remove the debris. The supernatants were transferred to fresh tubes and each protein sample was

quantified by performing a BCA assay. Twenty µg of proteins were loaded on each well of NuPAGE® Novex® 4-12% Bis-Tris gels (Invitrogen) for SDS-PAGE (120 V for 1.5 hr) in NuPAGE® MES SDS running buffer (Invitrogen). The proteins were then transferred to PVDF membranes in NuPAGE® transfer buffer (Invitrogen) at 30 V for an hour. The membranes were blocked with TBST (tris-buffered saline with 0.1% Tween-20) buffer containing 5% (w/v) nonfat dry milk for an hour and then washed with TBST buffer 3 times for 5 min each. The membranes were incubated with rabbit polyclonal anti-Keap1 antibody (Abcam Inc., Cambridge, MA, #ab139729), and rabbit polyclonal anti-β actin antibody (Abcam, #ab8227) separately in TBST buffer containing 5% bovine serum albumin (BSA) at 4°C overnight. After rinsing 3 times for 5 min each, the membranes were incubated with goat polyclonal antibody to rabbit IgG conjugated with horseradish peroxidase (HRP) (Abcam, #ab6721) for an hour and then washed 3 times. The protein blots were visualized by using WesternBright Quantum HRP substrate (Advansta, Menlo Park, CA) and the chemiluminescent images were taken in a FluorChem FC2 imaging system (Alpha Innotech, San Leandro, CA).

5.3.8 U87mg cell transfection

Human glioma U87mg cells were plated in 6-well plates at a density of 10^4 cells/cm^2 and grown until they reached 70-80% confluency. Cells were maintained in DMEM (Dulbecco's Modified Eagle Medium, Invitrogen, Carlsbad, CA) supplemented with 10% fetal bovine serum and 100 U/mL of penicillin/streptomycin and cultured in a humidified incubator containing 5% CO_2 at 37°C. The cells were transfected with Keap1 siRNA-peptide complex in DMEM either with or without serum for 3 hr and further incubated in a complete culture medium for 48 hr. The human Keap1 siRNA was

prepared at the University of Utah HSC Core Research Facility. The siRNA sequences are as following; (sense) 5'-GGCCUUUGGCAUCAUGAACTT-3', (antisense) 5'-GUUCAUGAUGCCAAAGGCCTG-3'.

5.3.9 Hemolysis assay

The hemolysis assay was performed following the protocol described by Yu et al. (20). Briefly, the whole blood drawn from two mice was stored in heparinized tubes. A measure of 2.5 mL of mouse whole blood was combined with 10 mL of Dulbecco's phosphate-buffered saline (DPBS) and the red blood cells (RBCs) were isolated by centrifugation at 10,000 × g for 5 min. The RBCs were washed with DPBS 5 times and then diluted in 40 mL of DPBS. Two hundred μL of the diluted RBCs were added to 400 μL of siRNA-peptide complex-containing DPBS suspensions. The siRNA-peptide complex was prepared at various molar ratios with 100 pmoles of siRNA. The mixture of RBC and siRNA-peptide complex was incubated for 4 hr at room temperature. Finally, the sample containing tubes were vortexed and centrifuged at 10,000 × g for 5 min. The supernatants were transferred to a 96-well plate and the absorbance for hemoglobin and the reference absorbance were measured at 577 nm and 655 nm of wavelength, respectively. The percentage of hemolysis was calculated as follows: Hemolysis % = [(sample absorbance - negative control) / (positive control - negative control)] x 100%.

5.3.10 Statistical analysis

The data were expressed as mean ± standard errors. The statistical analysis was conducted with one-way ANOVA followed by Tukey-Kramer HSD post-hoc analysis. The statistical significance was noted by asterisks (*$p < 0.05$; **$p < 0.01$; ***$p < 0.001$).

The graphs were generated using SigmaPlot 10.0 (Systat, San Jose, CA) and the statistical analysis was performed with JMP® v10.0 (SAS Institute Inc., Cary, NC).

5.4 Results

5.4.1 Brain targeting ability of the siRNA-carrier complex

To evaluate the brain-targeting ability of the siRNA/myr-TP-Tf complex and compare the direct vs. local injection effect, the siRNA-peptide complex was prepared with Cy5.5-labeled siRNA and administered into mice via either intracranial or retrobulbar routes. PBS-injected mice were used as a negative control and naked Cy5.5-siRNA-injected mice were included to distinguish the siRNA carrier effect. The siRNA/myr-TP-Scr complex-injected mice were used to compare the brain targeting effect. Following the injection, the fluorescence from Cy5.5-siRNA was imaged at 1 hr, 2 hr, 24 hr, and 48 hr postinjection. In accordance with our expectation, the mice given a direct injection of Cy5.5-siRNA displayed intense and focused fluorescence on the brain areas up to 48 hr postinjection regardless of the presence of the peptide carrier and targeting moiety (Figure 5.2, A-D). There was almost no difference in fluorescence intensity in the brain areas among Cy5.5-siRNA injected groups, but the naked Cy5.5-siRNA injected one slightly lost the intensity at 48 hr postinjection implying that the peptide-based siRNA carriers help sustain the siRNA accumulation in the brain. Overall, the images from intracranial injection groups showed that direct injection ensures siRNA-peptide complex delivery to the brain.

On the contrary, the mice given a retrobulbar injection of Cy5.5-siRNA displayed little or lower fluorescence intensity on the brain areas compared to the intracranial injection group counterparts (Figure 5.2, E-H). Nonetheless, the mouse administered

with Cy5.5-siRNA/myr-TP-Tf complex showed better fluorescence distribution on the brain area at every time-point compared to other groups. While naked Cy5.5-siRNA- and the Cy5.5-siRNA/myr-TP-Scr complex-injected mice had the fluorescence signal only in the area close to the injection sites at 1 hr and 4 hr postinjection and almost no signal after that, the Cy5.5-siRNA/myr-TP-Tf complex-injected mice had measurable fluorescence on the brain area, which was observed up to 48 hr postinjection with a declined intensity. It appeared that the naked Cy5.5-siRNA and the Cy5.5-siRNA/myr-TP-Scr complex do not readily reach brain tissues when systemically administered, whereas the Cy5.5-siRNA/myr-TP-Tf complex was able to get into the brain to some extent as manifested by detectable fluorescence signal on the brain area. Compared to the intracranial injection group, however, the retrobulbar injection of Cy5.5-siRNA/myr-TP-Tf complex achieved a limited distribution of the fluorescence, being mostly focused on the olfactory bulb and the frontal lobe area. This result led us to presume that the proximity to the injection site also influences the distribution of the siRNA-peptide complex. There were some autofluorescence exhibited by feet and tails of the mice and this should be distinguished from the Cy5.5-associated fluorescence. The belly-side up positions of the mice was also monitored at each time-point to examine the fluorescence distribution over the whole body (Figure 5.3). Although there were some changes in the fluorescence distribution along the time course, it was too ambiguous to determine whether the fluorescence originated from the Cy5.5 or not because of the autofluorescence exerted from the mouse body (e.g., dark agouti colored coat, feet, tails, bare skins, feces).

5.4.2 Functional target gene silencing

To evaluate the target gene silencing effect, the hPAP transgenic mice were injected with Keap1 siRNA-peptide complex 3 times in 24 hr intervals either via intracranial or retrobulbar routes. A day after the last injection, mice were euthanized for brain isolation. The brain tissues at the injection sites (for intracranial injection groups) and the frontal lobe areas (for retrobulbar injection groups) were collected and used for the hPAP assay to examine the Keap1 gene downregulation effect. As a negative control for the hPAP activity, brain tissues from the hPAP (-) mice were included in the hPAP assay. In the intracranial injection groups, all of the Keap1 siRNA-injected groups showed significantly increased hPAP activities compared to the PBS-injected control group (Figure 5.4A); this indicates that the Keap1 gene was successfully silenced following the Keap1 siRNA administration. It was consistent with the imaging result where the direct intracranial injection groups exhibited a strong and persistent fluorescence signal of Cy5.5-siRNA in the brain areas (Figure 5.2). Among the intracranial injection groups, the Keap1 siRNA/myr-TP-Tf complex-injected group showed the most dramatic increase in hPAP activity on average by 24.6-fold compared to the PBS control, while the naked Keap1 siRNA-injected group and the Keap1 siRNA/myr-TP-Scr complex-injected group elicited 2.5-fold and 9.9-fold increases, respectively. This result clearly demonstrates that the myr-TP-Tf peptide ensures enhanced siRNA delivery and functional target gene silencing compared to the nontargeting myr-TP-Scr peptide, as well as the naked form of siRNA. The nontargeting myr-TP-Scr peptide also showed approximately 3-fold higher hPAP activity than the naked Keap1 siRNA-injected group, indicating that the cell-penetrating peptide itself has

a beneficial role in siRNA delivery. Collectively, the Keap1 siRNA/myr-TP-Tf complex-injected group showed the highest increase in hPAP activity, which suggests that not only the cell-penetrating peptide, but also the brain-targeting moiety contributes to the favorable cellular uptake of siRNA-peptide complex and the effective RNAi.

In the retrobulbar injection groups, the increase in hPAP activity was also observed from the Keap1 siRNA-injected groups (Figure 5.4B). However, the extent of the hPAP activation was quite less than those found in the intracranial injection groups: the naked Keap1 siRNA-injected group (1.8-fold), the Keap1 siRNA/myr-TP-Tf complex-injected group (3.3-fold), and the Keap1 siRNA/myr-TP-Scr complex-injected group (1.6-fold). Although the intracranial injection groups showed more dramatic increases in hPAP reporter activity, the myr-TP-Tf peptide complex still proved to have better brain targeting ability compared to the naked siRNA or the nontargeting myr-TP-Scr peptide complex, displaying the highest hPAP activity increase among other groups of the retrobulbar injection. This result indicates that the systemic administration of the siRNA/myr-TP-Tf complex can be a valid approach for brain-targeted RNAi therapy. To improve RNAi effect, however, it seems that a follow-up study is required to optimize the dose, number of injections, injection intervals, etc.

The protein and mRNA levels of Keap1 were further examined by performing Western blot and qRT-PCR experiments. In the intracranial injection groups, the Keap1 siRNA/myr-TP-Tf complex-injected group showed reduced Keap1 protein expression, which was consistent with the hPAP activity result. This indicates the successful knockdown of the Keap1 gene (Figure 5.5A). However, the Keap1 protein levels were not in accordance with the hPAP activity trend, especially for the retrobulbar injection

groups (Figure 5.5B). Moreover, the qRT-PCR did not yield the matched results with the hPAP activity (Figure 5.6A and B). There was no significant difference in Keap1 mRNA levels among groups in both the intracranial and the retrobulbar injection groups. We presume that this was because the brain tissues collected for these assays were located apart from where the siRNA-peptide complex could reach and that the data were not congruent with the hPAP assay result. To elucidate the RNAi effect thoroughly, an additional number of mice should be included and the brain tissues need to be collected region by region for a more detailed gene expression analysis.

5.4.3 Other considerations for *in vivo* application

To examine any adverse effects associated with the siRNA-peptide complex, we conducted postprocedural monitoring during the injection period by measuring the body weight and examining the activity or behavioral changes of the mice. The body weight of the mice was measured every other day and no significant changes were observed (Figure 5.7). In addition, there were no noticeable alterations in appearance or behaviors among different groups during the injection course, indicating that the siRNA-peptide complex administration does not affect the general health of the animals.

Prior to *in vivo* administration, an *in vitro* experiment was performed to determine whether the siRNA-peptide complex can transfect the neuronal cells in the presence of serum, a physiologically relevant environment. The Keap1 siRNA/myr-TP-Tf complex were transfected into U87mg cells for 3 hr either with or without serum and the cells were collected at 48 hr posttransfection for the mRNA and protein level analysis. The Keap1 mRNA expression level was reduced to 28.2% in the serum-free condition, and to 51.8% for the serum present condition, showing that the presence of serum may interfere

with the cellular uptake of the siRNA-peptide complex (Figure 5.8A). Even so, the Keap1 silencing effect was still significant for the serum-containing condition compared to the nontreated control group, validating the utility of the siRNA-peptide complex for *in vivo* application (Figure 5.8A and D). The Keap1 silencing did not affect the Nrf2 mRNA expression level, consistent with our previous result (Figure 5.8B). The expression of Nqo1 (NAD(P)H dehydrogenase, quinone 1), one of the ARE downstream genes, was found to be increased by 454.7% for the serum-free condition and by 167.1% for the serum-present condition. Although the difference between the control and the serum-present condition was not statistically significant, the increasing expression pattern still indicated that the Keap1 RNAi was followed by ARE activation under the serum-containing condition as well (Figure 5.8C).

To investigate the potential adverse interaction between the siRNA-peptide complex and RBCs (red blood cells) in the bloodstream, a hemolysis assay was conducted. The siRNA-peptide complex was prepared at varied molar ratios and combined with the diluted mouse RBCs. Along with the increasing molar ratio of siRNA to peptide carrier, higher hemolytic activity was observed (Figure 5.9). This was expected to a certain degree because the cationic surface charge of the siRNA-peptide complex would possibly perturb the membranes of RBCs, causing them to leak out hemoglobin (21). The siRNA-peptide complex prepared at 1:20 (siRNA to peptide) molar ratio, which was relevant to the dose used in this study, resulted in approximately 10% of hemolysis (implying a slightly toxic property). Among ~10% of hemolytic activity, in the strict sense, the water content from the siRNA and the peptide suspension accounted for 1.8% (data now included). According to a study on the chitosan-based

DNA delivery system, a hemolytic activity less than 15% is regarded as nontoxic and considered suitable for intravenous administration (22). This supports the siRNA-peptide complex as a viable mode for *in vivo* RNAi application.

5.5 Discussion

Collectively, the data presented in the current study showed that the direct injection of the siRNA-peptide complex to the brain cortex ensures surpassing performance with regard to brain-targeted siRNA delivery and the target gene downregulation effect. Despite the relatively lower RNAi effect, the retrobulbar injection of the siRNA/myr-TP-Tf complex still proved its brain targeting ability and functional target gene silencing capability compared to the naked siRNA and the nontargeting complex. The absence of evident toxicity issues and acceptably minor hemolytic activity at current doses also substantiate the *in vivo* utility of the siRNA-peptide complex. Overall, the results described herein suggest that the myr-TP-Tf peptide can serve as a useful tool to achieve brain-targeted siRNA delivery both via local and systemic administration.

It is understandable that the direct injection of the siRNA-peptide complex to the brain cortex produced a greater gene silencing effect than the systemic administration; apparently because the intracranial route allows direct access of the agent to the focused brain parenchyma with higher concentration while obviating the need for passing through the BBB. Furthermore, the direct injection provides a pharmacokinetic benefit owing to the advantageous brain distribution of the therapeutics compared to the systemic administration (23). The direct injection effect may be even more enhanced by applying the convection-enhanced delivery (CED) technology where a positive pressure creating

pump infuses the agent through intracranially placed catheters (24,25). Notwithstanding advantages of direct injection, its actual application may involve complex and invasive procedures, which can be a limiting factor if multiple injections over an extended period are required to elicit a desired therapeutic effect. Practically, the systemic administration is a preferred method as it is minimally invasive, less costly, and relatively favorable for patient convenience. As learned from the imaging study, however, the brain targeting ability of the siRNA/myr-TP-Tf complex was shown to be weaker in retrobulbar injection groups (Figure 5.2) while the intracranial injection group displayed an intense fluorescence signal in the brain area even up to 96 hr postinjection (data not shown). In line with the imaging result, the target gene downregulation effect represented by the hPAP activity was also a lot stronger in the intracranial injection groups than in the retrobulbar injection groups (Figure 5.4). Even though the current formulation proved its brain targeting and gene silencing ability in retrobulbar injection groups, the results obtained in this study informs us that further optimization of the siRNA-peptide complex is needed to be fully functional for the systemic administration approach.

As a refinement plan, the transferrin receptor (TfR)-binding short peptide sequence of the myr-TP-Tf can be replaced with other types of brain-specific moieties for improved siRNA accumulation in the brain. Although the siRNA/myr-TP-Tf complex showed its ability to reach brain tissues compared to the naked siRNA and the nontargeting complex, the TfR may not be an ideal targeting receptor because of its ubiquitous expression on other peripheral organs (26). Depending on the siRNA species loaded on the complex, nonspecific uptake of the siRNA-peptide complex by other organs might disturb the normal gene regulation and cause severe adverse effects. In an

effort to accomplish brain-targeted drug delivery, researchers have attempted diverse brain-targeting moieties for the receptors, including LDLR-related protein (LRP1) (27), insulin receptor (28), diphtheria toxin receptor (29), acetylcholine receptor (30), leptin receptor (31), etc. However, these receptors are not exclusively found on the brain endothelium either. To optimize the brain targeting ability of the siRNA-peptide complex, further research endeavors are encouraged for the identification of novel brain-specific receptors and receptor targeting moieties that can bind to those receptors with high affinity.

Another consideration for enhancing the efficacy of the systemic administration is to optimize the dosage regimen. In the current study, only a single dosage protocol (three injections of 50 μg of siRNA in 24 hr intervals for the retrobulbar injection group) was tested due to the limited number of animals per group, which is a major limiting factor. In addition, the brain tissues collected from the same mouse were divided for multiple assays including the hPAP assay, Western blotting, and qRT-PCR. This made it difficult to examine the gene knockdown effect precisely, particularly because of the differential RNAi effect over the brain tissues. By increasing the number of animals per group, a range of multiple doses from high to low needs to be further tested along with the adjustment of the number of injections and the injection intervals in order to find an optimal dosage protocol that maximizes the gene silencing effect of the siRNA-peptide complex. In addition, a more thorough gene expression analysis should be followed with brain tissues at specific regions collected from separate mice for each assay. Concerning the dosage adjustment, however, it should be noted that the cationic charged carrier may cause toxicity issues (32-34), which limits the amount of the peptide that can be used for

the systemic administration. As tested in the hemolysis assay, the myr-TP-Tf peptide showed a slight hemolytic activity (~10%) though it was still considered within a safe range (Figure 5.9). To prevent excess hemolysis at high doses of the siRNA-peptide complex, the PEGylation strategy can be used for the siRNA carrier design. Indeed, studies have shown that the PEGylated drug delivery systems exhibited significantly reduced hemolytic activities compared to the nonmodified ones (35-37), possibly because the PEG coating provides the steric hindrance that lowers the interaction between the drug-loaded systems and the RBCs in the bloodstream (38,39). In addition, the PEGylation approach can also protect the siRNA-peptide complex from the reticuloendothelial system (RES)-mediated clearance (40).

To step forward to the clinical setting, not only the RNAi therapeutic effect, but also the biodistribution pattern and pharmacokinetic properties of the siRNA-peptide complex should be further elucidated. Although the fluorescently-labeled siRNA was used in the imaging study, it did not clearly visualize the biodistribution of the siRNA-peptide complex, largely because of the autofluorescence from the hPAP transgenic mice (Figure 5.3). To investigate the potential nonspecific absorption of the siRNA-peptide complex to other peripheral organs, we need to increase the number of animals and perform *ex vivo* organ imaging over multiple time-points, which eliminates the confusion from the whole body autofluorescence. As the peptide carriers were not labeled fluorescently, it may not be conclusive as to whether the fluorescence indicates the siRNA in the peptide complex form or just free siRNA. We have attempted to use a 5-FAM-labeled peptide carrier, but it failed to maintain the identical siRNA condensation behavior (data not shown). To clarify the biodistribution of the siRNA and peptide

carrier individually, the peptide carriers may need to be labeled with alternative dyes or radioactive isotopes that do not interfere with the normal electrostatic interaction between the peptide and the siRNA.

RNAi therapy has received a spotlight for its powerful gene modulation ability in pathological conditions. Regarding various neurodegenerative disorders, researchers have suggested multiple RNAi targets that include variants of APP, BACE1, presenilin 1 and 2 for AD, α-synuclein for PD, ataxin-1 for spinocerebellar ataxia, etc. Although RNAi approaches targeting those genes have shown promising therapeutic results in many preclinical validation studies with rodent models, there is no successful RNAi drug available for treating neurodegenerative disorders, yet. This is because the siRNAs are vulnerable to the serum nucleases in the bloodstream and are unable to cross the BBB, which all result in poor accumulation in the target site. Considering the clinical benefits from the highly specific and effective gene silencing mechanism of the RNAi, it is imperative to develop RNAi carrying vehicles that can protectively load siRNAs and functionally deliver them to the brain parenchyma. Our current work is in line with this effort and further research should also continue.

To conclude, the *in vivo* data here validated the myristoylated cell-penetrating peptide equipped with a brain-targeting moiety as a functional brain-targeted siRNA delivery vehicle. As a next step in the preclinical stage, we can administer therapeutic siRNAs/peptide complex to AD or other types of NDD animal models and evaluate the therapeutic outcome with regard to target gene knockdown, as well as the symptomatic and behavioral improvement. We expect that further optimization of the carrier design and refinement of the dosage will advance the RNAi therapeutic effect in living systems.

Table 5.1. qRT-PCR primer sequences

Gene	Forward primer	Reverse primer
mGAPDH	5'AACTTTGGCATTGTGGAAGG3'	5'TGTGAGGGAGATGCTCAGTG3'
mKeap1	5'AAGGACCTTGTGGAAGACCA3'	5'CCCTGTCCACTGGAATTGAT3'
hGAPDH	5'CCACTCCTCCACCTTTGAC3'	5'ACCCTGTTGCTGTAGCCA3'
hKeap1	5'CAGATTGGCTGTGTGGAGTT3'	5'GCTGTTCGCAGTCGTACTTG3'
hNrf2	5'ATAGCTGAGCCCAGTATC3'	5'CATGCACGTGAGTGCTCT3'
hNQO1	5'CAGTGGTTTGGAGTCCCTGCC3'	5'TCCCCGTGGATCCCTTGCAG3'

(m: mouse, h: human)

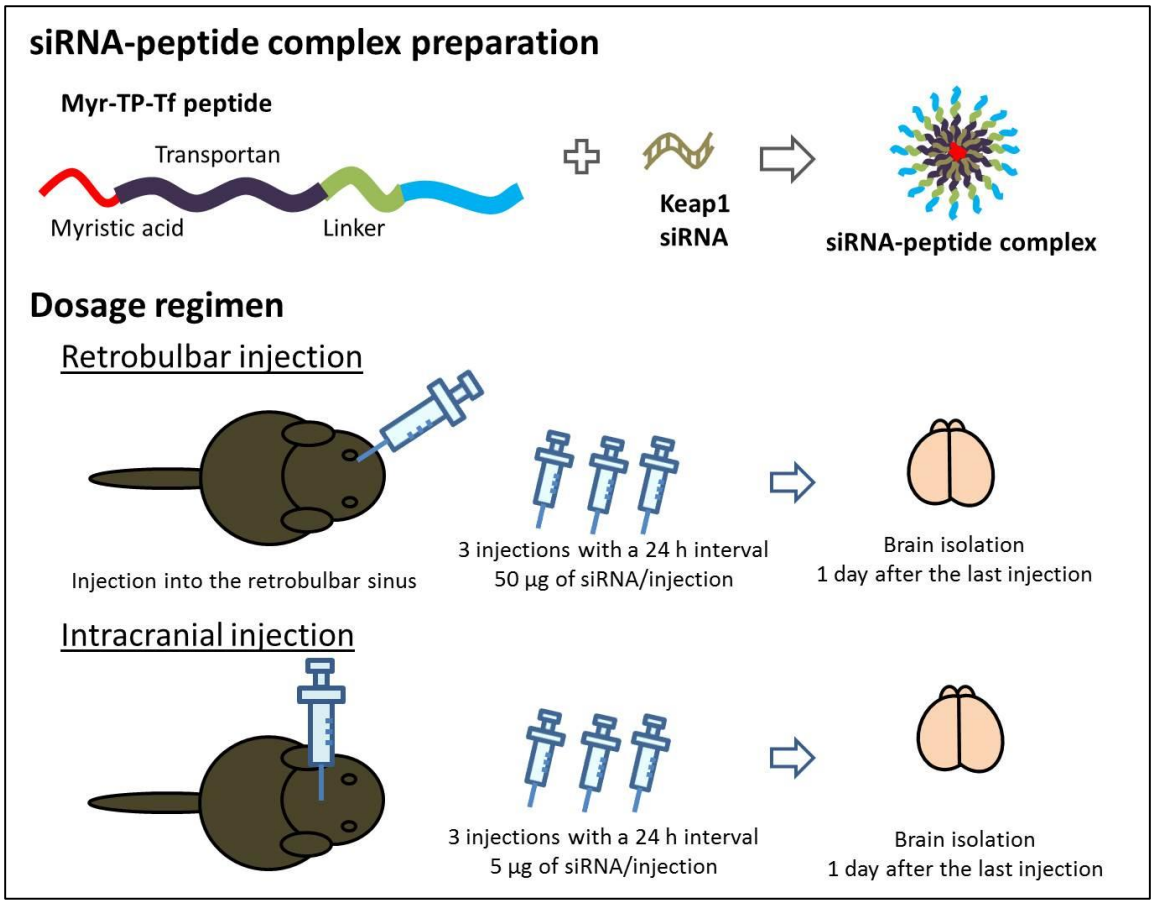

Figure 5.1. Illustration of the siRNA-peptide complex preparation and the dosage regimen for the retrobulbar and intracranial injections for adult mice. All siRNA-peptide complex suspensions were freshly prepared in sterile phosphate buffered saline and incubated at room temperature for 20 min before injection. In the imaging study, animals were given a single injection of fluorescently labeled siRNA-peptide complex and immediately subjected to the imaging.

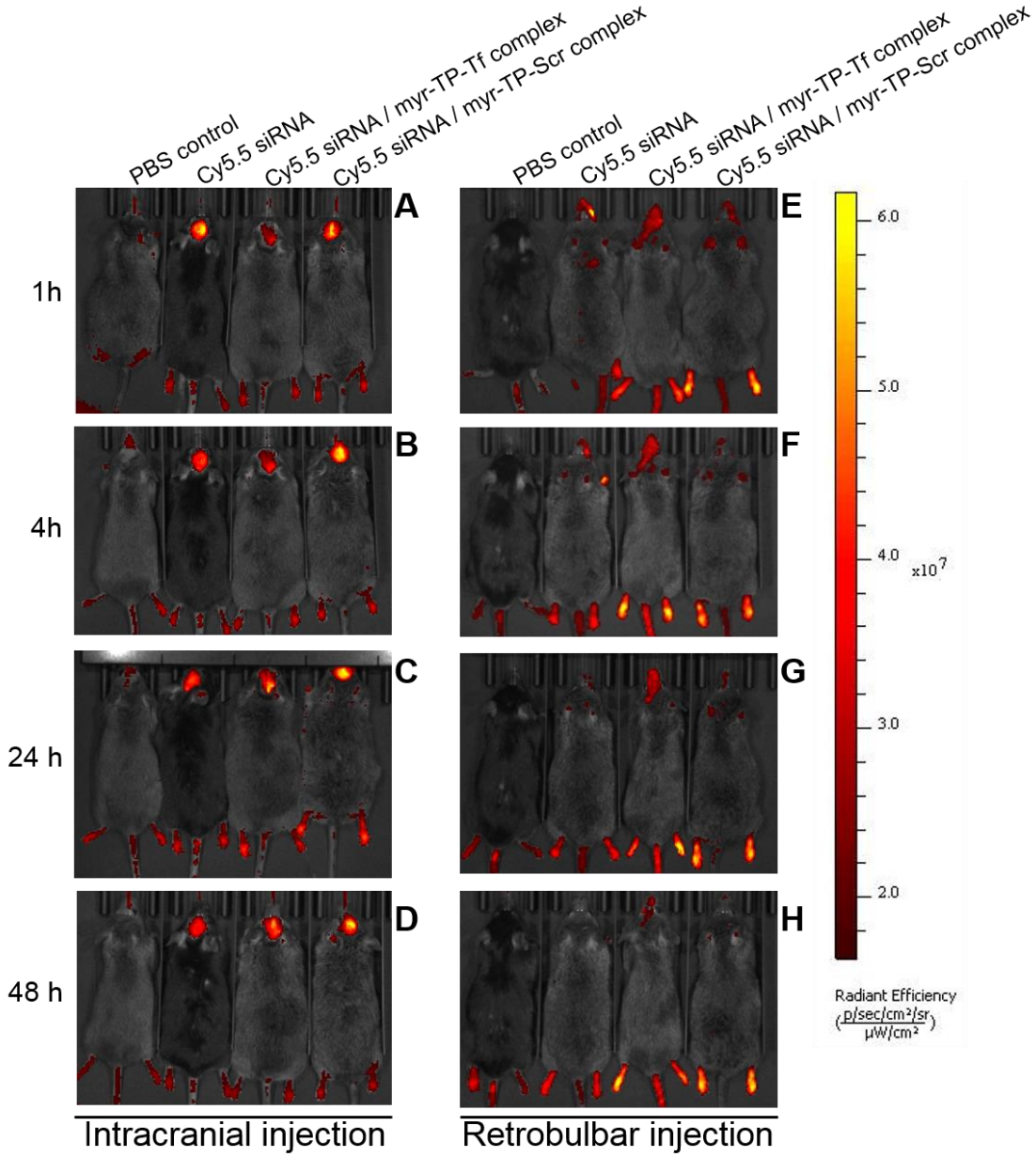

Figure 5.2. Fluorescence imaging of mice injected with Cy5.5-labeled siRNA (belly down). The fluorescence signal was taken at 1 hr, 4 hr, 24 hr and 48 hr postinjection. Mice were lined up (from left to right) as PBS control, naked Cy5.5-siRNA, Cy5.5-siRNA/myr-TP-Tf complex, and Cy5.5-siRNA/myr-TP-Scr complex-injected ones. The intracranial injection groups are shown in left panel (A, B, C, and D) and the retrobulbar injection groups in right panel (E, F, G, and H).

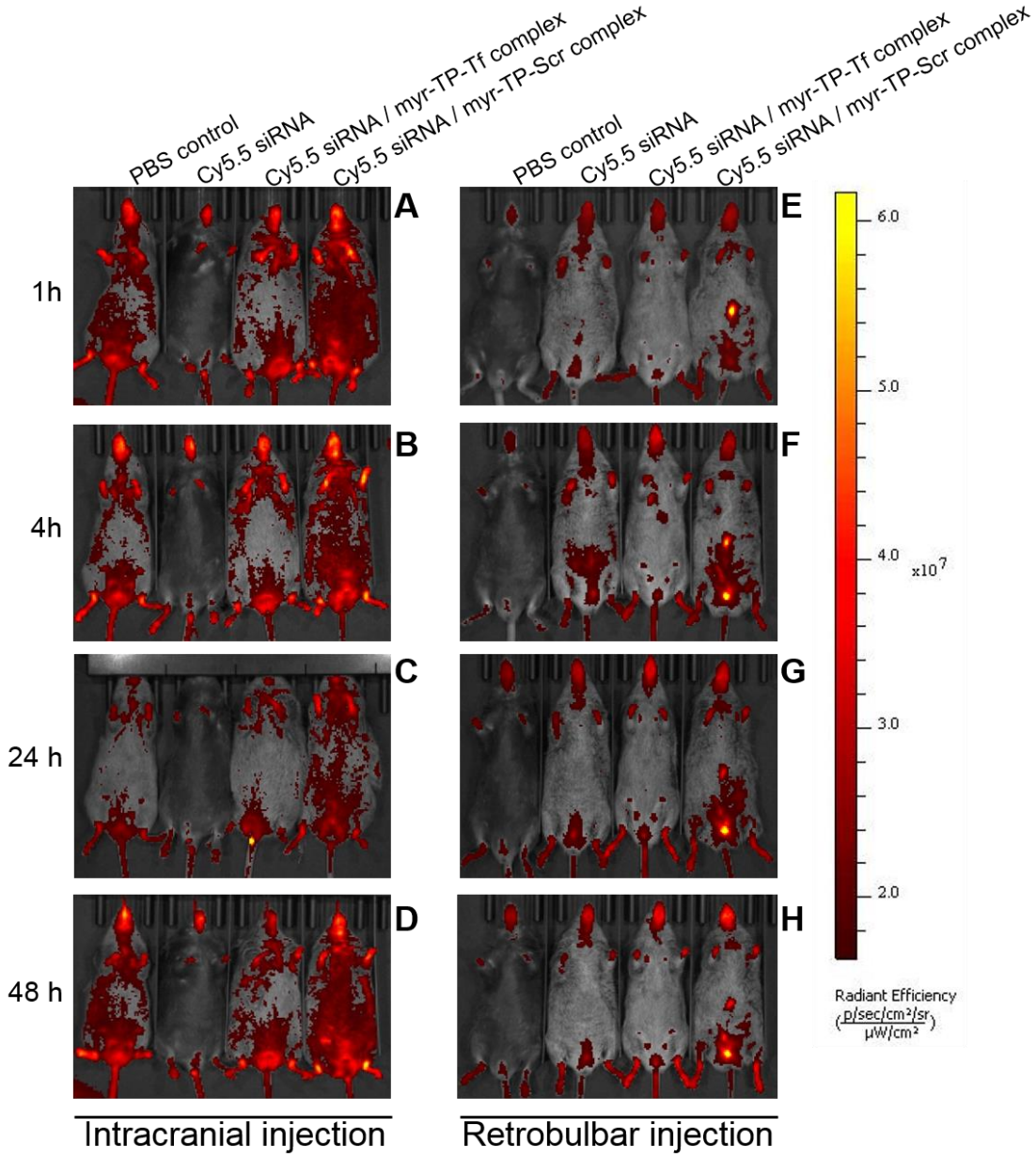

Figure 5.3. Fluorescence imaging of mice injected with Cy5.5-labeled siRNA (belly up). The fluorescence signal was taken at 1h, 4h, 24h and 48h post-injection. Mice were lined up (from left to right) as PBS control, naked Cy5.5-siRNA, Cy5.5-siRNA/myr-TP-Tf complex, and Cy5.5-siRNA/myr-TP-Scr complex-injected ones. The intracranial injection groups are shown in left panel (A, B, C, and D) and the retrobulbar injection groups in right panel (E, F, G, and H).

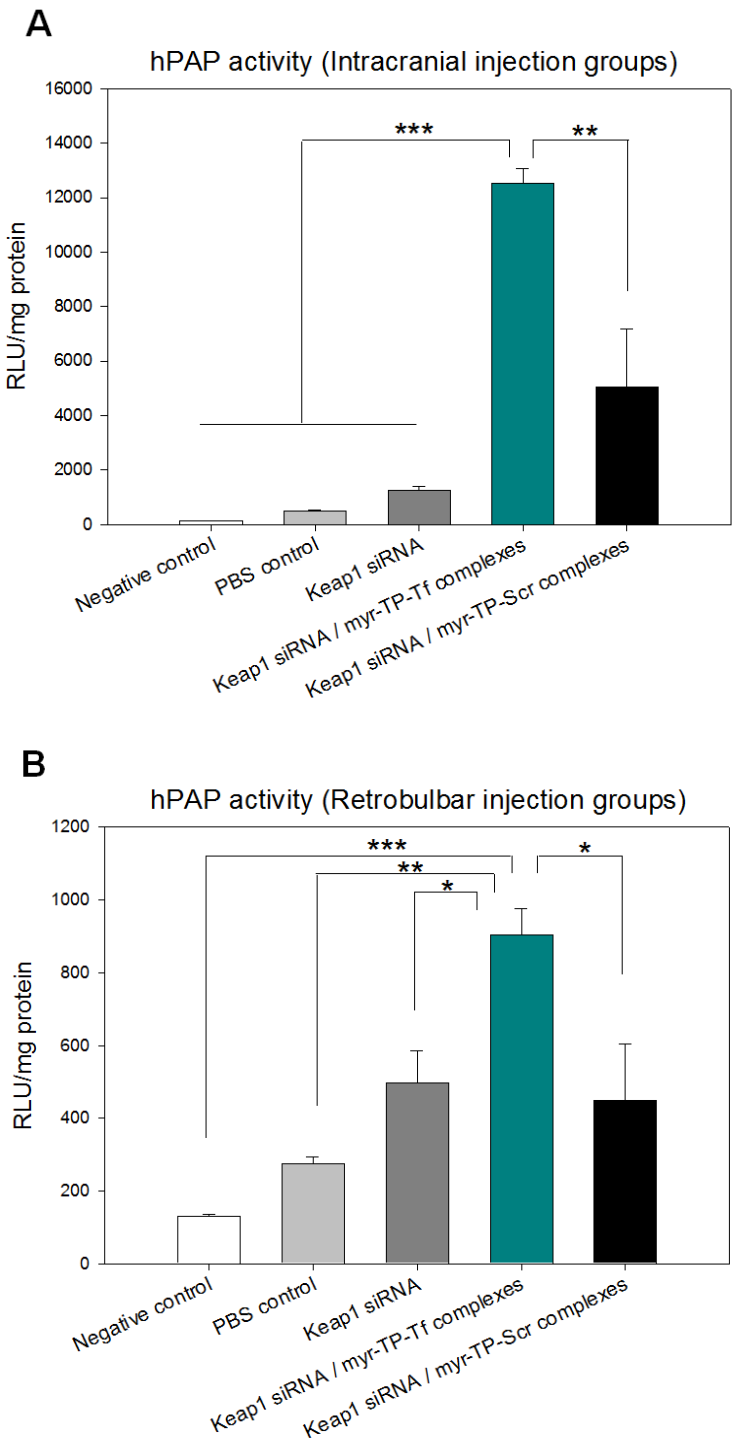

Figure 5.4. hPAP activity. Relative hPAP activity in brain tissues of the Keap1 siRNA-injected mice were examined via luminescence measurements. (A) hPAP activity in intracranial injection groups; and (B) hPAP activity in retrobulbar injection groups. Data are expressed as mean ± standard error. One-way ANOVA was conducted with Tukey-Kramer HSD post-hoc analyses (n=3/group, *$p < 0.05$; **$p < 0.01$; ***$p < 0.001$).

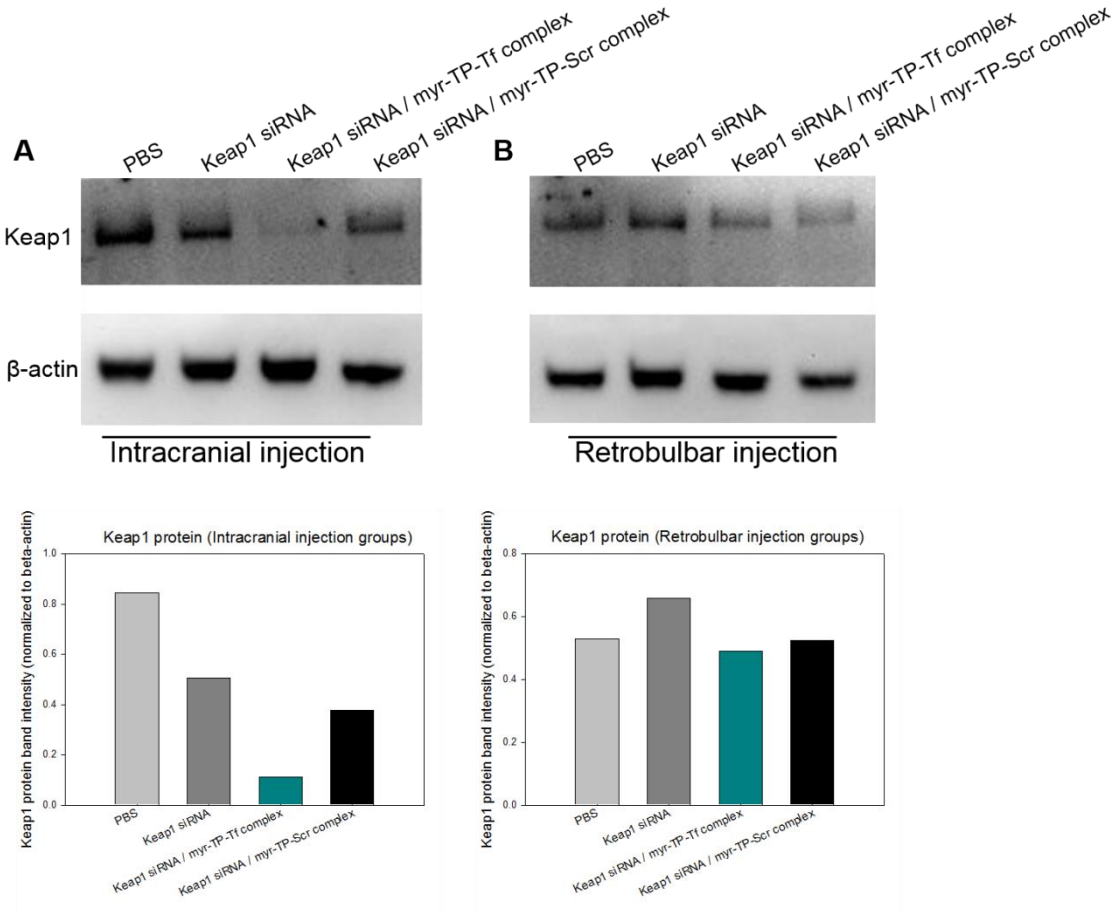

Figure 5.5. Western blot analysis of Keap1 protein expression level. (A) Keap1 protein level in intracranial injection groups; and (B) Keap1 protein level in retrobulbar injection groups.

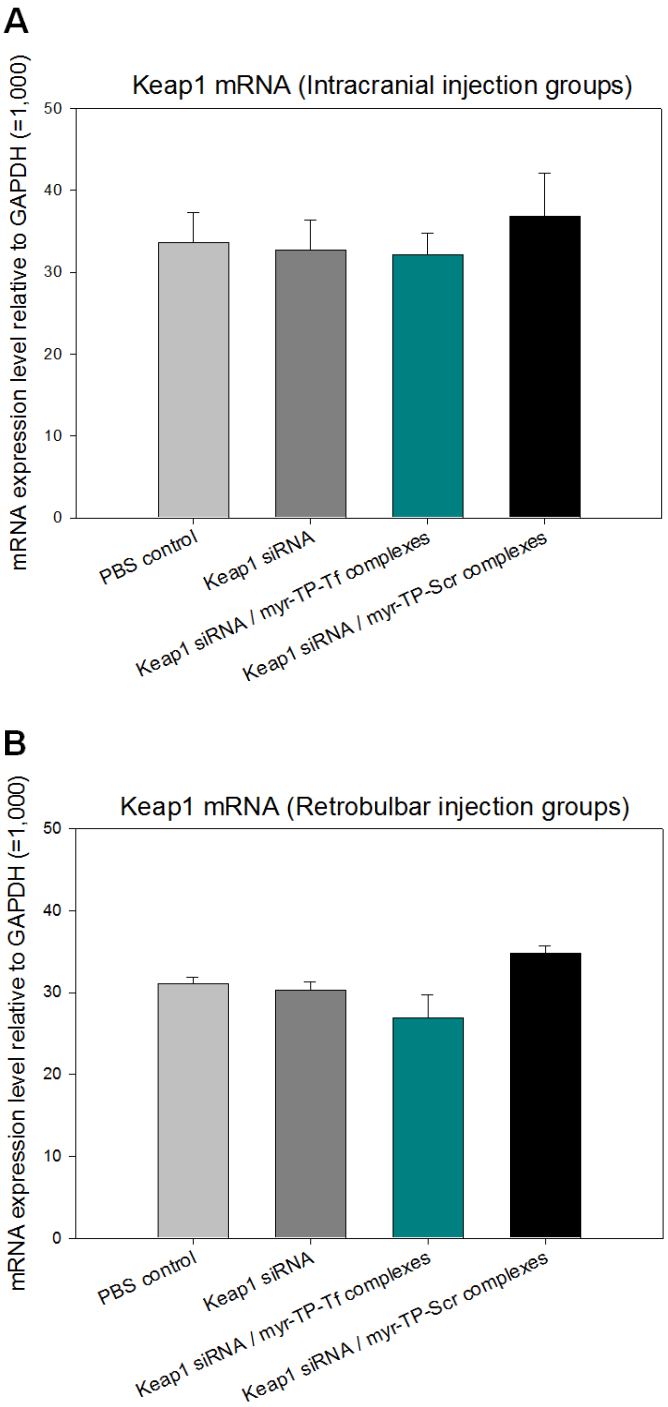

Figure 5.6. qRT-PCR analysis of Keap1 mRNA expression level (n=3/group). (A) Keap1 mRNA level in intracranial injection groups; and (B) Keap1 mRNA level in retrobulbar injection groups.

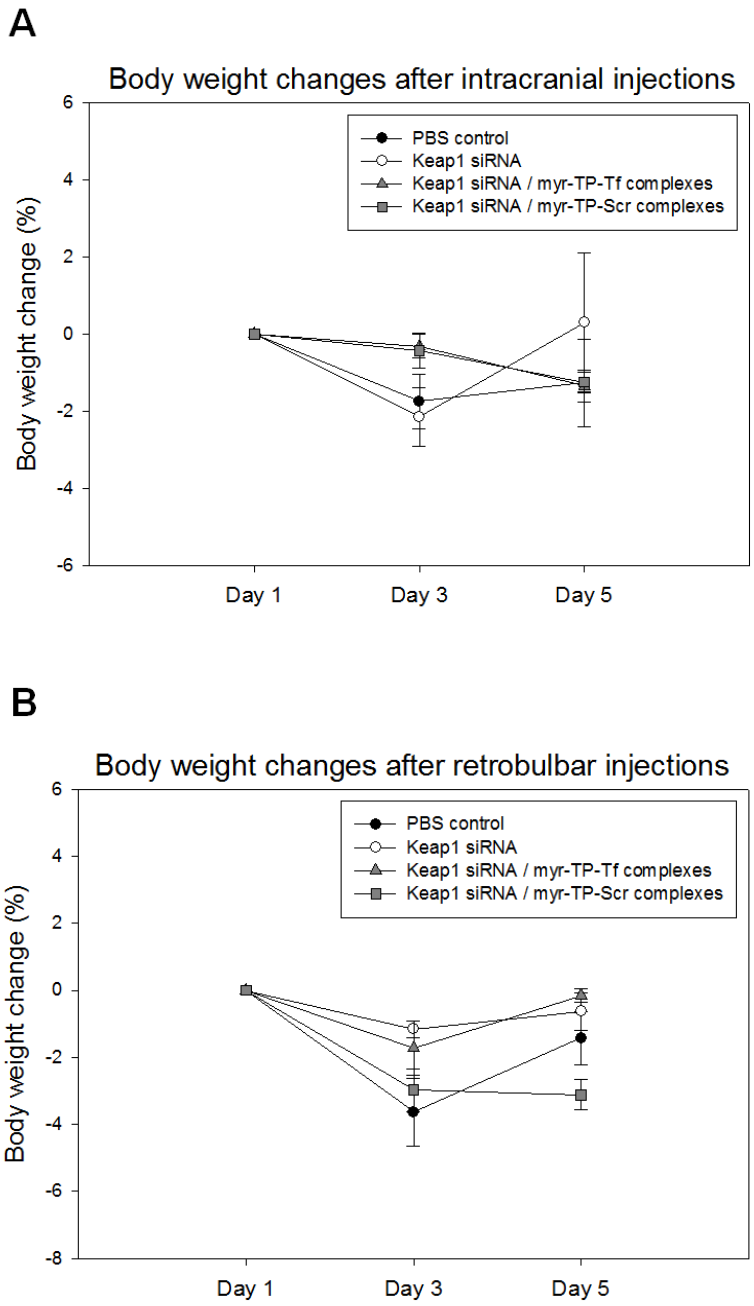

Figure 5.7. Body weight monitoring during the course of injections (n=3/group). (A) Body weight changes in intracranial injection groups; and (B) body weight changes in retrobulbar injection groups.

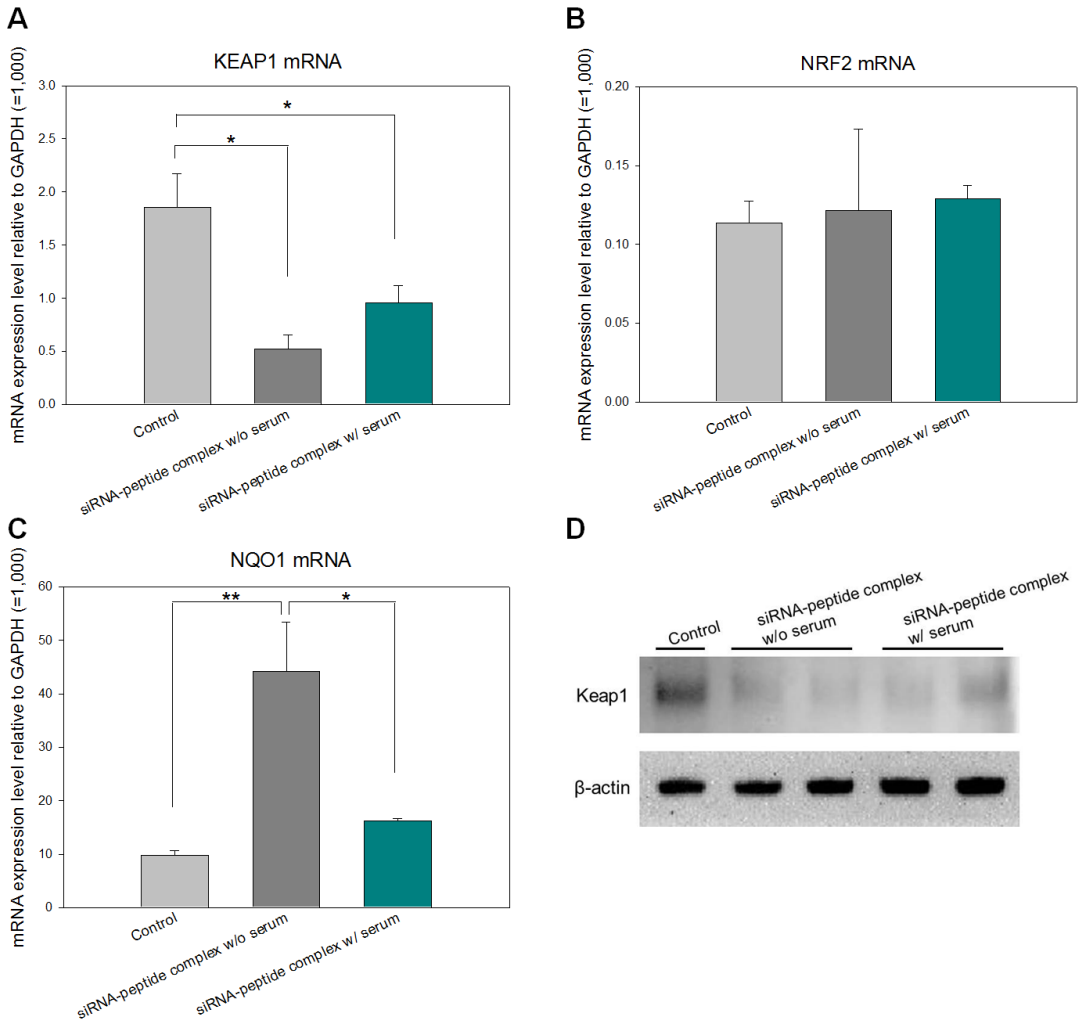

Figure 5.8. Transfection of Keap1 siRNA/myr-TP-Tf complex to U87mg cells in the presence and absence of serum (n=3/group). Cells were transfected with Keap1 siRNA/myr-TP-Tf complex for 3 hr with or without serum and further incubated for 48 hr in a complete medium to examine the serum effect in transfection and gene downregulation. (A) Keap1 mRNA level; (B) Nrf2 mRNA level; (C) Nqo1 mRNA level; and (D) Keap1 protein expression level.

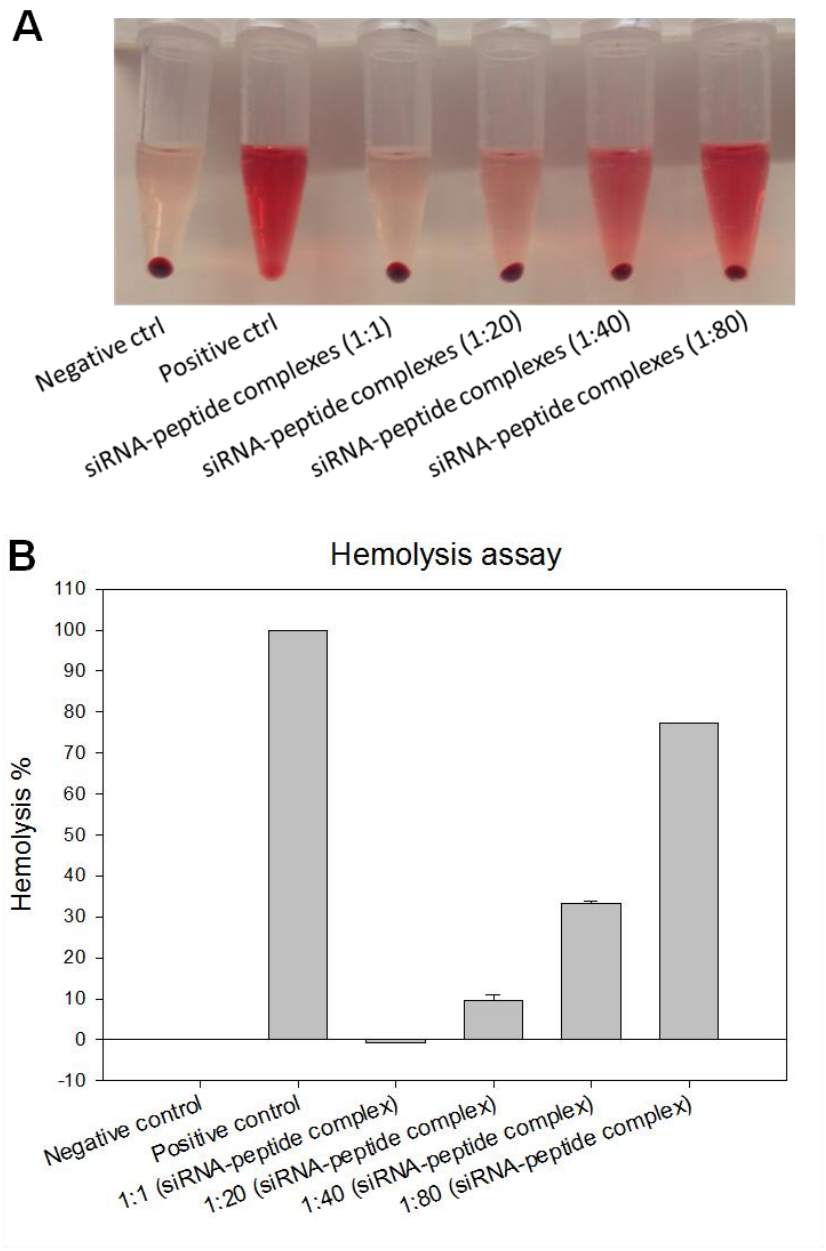

Figure 5.9. Hemolysis assay on siRNA-peptide complex prepared at various siRNA to peptide molar ratios (n=2/group). (A) Visual representation of the hemolytic activity; and (B) the percentage of hemolysis of each preparation relative to the positive control.

5.6 References

1. Cummings JL, Morstorf T, Zhong K. Alzheimer's disease drug-development pipeline: few candidates, frequent failures. Alzheimers Res Ther 2014;6:37.

2. Yiannopoulou KG, Papageorgiou SG. Current and future treatments for Alzheimer's disease. Ther Adv Neurol Disord 2013;6:19-33.

3. Boudreau RL, Rodríguez-Lebrón E, Davidson BL. RNAi medicine for the brain: progresses and challenges. Hum Mol Genet 2011;20:R21-R27.

4. Davidson BL, Paulson HL. Molecular medicine for the brain: silencing of disease genes with RNA interference. Lancet Neurol 2004;3:145-49.

5. Evin G, Hince C. BACE1 as a therapeutic target in Alzheimer's disease: rationale and current status. Drug Aging 2013;30:755-64.

6. Singer O, Marr RA, Rockenstein E, Crews L, Coufal NG, Gage FH, et al. Targeting BACE1 with siRNAs ameliorates Alzheimer disease neuropathology in a transgenic model. Nat Neurosci 2005;8:1343-49.

7. Brunden KR, Trojanowski JQ, Lee VM-Y. Advances in tau-focused drug discovery for Alzheimer's disease and related tauopathies. Nat Rev Drug Discov 2009;8:783-93.

8. Piedrahita D, Hernández I, López-Tobón A, Fedorov D, Obara B, Manjunath B, et al. Silencing of CDK5 reduces neurofibrillary tangles in transgenic Alzheimer's mice. J Neurosci 2010;30:13966-76.

9. Phiel CJ, Wilson CA, Lee VM-Y, Klein PS. GSK-3α regulates production of Alzheimer's disease amyloid-β peptides. Nature 2003;423:435-39.

10. Kobayashi M, Yamamoto M. Molecular mechanisms activating the Nrf2-Keap1 pathway of antioxidant gene regulation. Antioxid Redox Sign 2005;7:385-94.

11. Kuwahara H, Yokota T, Mizusawa H. Delivery of siRNA into the blood-brain barrier: recent advances and future perspective. Ther Deliv 2012;3:417-20.

12. Pardridge WM. CNS drug design based on principles of blood-brain barrier transport. J Neurochem 1998;70:1781-92.

13. Bumcrot D, Manoharan M, Koteliansky V, Sah DW. RNAi therapeutics: a potential new class of pharmaceutical drugs. Nat Chem Biol 2006;2:711-19.

14. Gao Y, Liu X-L, Li X-R. Research progress on siRNA delivery with nonviral carriers. Int J Nanomedicine 2011;6:1017-25.

15. Barnaby SN, Lee A, Mirkin CA. Probing the inherent stability of siRNA immobilized on nanoparticle constructs. P Natl Acad Sci 2014;111:9739-44.

16. Youn P, Chen Y, Furgeson DY. A myristoylated cell-penetrating peptide bearing a transferrin receptor-targeting sequence for neuro-targeted siRNA delivery. Mol Pharmaceutics 2014;11:486-95.

17. Yardeni T, Eckhaus M, Morris HD, Huizing M, Hoogstraten-Miller S. Retro-orbital injections in mice. Lab Animal 2011;40:155.

18. Socher M, Kuntz J, Sawall S, Bartling S, Kachelrieß M. The retrobulbar sinus is superior to the lateral tail vein for the injection of contrast media in small animal cardiac imaging. Lab Animal 2014;48:105-13.

19. Gan L, Johnson DA, Johnson JA. Keap1-Nrf2 activation in the presence and absence of DJ-1. Eur J Neurosci 2010;31:967-77.

20. Yu T, Malugin A, Ghandehari H. Impact of silica nanoparticle design on cellular toxicity and hemolytic activity. ACS nano 2011;5:5717-28.

21. Dobrovolskaia MA, Aggarwal P, Hall JB, McNeil SE. Preclinical studies to understand nanoparticle interaction with the immune system and its potential effects on nanoparticle biodistribution. Mol Pharmaceutics 2008;5:487-95.

22. Richardson SW, Kolbe HJ, Duncan R. Potential of low molecular mass chitosan as a DNA delivery system: biocompatibility, body distribution and ability to complex and protect DNA. Int J Pharm 1999;178:231-43.

23. Misra A, Ganesh S, Shahiwala A, Shah SP. Drug delivery to the central nervous system: a review. J Pharm Pharm Sci 2003;6:252-73.

24. Debinski W, Tatter SB. Convection-enhanced delivery for the treatment of brain tumors. Expert Rev Neurother 2009;9:1519-27.

25. Bidros DS, Liu JK, Vogelbaum MA. Future of convection-enhanced delivery in the treatment of brain tumors. Future Oncol 2010;6:117-25.

26. Qian ZM, Li H, Sun H, Ho K. Targeted drug delivery via the transferrin receptor-mediated endocytosis pathway. Pharmacol Rev 2002;54:561-87.

27. Bertrand Y, Currie JC, Demeule M, Régina A, Ché C, Abulrob A, et al. Transport characteristics of a novel peptide platform for CNS therapeutics. J Cell Mol Med 2010;14:2827-39.

28. Banks WA. The source of cerebral insulin. Eur J Pharmacol 2004;490:5-12.

29. Gaillard PJ, Brink A, de Boer AG. Diphtheria toxin receptor-targeted brain drug delivery. Int Congr Ser 2005;1277:185-98.

30. Kumar P, Wu H, McBride JL, Jung KE, Kim MH, Davidson BL, et al. Transvascular delivery of small interfering RNA to the central nervous system. Nature 2007;448:39-43.

31. Tosi G, Badiali L, Ruozi B, Vergoni AV, Bondioli L, Ferrari A, et al. Can leptin-derived sequence-modified nanoparticles be suitable tools for brain delivery? Nanomedicine 2012;7:365-82.

32. Fischer D, Li Y, Ahlemeyer B, Krieglstein J, Kissel T. *In vitro* cytotoxicity testing of polycations: influence of polymer structure on cell viability and hemolysis. Biomaterials 2003;24:1121-31.

33. Lee HJ, Pardridge WM. Monoclonal antibody radiopharmaceuticals: cationization, pegylation, radiometal chelation, pharmacokinetics, and tumor imaging. Bioconjugate Chem 2003;14:546-53.

34. Domański D, Klajnert B, Bryszewska M. Influence of PAMAM dendrimers on human red blood cells. Bioelectrochemistry 2004;63:189-91.

35. Yu Nie LJ, Ding H, Xie L, Li L, He B, Wu Y, et al. Cholesterol derivatives based charged liposomes for doxorubicin delivery: preparation, *in vitro* and *in vivo* characterization. Theranostics 2012;2:1092.

36. He Q, Zhang J, Shi J, Zhu Z, Zhang L, Bu W, et al. The effect of PEGylation of mesoporous silica nanoparticles on nonspecific binding of serum proteins and cellular responses. Biomaterials 2010;31:1085-92.

37. Lu J, Chuan X, Zhang H, Dai W, Wang X, Wang X, et al. Free paclitaxel loaded PEGylated-paclitaxel nanoparticles: preparation and comparison with other paclitaxel systems *in vitro* and *in vivo*. Int J Pharm 2014.

38. Veronese FM, Pasut G. PEGylation, successful approach to drug delivery. Drug Discov Today 2005;10:1451-58.

39. Knop K, Hoogenboom R, Fischer D, Schubert US. Poly (ethylene glycol) in drug delivery: pros and cons as well as potential alternatives. Angew Chem Int Ed 2010;49:6288-308.

40. Jokerst JV, Lobovkina T, Zare RN, Gambhir SS. Nanoparticle PEGylation for imaging and therapy. Nanomedicine 2011;6:715-28.

CHAPTER 6

CONCLUSIONS AND FUTURE WORK

6.1 Conclusions

The RNAi approach can serve as a promising mode of treatment for neurodegenerative disorders. In order to achieve the brain-targeted delivery of therapeutic siRNAs, we have designed a myristoylated cell-penetrating peptide equipped with a transferrin-receptor targeting peptide sequence (myr-TP-Tf). In the *in vitro* characterization study, we have found that the myr-TP-Tf peptides optimally encapsulated siRNAs at a 20: 1 molar ratio (peptide to siRNA) where the siRNAs exhibited prolonged stability against the serum and RNase A. The siRNA-peptide complex displayed spherical structures with fairly small size (~100 nm in diameter) and a moderately positive surface potential value (~23 mV); this was generally in accordance with our expectation for the siRNA carrier physicochemical characteristics. In addition, the peptide-siRNA complex successfully delivered bioactive siRNA in both the immortalized brain cell line and primary brain cells and significantly downregulated the target gene expression. The siRNA transport across the brain endothelial cell monolayer in the transwell system indicated the capability of myr-TP-Tf to deliver the siRNA across the BBB model *in vitro*. Overall, the myr-TP-Tf peptide demonstrated its potential as a siRNA carrier for brain-targeted delivery.

We proposed Keap1 protein downregulation as a therapeutic approach for NDDs

in order to provide cytoprotection to the brain cells against oxidative stress and neurodegenerative conditions. Using the myr-TP-Tf carrier, we examined the neuroprotective effect of Keap1 RNAi in a human glioma cell line under Aβ peptide and H_2O_2-mediated oxidative stress. Our findings showed that the Keap1 RNAi enhanced the endogenous antioxidant capacity, possibly through the Nrf2-mediated activation of a variety of antioxidant and detoxifying proteins. Furthermore, the Keap1 RNAi groups exhibited higher cell viability and less oxidative damages under oxidative assault, compared to the control groups. The basal autophagy level was also relatively maintained in the Keap1 RNAi group while the control group had an elevated level of autophagic activity. Therefore, it is concluded that the Keap1 RNAi has a promising therapeutic potential for brain cells under the pathological oxidative stress condition such as in many NDDs.

Finally, we have conducted *in vivo* validation of the siRNA-peptide complex to examine its brain targeting ability and its functional target gene silencing effect in a living system. The fluorescently labeled siRNA revealed that the systemic administration of the myr-TP-Tf complex into adult mice was able to deliver siRNAs to the brain parenchyma compared to the naked siRNA or nontargeting complex, thereby demonstrating its brain targeting ability. Successful siRNA delivery was also manifested by the activation of a reporter protein from the harvested brain tissues. However, the brain accumulation extent and the target gene downregulation effect were more pronounced in direct local administration groups than the systemic administration groups. Hence, we conclude that the myr-TP-Tf peptide possesses promising properties as a brain-targeted siRNA carrier *in vivo* as well, but the carrier design may need to be

optimized in order to fine-tune the targeting ability and ultimately maximize the therapeutic effects.

6.2 Experimental design for a complete *in vivo* study

Based on the preliminary *in vivo* results in Chapter 5, the experimental design herein is suggested for the further study to fully evaluate the brain targeting ability and the target gene silencing capacity of the siRNA-peptide complex in the living system. The RNAi effect from local administration vs. systemic administration was briefly compared in the preliminary study. In accordance with our expectation, the intracranial injection resulted in more prevalent brain accumulation of the siRNA as well as a greater target gene silencing effect compared to retrobulbar injection (Figure 5.2). However, the small number of animals per group was a major limiting factor in the previous study. In addition, the retrobulbar route may not be a feasible option for the clinical application even if it is widely used as an alternative route to tail vein injection in many preclinical studies. Moreover, there can be a benefit for the retrobulbar route in reaching the brain due to the close distance between the retrobulbar sinus and the brain area. In furture studies, more animals will be included to enhance the statistical power and the RNAi effect from two modes of systemic administration (retrobulbar injection vs. tail vein injection) will be compared.

To examine brain-targeting ability, siRNA labeled with near-infrared fluorescent dye such as Cy5.5 will be used to formulate the siRNA-peptide complex and the mice will be imaged in the *in vivo* fluorescence imaging system at various time-points (e.g.,1 hr, 3 hr, 8 hr, and 24 hr) after the injection. The experimental groups include PBS control group, Cy5.5 siRNA group, Cy5.5 siRNA/Myr-TP-Tf complex group, and Cy5.5

siRNA/Myr-TP-Scr complex group. To assess the distribution of the siRNA, the flipped position of the mice will be additionally taken at each time-point. The hPAP transgenic mice in the previous study displayed autofluorescence from various parts of the body which caused confusion with the siRNA fluorescence signals (Figure 5.3). In further study, mice with white coats such as Balb/c mice will be used instead to exclude the autofluorescence issue. In addition, *ex vivo* imaging at each time-point will be conducted for more precise analyses of the fluorscence distribution over the brain as well as other peripheral organs. In this same study, mice will be sacrified at each time-point and the primary organs (brain, heart, lung, liver, stomach, spleen, kindey, small intestines, large intestines, reproductive organs; testis for males and ovaries for females) will be isolated for immediate imaging. Both genders will be included to examine any gender-related response difference.

To evaluate the gene silencing effect, Keap1 siRNA will be administered to hPAP(+) transgenic mice and the hPAP activity will be examined from isolated brain tissues. In the previous study, only a single dosage regimen (3 injections of 50 μg siRNA/injection in 24 hr intervals) was tested; the effect in the retrobulbar injection groups was much lower than the one in the intracranial injection groups (Figure 5.4). In the further study, we suggest three different doses (50 μg siRNA, 100 μg siRNA, 150 μg siRNA) that follow the same injection repeats (3 injections) at the same interval (24 hr) to examine the dose-dependent gene silencing effect and any dose-associated toxicity issues. Previously, the Keap1 expression level was not correlated with the hPAP activity result for the retrobulbar injection groups (Figure 5.5 and 5.6). We thought that this was because the brain tissues used for all assays were collected from the same mouse due to a

lack of animals. To examine the target gene downregulation effect more precisely, we suggest using separate animals for each assay (hPAP assay, qRT-PCR, Western blot). These assays can also be conducted with the other organs, which may show significant fluorescence signals in the imaging study, to examine the nonspecific RNAi effect. During the course of study, the general health of the animals should be monitored everyday to check if there is any toxicity issues. The body weight will be measured and recorded everyday and any abnormalities in behaviors or activity will also be examined.

The required sample size per group was calculated using G*Power software 3.1 (IDRE Research Technology Group, Los Angeles, CA). The desired level of significance was set at 0.05 (α) and the power (1-β) was set at 0.9. When the medium effect size (0.5 by convention) was used, the required sample size was 86 subjects per group, which was too large for conducting actual experiments. Therefore, the parameters needed to be adjusted in a range of reasonable values. When we set 200 RLU/mg protein of hPAP activity as a minimally meaningful difference that we would like to detect, and used the standard deviations from the previous hPAP activity data (Figure 5.4B), the effect size became 1.33 and the calculated sample size was 13 per group. For 300 RLU/mg protein of hPAP activity as a minimally meaningful difference to be detected, the effect size was 2 and the required sample size was 7 per group. Here, the hPAP activity was converted to effect size in G*Power by putting the arbitrarily chosen mean difference (200 RLU/mg protein was attempted first as it was the mean difference between the PBS control group and the Keap1 siRNA-treated group) and the averaged standard deviation value (~150 mg/RLU) of the previous hPAP activity data. When the power is reduced from 0.9 to 0.8, the required sample size was 64 per group for the medium effect size (0.5), 10 per group

for an effect size of 1.33, and 6 per group for an effect size of 2. Considering that similar studies in the literature used 3-4 mice per group (30,31), we estimate that 6-13 mice per group would be fair enough for obtaining statistical significance if there is difference. The sample size for the imaging study was not calculated, but 4-5 animals seems appropriate for the visual examination of the fluorescence signals. Based on the experimental design described above and the calculated sample size, the experimental groups and the number of animals needed were determined as shown in Table 6.1. The required amounts and the estimated cost of the siRNA, peptides, and mice are listed in Table 6.2.

The number of mice in Table 6.1 may not be practical to perform the experiments considering time, cost, and labor. The required number can be reduced if 4 mice/group is used instead of 5 in the imaging study. Also, the mice for PBS group can be reduced as they serve as a negative control. In addition, only one gender can be included for the study. In the gene silencing study, the number of animals can be reduced if the same mouse is used for the three different assays (hPAP assay, qRT-PCR, Western blot), although it may compromise the precise gene silencing analyses. Alternatively, we may compare just two different doses instead of three. Again, only one gender can be included for this study to reduce the use of animals.

6.3 Future work

6.3.1 Optimization of the siRNA carriers

To improve the brain targeting ability of the siRNA-carrier complex, we can attempt and evaluate alternative brain-targeting moieties besides the TfR-binding sequence in further studies. The candidates can be borrowed from the natural ligands that

are known to bind to the receptors expressed on the brain endothelial cells. For example, the ligands for low-density lipoprotein receptor (LDLR), LDLR-related protein (LRP1), insulin receptor, and diphtheria toxin receptor can be incorporated in drug delivery vehicles to achieve brain-targeted drug delivery through the receptor-mediated transcytosis mechanism (1). The potential limitation in this approach is that the modified ligand binding may lead to disruptions in the normal biological functions of the natural ligands. In addition, the efficiency of the ligand conjugation is often unsatisfactory, depending on the complexity of the conjugation chemistry.

As another option, various brain-targeting short peptide sequences can be integrated into the carrier peptide. The short peptide sequences are compatible with our peptide-based siRNA carrier design and also favorable for scalable production using the solid phase peptide synthesis technique. The following are the examples of the brain-targeting peptide sequences that were investigated in the literature: the LRP1-binding sequence (TFFYGGSRGKRNNFKTEEY) (2), the acetylcholine receptor targeting sequence derived from the rabies virus glycoprotein (RVG) (YTIWMPENPRPGTNSRGKRASNG) (3), and the leptin-receptor binding peptide which is the sequence 12-32 (g21) of leptin (TLIKTIVTRINDISHTQSVSA) (4).

Other than using these known sequences, we can employ the phage display technology to screen the short peptide sequences that bind to the receptors on the brain endothelium. The TfR-binding sequence in the current construct was originally found by using this technique (5). By introducing the phages that display the candidate short peptide sequences into mice or rats and performing *in vivo* brain perfusion, the peptide sequences with high affinity to the brain endothelium can be identified. Once the carrier

constructs with new targeting sequences are prepared, physicochemical characterization and *in vitro* transfection studies should be conducted to assess the capability in regard to the siRNA encapsulation, serum stability, and functional silencing of the target gene. In addition, any cytotoxic effects from the new constructs should also be examined. The peptide sequence that proves to have the most promising properties in all aspects will be chosen as an optimized peptide-based siRNA carrier.

6.3.2 Efficacy assessment of the siRNA-peptide complex treatment in NDD animal models

RNAi therapy using the siRNA-carrier complex should eventually be applied in NDD animal models in order to comprehensively evaluate the therapeutic efficacy and the safety profile of the treatment. In AD treatment, as briefly introduced in Chapter 2, the examples of the therapeutic siRNAs that can be loaded on the carrier complex are as follows: the Keap1 siRNA for rescuing the Nrf2 activity to enhance the cellular antioxidant capacity; the APP (amyloid precursor protein) siRNA to reduce the production of the Aβ peptide by directly suppressing the APP expression from upstream; the BACE (beta secretase 1) siRNA to downregulate the enzyme that is responsible for generating the Aβ peptide via the APP cleavage; and the CDK5 (cyclin-dependent kinase 5) siRNA to reduce the tau phosphorylation activity. We can even attempt a combinatorial approach with mixtures of more than one therapeutic siRNA to examine any additive or synergistic effects concerning the therapeutic benefits.

The therapeutic or disease modifying effects of the treatment can be evaluated from various angles. On the pathophysiological level, the followings are positive indicators of treatment efficacy: a significant reduction in Aβ peptide levels in CSF,

decreased formation of amyloid plaques and neurofibrillary tangles in brain tissues, reduced inflammatory markers in body fluids, and declined levels of oxidative damage markers such as lipid peroxidation products and protein carbonyls (6). In regard to the memory dysfunction, cognitive enhancement can be assessed by evaluating learning and memory skills based on performance in various behavioral tests such as spatial navigation tests, passive/active avoidance learning tests, cued/contextual learning tests, and schedule-induced learning tests. Concerning the BPSD (behavioral and psychological signs and symptoms of dementia)-related symptoms, the noncognitive symptoms can be examined with the following tests: aggressive behavior tests, activity disturbances tests, depression-related symptoms tests, anxiety/fear tests (6).

The safety of the siRNA-carrier complex in *in vivo* application will also be assessed. Importantly, the treatment should not result in increased mortality and morbidity. The following five aspects of the animal's condition are commonly monitored to evaluate general adverse effects from treatment: the body weight, physical appearance, measurable clinical signs, unprovoked behavior and response to external stimuli (7). The behavioral abnormalities as a part of NDD symptoms in NDD animal models should be carefully differentiated from the treatment-caused alterations. Another consideration is the immunogenicity issue involved in the siRNA as well as the peptide carriers. It was reported that siRNAs could induce interferons and immunostimulatory cytokines depending on their nucleotide sequences (8). Therefore, we need to analyze the animal serum before and after the treatment to examine whether the treatment leads to antibody production against the carrier peptide and whether the levels of diverse cytokines and chemokines are influenced by the treatment. The improved therapeutic outcome and the

absence of adverse signs will be encouraging evidence for the use of our siRNA carrier system as a promising therapeutic approach for NDDs.

Table 6.1. The experimental groups and the number of animals needed.

Study	Approach	Group	Time	hPAP(+) ♂	hPAP(+) ♀	Balb/c ♂	Balb/c ♀
Imaging study	Tail vein injection	PBS	1 h	-	-	5/time-point *4 =20	5/time-point *4 =20
			3 h				
			8 h				
			24 h				
		Cy5.5 siRNA	1 h	-	-	5/time-point *4 =20	5/time-point *4 =20
			3 h				
			8 h				
			24 h				
		Cy5.5 siRNA /Myr-TP-Tf complex	1 h	-	-	5/time-point *4 =20	5/time-point *4 =20
			3 h				
			8 h				
			24 h				
		Cy5.5 siRNA /Myr-TP-Scr complex	1 h	-	-	5/time-point *4 =20	5/time-point *4 =20
			3h				
			8 h				
			24 h				
	Retrobulbar injection	PBS	1 h	-	-	5/time-point *4 =20	5/time-point *4 =20
			3 h				
			8 h				
			24 h				
		Cy5.5 siRNA	1 h	-	-	5/time-point *4 =20	5/time-point *4 =20
			3 h				
			8 h				
			24 h				
		Cy5.5 siRNA /Myr-TP-Tf complex	1 h	-	-	5/time-point *4 =20	5/time-point *4 =20
			3 h				
			8 h				
			24 h				
		Cy5.5 siRNA /Myr-TP-Scr complex	1 h	-	-	5/time-point *4 =20	5/time-point *4 =20
			3 h				
			8 h				
			24 h				

Study	Approach	Group	Dose	hPAP(+) ♂	hPAP(+) ♀	Balb/c ♂	Balb/c ♀
Gene silencing study	Tail vein injection	PBS	-	7 mice	7 mice	-	-
		Keap1 siRNA	50 µg	7/dose * 3 doses * 3 assays = 63	7/dose * 3 doses * 3 assays = 63	-	-
			100 µg				
			150 µg				
		Keap1 siRNA /Myr-TP-Tf complex	50 µg	7/dose * 3 doses * 3 assays = 63	7/dose * 3 doses * 3 assays = 63	-	-
			100 µg				
			150 µg				
		Keap1 siRNA /Myr-TP-Scr complex	50 µg	7/dose * 3 doses * 3 assays = 63	7/dose * 3 doses * 3 assays = 63	-	-
			100 µg				
			150 µg				
	Retrobulbar injection	PBS	-	7 mice	7 mice	-	-
		Keap1 siRNA	50 µg	7/dose * 3 doses * 3 assays = 63	7/dose * 3 doses * 3 assays = 63	-	-
			100 µg				
			150 µg				
		Keap1 siRNA /Myr-TP-Tf complex	50 µg	7/dose * 3 doses * 3 assays = 63	7/dose * 3 doses * 3 assays = 63	-	-
			100 µg				
			150 µg				
		Keap1 siRNA /Myr-TP-Scr complex	50 µg	7/dose * 3 doses * 3 assays = 63	7/dose * 3 doses * 3 assays = 63	-	-
			100 µg				
			150 µg				
Total				392 mice	392 mice	160 mice	160 mice

Table 6.2. Required amounts and the estimated cost of the siRNA, peptides, and mice.

Materials	Amount/injection	Required amount	Estimated cost
Cy5.5 siRNA (Imaging study)	50 µg of siRNA (=4 nmoles)	4 nmoles/injection * single injection * 5 mice/time-point * 4 time-points* 3 groups * 2 routes of administration * 2 genders →Total 960 nmoles.	Core facility charges $7.00/base for 1 µmole scale, $20.00 for set up fee, $75.00 for HPLC purification and $150.00 for Cy5.5 conjugation. 200 nmol RNAi syntheses generally give 40 -70 nmoles of desalted material (20-35% yield). If 5 µmoles are requested, $7.00* 21 nt*2 strands *5 + $75.00 + $20.00+ $150.00= $1,715
mKeap1 siRNA (Gene silencing study)	50 µg of siRNA (=4 nmoles) 100 µg of siRNA (=8 nmoles) 150 µg of siRNA (=12 nmoles)	4 nmoles/injection * 3 injections * 7 mice/assay * 3 assays * 3 groups * 2 routes of administration * 2 genders = 3,024 nmoles for 50 µg of siRNA dose. 6,048 nmoles for 100 µg of siRNA dose and 9,072 nmoles for 150 µg of siRNA dose. →Total 18.144 µmoles.	If 50 µmoles are requested, $7.00* 21 nt*2 strands *50 + $75.00 + $20.00 = $14,795
Myr-TP-Tf peptide (Imaging study + Gene silencing study)	50 µg of siRNA (80 nmoles of peptides) 100 µg of siRNA (160 nmoles of peptides) 150 µg of siRNA (240 nmoles of peptides)	80 nmoles/injection * single injection * 5 mice/time-point * 4 time-points* 2 routes of administration * 2 genders =6,400 nmoles of peptide (Imaging study) 80 nmoles/injection * 3 injections * 7 mice/assay * 3 assays * 2 routes of administration * 2 genders = 20,160 nmoles for 50 µg of siRNA dose. 40,320 nmoles for 100 µg of siRNA dose, and 60,480 nmoles for 150 µg of siRNA dose are needed (Gene silencing study) →Total 127.36 µmoles.	127.36 µmoles corresponds to 570 mg of peptide. Selleckchem provides significant discount for the large scale synthesis. $109.80/amino acid for 1,000 mg * 43 amino acid= $4,721.40 (+ myristic acid conjugation fee)
Myr-TP-Scr peptide (Imaging study + Gene silencing study)	50 µg of siRNA (80 nmoles of peptides) 100 µg of siRNA (160 nmoles of peptides) 150 µg of siRNA (240 nmoles of peptides)	80 nmoles/injection * single injection * 5 mice/time-point * 4 time-points* 2 routes of administration * 2 genders =6,400 nmoles of peptide (Imaging study) 80 nmoles/injection * 3 injections * 7 mice/assay * 3 assays * 2 routes of administration * 2 genders = 20,160 nmoles for 50 µg of siRNA dose. 40,320 nmoles for 100 µg of siRNA dose, and 60,480 nmoles for 150 µg of siRNA dose are needed (Gene silencing study) →Total 127.36 µmoles.	127.36 µmoles corresponds to 570 mg of peptide. Selleckchem provides significant discount for the large scale synthesis. $109.80/amino acid for 1,000 mg * 43 amino acid= $4,721.40 (+ myristic acid conjugation fee-not sure)
Animal	Type	Required number of animals	Estimated cost
Mice	Balb/c mice	160-320 mice (Adjustable depending on the experimental design)	Balb/c mice from the Jackson laboratory are priced as following; 15 week-old mouse: $36.75/animal $36.75 * 320 mice =$11,760.00 $36.75 * 160 mice =$5,880.00
	hPAP (+) mice	392-784 mice (Adjustable depending on the experimental design)	Depends on the Dr.Jeffrey Johnson lab

6.4 References

1. Abbott NJ, Patabendige AA, Dolman DE, Yusof SR, Begley DJ. Structure and function of the blood–brain barrier. Neurobiol Dis 2010;37:13-25.

2. Bertrand Y, Currie JC, Demeule M, Régina A, Ché C, Abulrob A, et al. Transport characteristics of a novel peptide platform for CNS therapeutics. J Cell Mol Med 2010;14:2827-39.

3. Kumar P, Wu H, McBride JL, Jung KE, Kim MH, Davidson BL, et al. Transvascular delivery of small interfering RNA to the central nervous system. Nature 2007;448:39-43.

4. Tosi G, Badiali L, Ruozi B, Vergoni AV, Bondioli L, Ferrari A, et al. Can leptin-derived sequence-modified nanoparticles be suitable tools for brain delivery? Nanomedicine 2012;7:365-82.

5. Lee JH, Engler JA, Collawn JF, Moore BA. Receptor mediated uptake of peptides that bind the human transferrin receptor. Eur J Biochem 2001;268:2004-12.

6. Van Dam D, De Deyn PP. Drug discovery in dementia: the role of rodent models. Nat Rev Drug Discov 2006;5:956-70.

7. Morton D, Griffiths P. Guidelines on the recognition of pain, distress and discomfort in experimental animals and an hypothesis for assessment. Vet Rec 1985;116:431-36.

8. Judge AD, Sood V, Shaw JR, Fang D, McClintock K, MacLachlan I. Sequence-dependent stimulation of the mammalian innate immune response by synthetic siRNA. Nat Biotechnol 2005;23:457-62.